TYCO LABORATORIES, INC., BEAR HILL, WALTHAM, MASSACHUSETTS 02154 TELEPHONE 617 899-1650

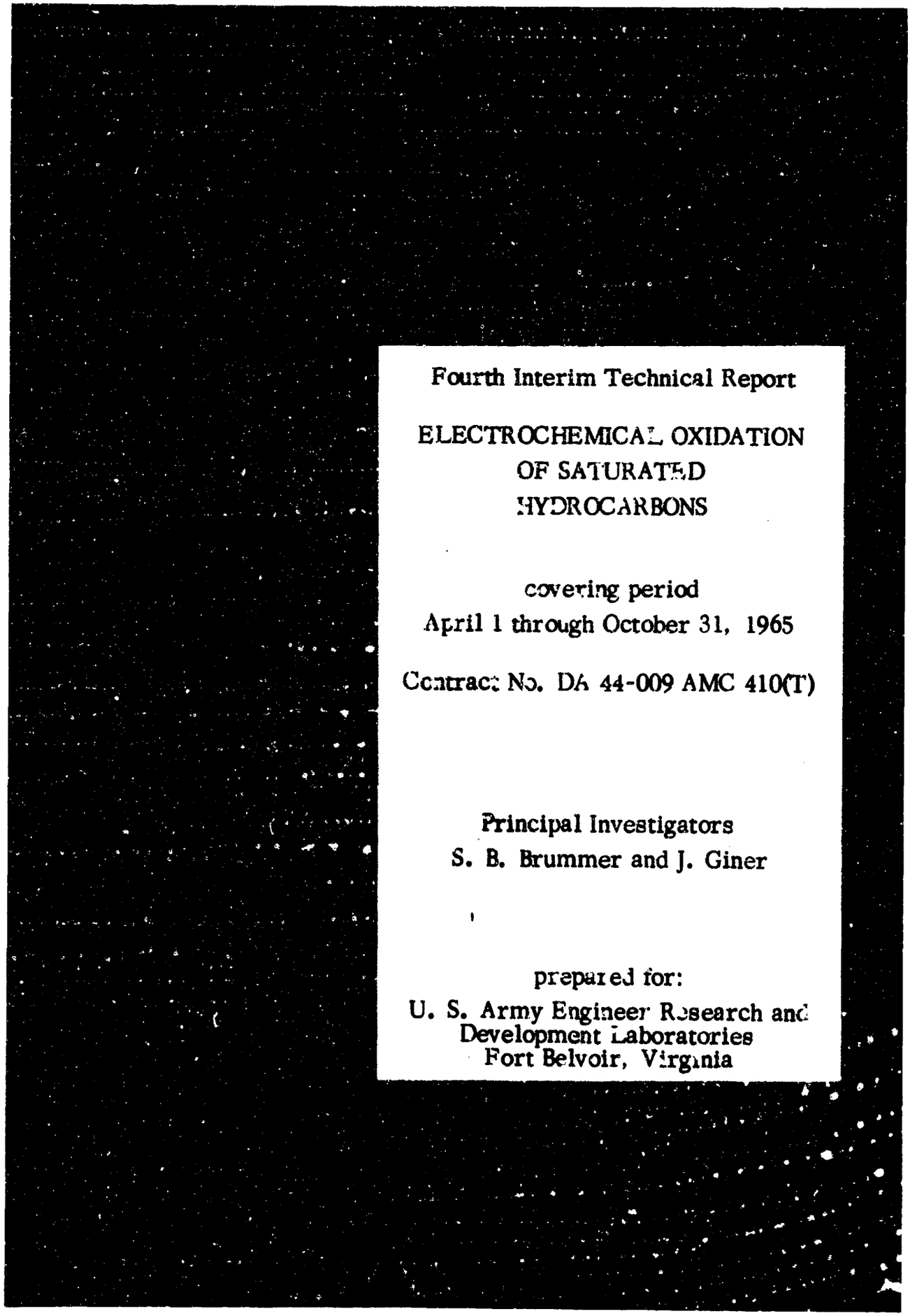

Fourth Interim Technical Report

ELECTROCHEMICAL OXIDATION OF SATURATED HYDROCARBONS

covering period
April 1 through October 31, 1965

Contract No. DA 44-009 AMC 410(T)

Principal Investigators
S. B. Brummer and J. Giner

prepared for:
U. S. Army Engineer Research and Development Laboratories
Fort Belvoir, Virginia

TYCO LABORATORIES, INC.
Bear Hill
Waltham 54, Massachusetts

Fourth Interim Technical Report

ELECTROCHEMICAL OXIDATION OF SATURATED HYDROCARBONS

covering period
April 1 through October 31, 1965

Contract No. DA 44-009 AMC 410(T)

Principal Investigators
S. B. Brummer and J. Giner

prepared for:
U. S. Army Engineer Research and Development Laboratories
Fort Belvoir, Virginia

CONTENTS

CONTENTS (Cont.)

List of Figures

ABSTRACT TO SECTION I

The mechanism of the oxidative adsorption of propane on smooth platinum from concentrated phosphoric acid solutions has been studied from 80 - 140°C. Measurements have been made using anodic and cathodic chronopotentiometry in conjunction with rapidly - applied potentiostatic techniques. Experiments with rotating disk and with platinum foil electrodes show that adsorption onto a clean electrode is limited by diffusion in solution. Total propane adsorption, at a given potential, measured either anodically or cathodically, is independent of the temperature in the range 80 - 140°C. Comparison of the limiting values of the two measurements suggests that the average oxidation state of the adsorbate is independent of the potential ($\geq$ 0.3 v) and of the temperature. Potentiostatic anodic desorption studies show, however, that this is not so and show that the detailed "structure" of the adsorbate is a function of the potential and the temperature. Three distinct adsorbed residues appear to be present, (A), (B), and (C). These appear to release respectively, 1.8, 1.3 and ~ 6 electrons per covered Pt site when oxidized. Potentiostatic cathodic desorption measurements indicate the presence of another adsorbed material, which may be physically adsorbed C_3H_8. When the presence of this material is allowed for, (A) and (B) appear to be the same and release a little more than 1 electron/site when oxidized.

ABSTRACT TO SECTION II

Physical parameters of platinum black catalysts have been selected and determined for material characterization and are being correlated with catalytic activity as fuel cell anodes. The platinum black catalysts have been precipitated from aqeuous solution and their structural and morphological properties are being studied using X-ray diffraction, electron-microscopy, electron-diffraction and B.E.T. adsorption. Physical characterization of the catalysts has aimed at elucidating atomic factors (i.e. factors involving

the specificity of the various atomic sites of the crystal surface) such as size, morphology of the elementary crystallites, stored-energy, crystal imperfections. Also, studies have been directed at elucidating structural factors (i.e. factors involving the state of aggregation) such as agglomeration, size distribution and crystal orientation of the deposits. Absolute values of average particle size were obtained by electron microscope shadowgraphy and evaluation of X-ray line broadening. Particle size distribution was obtained by shadowgraphy and from spot size evaluation of electron diffraction of low-index reflections from the small single crystallites of platinum. Comparison of the values obtained by the last method with the other values leads to the conclusion that particles of the black are monocrystalline. A log-normal Gaussian particle size distribution of the form

$$P(x)\,dx = \frac{ah}{\sqrt{\pi}} \exp\left(-\frac{1}{4h^2}\right) \cdot \exp\left(-h^2 \ln^2 ax\right) dx$$

was derived with the constant h a measure of the distribution spread. Within experimental error, these methods (X-ray, electron-shadowgraph) and the B.E.T. adsorption, give good agreement for the particle size and size distribution. The X-ray method is being used to evaluate the energy stored during precipitation. The catalytic activity of the blacks is being correlated with these physical parameters of the catalysts.

ABSTRACT TO SECTION III

The corrosion resistance of tantalum alloys and intermetallic compounds in concentrated phosphoric acid has been investigated from 80 - 150°C. Tantalum is less corrodible in these solutions than any other non-noble metal. Alloys of tantalum with titanium (up to 60 a % Ti) show promising corrosion resistance as does the intermetallic compound $TaNi_3$.

INTRODUCTION

The work described in this report is concerned with the practical implementation of the hot concentrated phosphoric acid, direct oxidation, hydrocarbon fuel cell. Experiments in this period have been concerned with three aspects of the over-all problem: the mechanism of the hydrocarbon to carbon dioxide reaction on a platinum anode, the role of surface morphology and surface defect structure in optimizing the characteristics of dispersed platinum-metal catalysts, and the development of suitable corrosion resistant structural materials for use in the acid electrolyte. The mechanism study, described in section I of the report, is a continuation of work previously reported[1, 2] and is concerned with an investigation of the oxidative adsorption of propane on smooth platinum. Both the surface morphology study and the corrosion program were initiated in this report period. They are described in sections II and III respectively. A summary of the experimental findings is appended to each section and is also contained in the abstract at the beginning of this report.

I. MECHANISM OF OXIDATIVE ADSORPTION OF HYDROCARBONS ON PLATINUM

1. Introduction

In the hot concentrated phosphoric acid direct-oxidation hydrocarbon fuel cell, the major limitation is the performance of the anode. The aim of this part of the research program is to provide basic information on the functioning of the anode. Work reported here is a continuation of that described previously[1-4], and we have continued our investigation of the oxidative adsorption of propane at smooth platinum electrodes. Almost all the measurements in this period have been concerned with studying the residues which accumulate during the progress of the adsorption of propane. Most of these studies were made at 130°C with concentrated phosphoric acid electrolyte. Studies of diffusional processes have also been made using a platinum foil and a rotating platinum disk electrode.

Details of the experiments we have carried out are described in the sections which follow. To assist in this description, a glossary of symbols is presented at the end of section I of this report.

2. Experimental

Most of the experimental details have been described in our previous reports[1, 2] and we will indicate in the appropriate results section whenever our procedures differ from those reported previously. There are, however, two general points of procedure which should be mentioned here: In order to attain greater purity for the H_3PO_4, we have adopted the procedure of crystallization. The method is to filter the 85% A.C.S. or food-grade H_3PO_4 through glass and then to crystallize it by cooling it slowly, while adding seed crystals to prevent undercooling. The seed crystals are prepared by vigorous cooling of 85% H_2PO_4 with liquid N_2. The crystals separating from the melt are the 91.6% hemi-hydrate[14]. These are filtered under suction and are allowed to surface-melt while on the filter to help reject impurities. They are remelted, slightly diluted with triply-distilled water, and recrystallized, as before. They are crystallized four times in all and then, as before, are refluxed for 48 hours with 50% vol/vol

of 30% H_2O_2 solution. The excess H_2O, produced from the decomposition of the H_2O_2, is boiled off to give the required concentration of H_3PO_4. The results of this procedure are variable. In the best instances, we have obtained a solution of previously unparalleled cleanliness and, for example, there is no difference between the Q_H (cathodic hydrogen charge measurements taken from 0.5 v vs. R.H.E.) determined at 130°C after 100 sec at 0.3 v and that determined 10 msec after anodic cleaning. In the worst instances, the fall in Q_H (with time after anodic pretreatment) is no better than is observed without crystallization. Even in this case, however, we have found that although Q_H decreases with time, implying contamination, the charging curve does not lose its characteristic shape. With uncrystallized acid, the curve invariably loses its shape after 100 sec at 0.3 v, even when Q_H scarcely decreases.

The above reflux with H_2O_2 is carried out in vycor. Previous experiments were performed in a vycor cell, following a report[5] that pyrex is corroded relatively rapidly in hot concentrated H_3PO_4. Some measurements at 130°C were, however, carried out in a pyrex cell without noticeable difference in the results. But, when we attempted to repeat our previous experiments at 80°C in the pyrex cell, we found that the C_3H_8 adsorption was considerably less than that we had found previously[1, 3]. Careful checking of our experimental procedure showed that if the hot H_3PO_4 was never in contact with pyrex we could reproduce our previous data. For this reason, we now reflux the H_3PO_4 in a vycor flask. The above behavior is anomalous, for it is expected that if anything is dissolved from pyrex by the H_3PO_4 it should occur more readily at the higher temperature. Thus, the effect of pyrex should be more marked at higher temperatures. However, we may suppose that the adsorption of C_3H_8 at 80°C occurs less readily than at 110°C and higher (which it must if there is a finite activation energy for chemisorption) and can thus be more readily poisoned. Then, a small impurity concentration (from the pyrex) could be more deleterious at the lower temperature.

For assistance with following the description of our results, as set out in the following sections, we include a glossary of the more widely used symbols at the end of section I of this report.

3. Studies of Diffusional Processes in C_3H_8 Adsorption

In the last report on this contract[2] some question was raised that the initial adsorption kinetics of C_3H_8 onto clean Pt are not diffusionally controlled. The view was expressed that the linear diffusion equation of Laitinen and Kolthoff[6] is not applicable for long times of adsorption at a wire electrode[7]. Calculations in the last report showed that any such discrepancy should be small in concentrated H_3PO_4 due to its high viscosity. To verify this, we have carried out experiments with a stagnant solution using a Pt-foil electrode, which better approximates the semi-infinite linear diffusion model than does a wire electrode. Both experiments show clearly that the adsorption of C_3H_8 onto clean, smooth Pt is limited by diffusion in the solution. These experiments will now be described in greater detail.

The experiments with the Pt foil was carried out with 80% (13 M) H_3PO_4 saturated with C_3H_8 at 130°C. Measurements were made of the decrease of θ_H^t with time of adsorption at 0.3 v. We see (Fig. I-1) that θ_H^t decreases linearly with $\tau_{ads}^{\frac{1}{2}}$ for at least the first 25 sec of adsorption time. This would substantiate the previous conclusion that the adsorption is diffusion limited, which was based on experiments with the wire electrode.

The experiments with the rotating disk assembly were carried out at 80°C with the 91.6% hemi-hydrate (16.1 M) acid. Here, we wished not only to establish that the adsorption rate is diffusionally controlled, but also to study the kinetics of the adsorption step. To accomplish this, we worked at a lower temperature where the rate of the adsorption step would be lower. The experiment consisted of activating the electrode as previously reported[1, 2], adsorbing at fixed potential for various τ_{ads}, and then stripping the adsorbate anodically with a large galvanostatic pulse (~ 100 - 200 ma/real cm^2). This procedure was repeated for values of τ_{ads} from 10 msec to 10 sec at 0.22 v and 0.3 v. Previously, it was noted that anodic charging does not give an unambiguous measure of $C_3H_{8_{ads}}$ because the C_3H_8, once

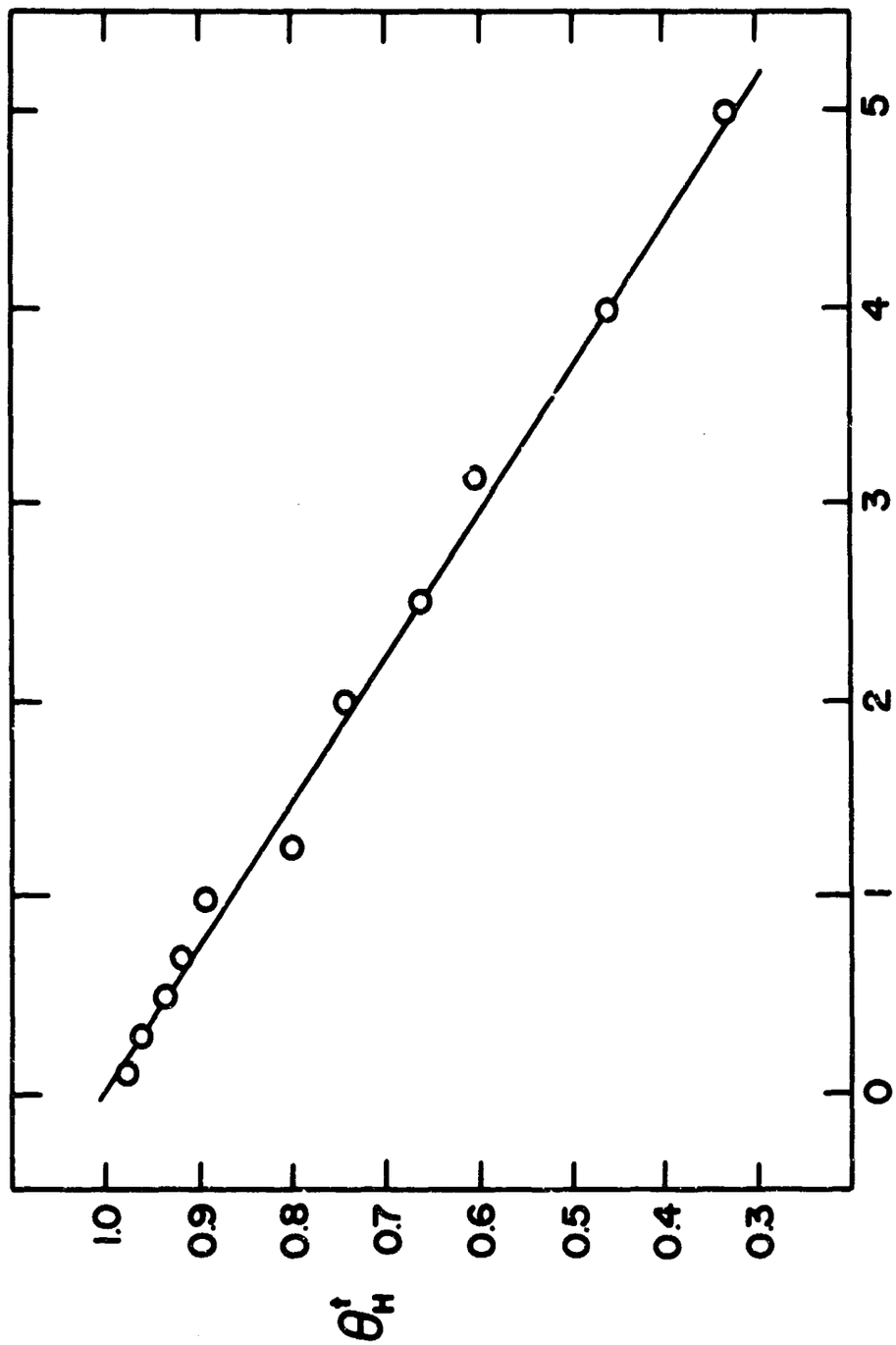

Fig.I-1 Adsorption of C_3H_6 at 0.3V at 130°C on Pt foil

adsorbed, starts to oxidize. Consequently, we have largely confined our studies to low potentials and relatively short times of adsorption. Here, we know from our previous work that the extent of this oxidation is insignificant. It would, of course, be possible to use cathodic charging in this context, but we have preferred the anodic charging, where possible, because of its greater sensitivity.

Before presenting the data, we shall derive the expressions which are expected for the adsorption rate if the process is controlled by mass transport to the rotating disk electrode. The flux of material to the electrode is given by the Levich equation[8] which, when modified according to Gregory and Riddiford[9], gives:

$$i = \frac{0.554\ nFD^{2/3}\ \nu^{-1/6}\ \omega^{1/2}C}{0.8934 + 0.316\ (D/\nu)^{0.36}}\ ,\ amp/gcm^2. \qquad (I.1)$$

Here, i is the current corresponding to the electrode reaction (involving n electrons) of the solution species, of bulk concentration C (mole/ml), and with a diffusion coefficient D (cm^2/sec); ν is the kinematic viscosity (stokes), F is the faraday, and ω is the angular velocity of the disk (sec^{-1}). Then, since i is constant for a given set of solution parameters, the charge Q passed in time τ as the result of the reaction of the material brought to the electrode by forced mass transport is:

$$Q = i\,\tau = \frac{0.554\ nFD^{2/3}\ \nu^{-1/6}\ \omega^{1/2}C\ \tau}{0.8934 + 0.316\ (D/\nu)^{0.36}}\ ,\ coul/gcm^2. \qquad (I.2)$$

For the anodic stripping of adsorbed C_3H_8 we would write:

$$Q_{ads}^{C_3H_8} = \frac{0.554\ nFD^{2/3}\ \nu^{-1/6}\ \omega^{1/2}C^{C_3H_8}\ \tau_{ads}}{0.8934 + 0.316\ (D/\nu)^{0.36}}\ ,\ coul/gcm^2. \qquad (I.3)$$

Here, n could be taken as 20, corresponding to the oxidation reaction $C_3H_{8_{ads}} \rightarrow CO_2$ - or as 17[2], corresponding to the oxidation of triply-bonded C_3H_8 to CO_2. We will take 17, in conformity with our previous results. For 91.6% H_3PO_4 at 80°C, the kinematic viscosity is 6.5×10^{-2} stokes[10]. If we take a preliminary value of $D^{C_3H_8}$ of 1.45×10^{-6}[2] to make the minor correction (< 1%) to the denominator of (I.3) and if we take $C^{C_3H_8}$ as 1.7×10^{-7} moles/ml[11], we obtain

$$Q_{ads}^{C_3H_8} = 0.086\ \omega^{1/2}\ \tau_{ads}\ D^{2/3},\ \text{coul/gcm}^2. \qquad (I.4)$$

Here ω is in rpm. Then, for diffusionally-controlled adsorption we expect $Q_{ads}^{C_3H_8}$ to increase linearly with time of adsorption and with $\omega^{1/2}$.

Data obtained with the rotating disk assembly described previously[2] for C_3H_8 adsorption from 91.6% H_3PO_4 at 80°C are shown in Figs. I.2-4. At 0.22 v (Fig. I.2) $Q_{ads}^{C_3H_8}$ does increase linearly with τ_{ads} except for short times of adsorption. Similarly at 0.3 v, $Q_{ads}^{C_3H_8}$ increases with τ_{ads} but, here, it quite rapidly tails off. This is because of the above mentioned partial oxidation of the adsorbed C_3H_8. The slopes of the linear region of the $Q_{ads}^{C_3H_8}$ vs. τ_{ads} lines of Figs. I.2 and I.3 are plotted against $\omega^{1/2}$ in Fig. I.4 and we find satisfactory linearity. Using the slope of the line in Fig. I.4, we calculate a value for $D^{C_3H_8}$ of 0.66×10^{-6} cm^2/sec. Experiments with the solution stagnant, i.e. where the semi-infinite linear diffusion conditions would apply, gave an initial slope for the $Q_{ads}^{C_3H_8}$ vs. $\tau_{ads}^{1/2}$ line of 2.5×10^{-4} coul/gcm^2. This gives a value of 0.71×10^{-6} cm^2/sec for $D^{C_3H_8}$, in good agreement with the rotating disk experiment. Using Walden's rule, these diffusion constants predict 6.9×10^{-6} and 7.4×10^{-6} for $D^{C_3H_8}$ in water at 25°C. This contrasts with values of 9.3×10^{-6} and 11.8×10^{-6} cm^2/sec, predicted earlier[4] for $D^{C_3H_8}$ in water at 25°C. The experimental value at 25°C is 12.1×10^{-6} cm^2/sec[12].

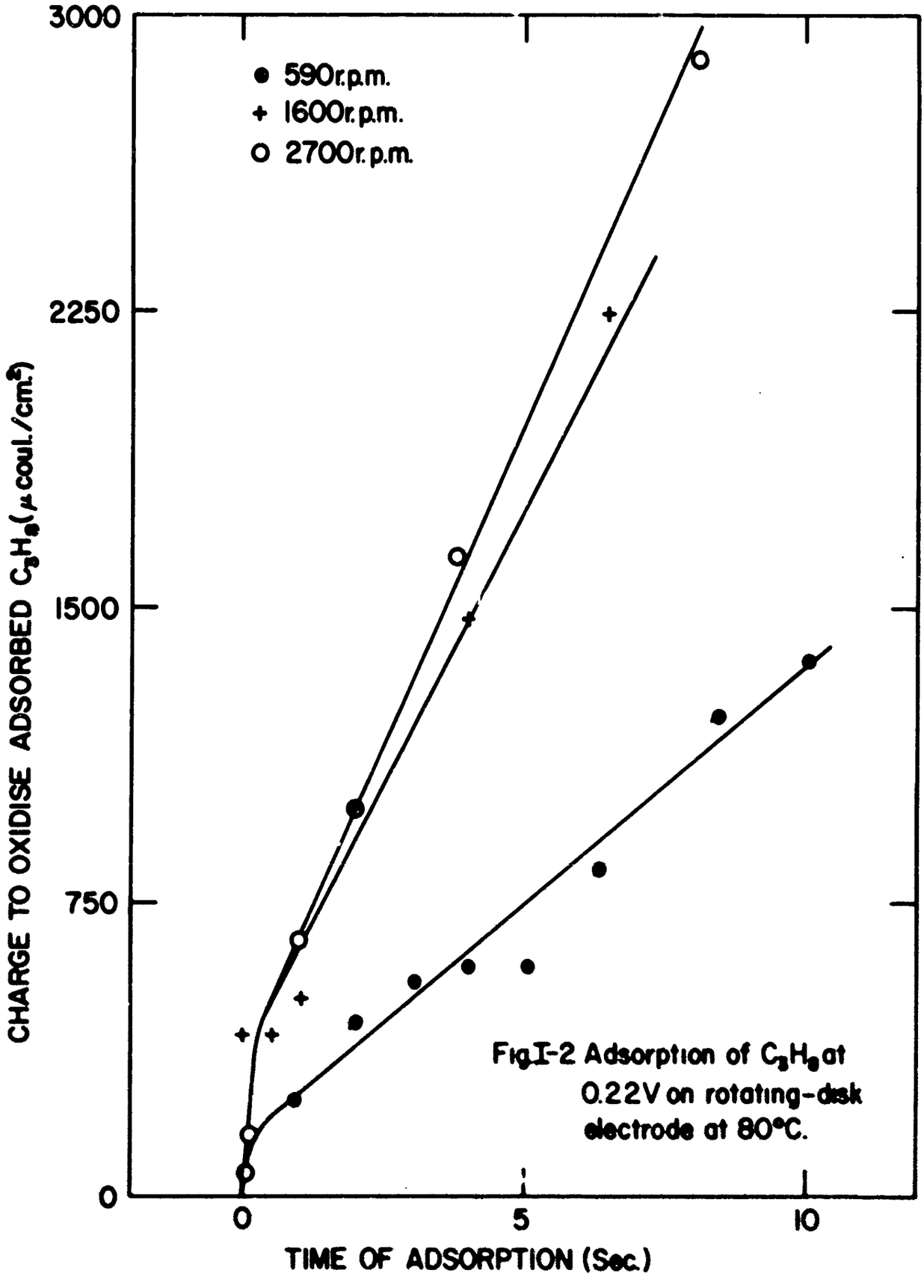

Fig.I-2 Adsorption of C_3H_8 at 0.22V on rotating-disk electrode at 80°C.

Fig. I-3 Adsorption of C_3H_8 at 0.3V on rotating-disk electrode at 80°C.

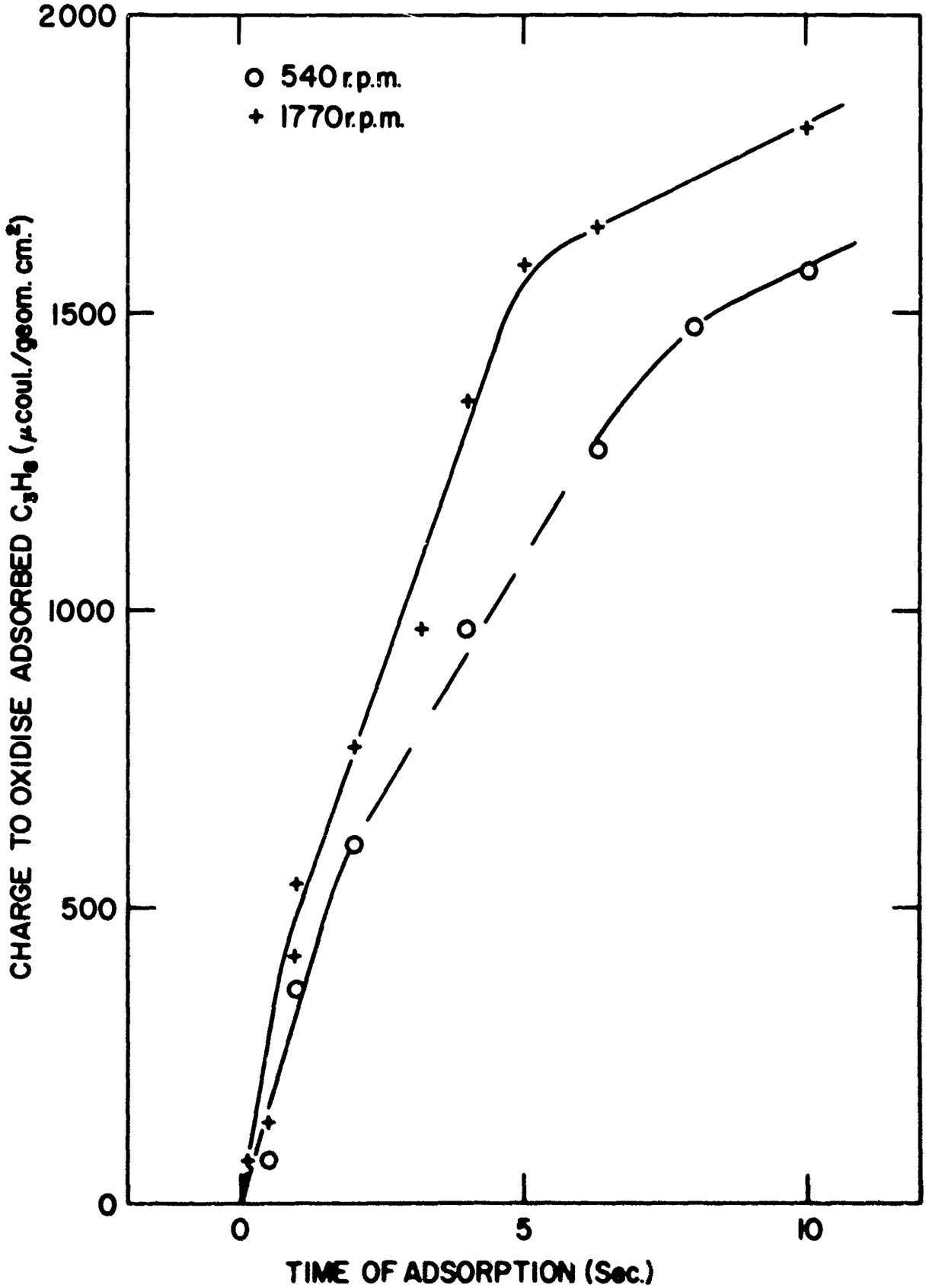

Fig. I-4 Slope of ($Q_{ads.}$ vs. $\tau_{ads.}$) vs. $\omega^{1/2}$

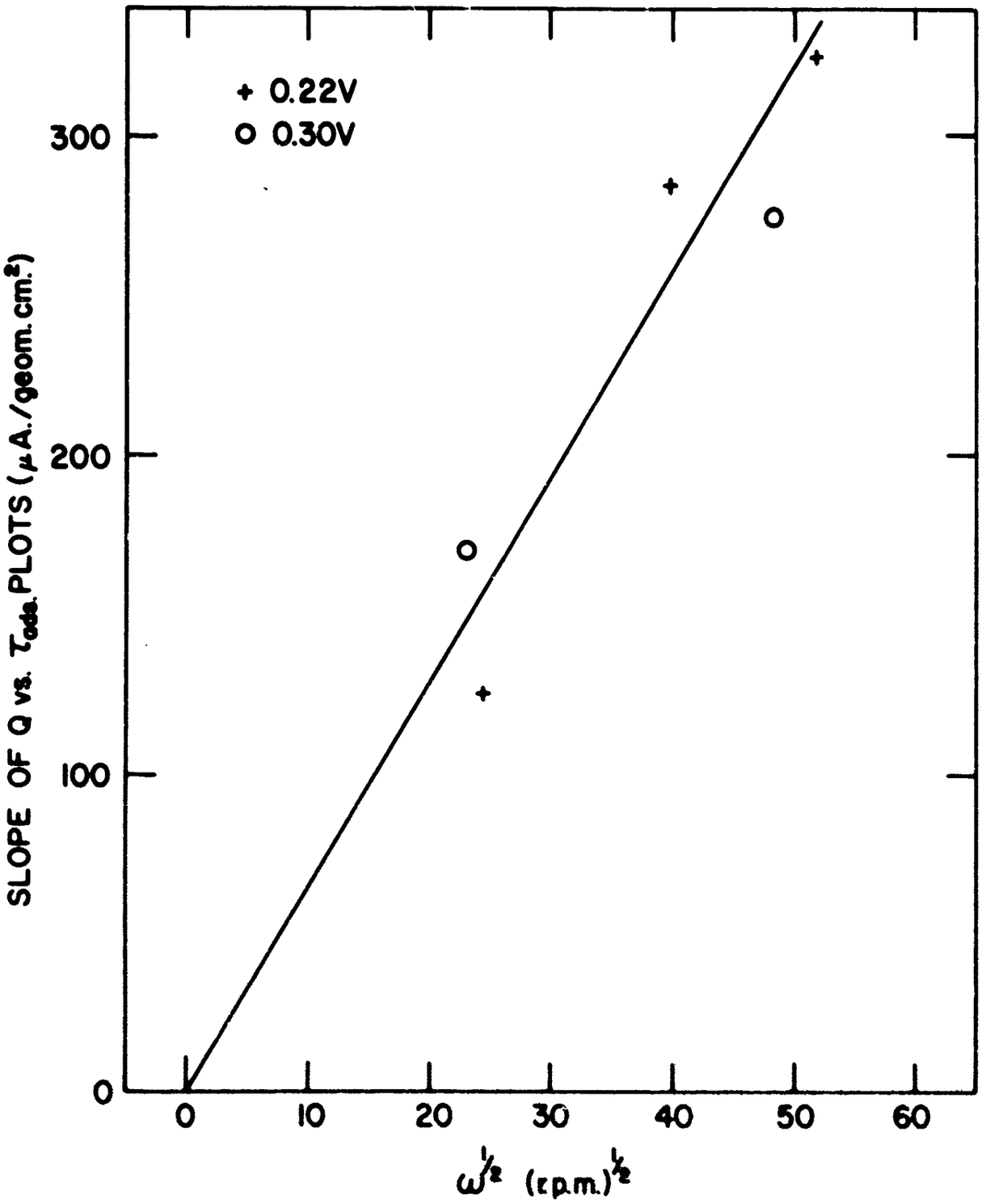

The general conclusion then must be that the adsorption rate is limited by diffusion. There are, however, two difficulties: the determined diffusional coefficients do not predict good values in room temperature water and the $Q_{ads}^{C_3H_8}$ vs. τ_{ads} plots are not linear, as noted, at low values of τ_{ads}. Both of these problems are, however, relatively minor. The Walden Rule is, even under the best of circumstances, only a moderate approximation and fails in aqueous solutions particularly badly[13]. In concentrated H_3PO_4 solutions, where very complex associated "structures" occur[14], the rule can only be used as an approximate guide for correlating diffusional coefficients determined under various conditions of viscosity, temperature, and concentration. On this basis, the present data give reasonable projections of the aqueous diffusional coefficients. The deviation from linearity at low τ_{ads} is expected in terms of the time required to establish steady-state convection conditions[15]. Thus, it must be concluded that diffusion is rate-limiting for C_3H_8 adsorption.

We have not as yet proceeded to examine the true kinetics of the adsorption process. This is because of difficulties with maintaining a clean solution when using the rotating disk electrode. Impurities enter the cell via the rotating assembly and are, of course, brought up to the electrode by forced convection. Their effect is most marked under conditions of non-diffusional control for C_3H_8 adsorption. We regard an improvement of the solution purity as the sine qua non for such measurements.

4. Verification of the Anodic Galvanostatic Charging Procedure

A typical anodic galvanostatic charging curve in the presence of $C_3H_{8_{ads}}$ is shown in Fig. I.5. This may be divided into 5 principal regions: Part I, where mainly the reaction $H \rightarrow H^+ + e^-$ occurs; Part II, from ~ 0.4 v to ~ 1 v, where mainly double layer charging occurs; Parts III and IV, where the main processes are electrode oxidation and adsorbate oxidation; and Part V, where the electrode is still being oxidized, and where some charge is also being put into O_2-evolution. The method which we have used to evalute what we have called (Q_{anodic}^{total}) is indicated in the figure. It is necessary

Fig. I-5 Potential-time trace during typical anodic galvanostatic pulse (100-200mA/real-cm²) at 130°C

to make arbitrary choices about the end-points of the charging curve. This is a particular problem at the more anodic end of the transient, i.e. between Parts IV and V of the curve. Here, even in the absence of adsorbed C_3H_8, the transition to steady O_2-evolution is very gradual and the potential is not substantially constant until about 2.4 v vs. R.H.E. (at 100 - 200 mA/r · cm^2; the potentials are iR-free). The method we have used is indicated in Fig. I.5. During IV, the E - τ curve is straight and we arbitrarily choose a potential during region V which is 4 oscilloscope divisions past the point where this linearity finishes. A tangent to the E - τ curve at this potential is then projected to meet the continuation of part IV. This intersection point occurs at 1.95 $\pm$ 0.05 v. An alternative procedure would, for example, be to select the anodic of the linear region, IV. This would overlook the observation that IV has a different slope in presence and absence of $C_3H_{8_{ads}}$. implying that some oxidation of $C_3H_{8_{ads}}$ occurs after the end of IV. Some projection of the line of region IV is necessary to take account of this oxidation. The validity of the procedure used can, in part, be judged from the very excellent independence of our measured values of $Q_{ads}^{C_3H_8}$ on the anodic current density i_a, which we have reported earlier[1, 4].

Despite this independence of $Q_{ads}^{C_3H_8}$ on i_a, it must be recognized that the procedure used is arbitrary and, nearly as bad, it is rather imprecise. In carrying out the desorption experiments described in the following sections, it was necessary to develop a highly self-consistent and preferably accurate method of measuring relatively small values of $Q_{ads}^{C_3H_8}$. To illustrate the problem, we may note that $Q_{ads}^{C_3H_8}$ is determined as the difference between the two quantities $(Q_{anodic}^{total})^{C_3H_8}$ and $(Q_{anodic}^{total})^{N_2}$. The latter is perhaps 400 μcoul/r · cm^2 with a mean deviation of $\pm$ 3%, i.e. ~ 12 μcoul/cm^2. When $Q_{ads}^{C_3H_8}$ is only about 50 μcoul/r · cm^2 the total error that can be introduced is $\pm$ 12 $\pm$ 15 ($\pm$ 3% on 450 for $(Q_{anodic}^{total})^{C_3H_8}$). Thus, we may only be able to quote $Q_{ads}^{C_3H_8}$ as 50 $\pm$ 27

μcoul/r · cm^2. This difficulty is largely eliminated if, instead of following the procedure outlined in Fig. I.5, we merely project region IV to some arbitrary potential and measure the charge passed from 0.7 v to this potential (say 1.95 v). Then, the uncertainty of the values is less than 1% in (Q^{total}_{anodic}) and, for 50 μcoul/r · cm^2 of adsorbate, we do not have a greater imprecision than ~ 9 μcoul/r. cm^2. The absolute error in $Q^{C_3H_8}_{ads}$ will be larger than this if our arbitrary choice of end-point is wrong. Because of the variation in the slope of IV as τ_{ads} varies, it makes a significant difference which potential we choose for the end-point. The magnitude of this effect is such that, for example, terminating at 1.9 or 2.4 v, we get apparent values for $Q^{C_3H_8}_{ads}$ of 149 and 174 μcoul/r. cm^2 for 1 sec adsorption at 0.3 v and 130°C, and values of 347 and 406 μcoul/r. cm^2 for 10 sec of adsorption.

To help decide which potential to use as the end-point, we have used another method to obtain $Q^{C_3H_8}_{ads}$. Here we adsorb the C_3H_8 for various times as before, and then strip it potentiostatically. This we do by raising the potential of the electrode such that no C_3H_8 adsorption normally occurs. Then, the adsorbed C_3H_8 will be oxidized or desorbed. Such stripping can be done at 0.7 v and up[13-4]. The charge passed at the stripping potential is measured and, after correction for double-layer and electrode oxidation effects, a value of $Q^{C_3H_8}_{ads}$ is obtained which can be compared with the galvanostatic determination.

This method has a number of significant advantages over the galvanostatic method, and, also, a number of disadvantages. A <u>major advantage</u> is that the correction for electrode oxidation and double-layer charging is much smaller and can, in addition, be made with greater certainty. For example, the $(Q^{total}_{anodic})^{N_2}$ value to be subtracted from the $(Q^{total}_{anodic})^{C_3H_8}$ values to give $Q^{C_3H_8}_{ads}$, is about 400 μcoul/r. cm^2 in the galvanostatic method and only ~ 70 μcoul/r. cm^2 for a potentiostatic jump from 0.3 to 0.9 v. In practice, this means that the imprecision in

the correction is only ~ 1 μcoul/r . cm^2 for the potentiostatic step method as against 5 μcoul/r . cm^2 for the galvanostatic method. In addition, this correction can be made with greater certainty for, integrating the charge over relatively long times (e.g. ~ 1 sec), one is more certain that the electrode oxidation is at its steady state corresponding to that potential, as determined in absence of C_3H_8. On the other hand, the extent of electrode oxidation during the fast anodic galvanostatic pulse, determined as it is by the relative kinetics of a number of fast processes, is less likely to be exactly the same as in the absence of C_3H_8. This effect is obviously small here because of the above-mentioned non-dependence of $Q_{ads}^{C_3H_8}$ on i_a. A <u>disadvantage</u> of the potentiostatic method is that one does not have control over the time-scale of the processes which occur during stripping. The speed of galvanostatic stripping can easily be varied in order to eliminate charge contributions from diffusional processes (either impurity effects or, more important, effects from C_3H_8 diffusing up to the electrode and oxidizing). With the potentiostatic technique, the oxidative desorption occurs at its natural rate, which is typically relatively slow, since the stripping potential is kept low to minimize electrode oxidation, and diffusional or desorption effects can be quite significant. This problem can be eliminated by varying the speed of oxidative desorption by varying the stripping potential. If the computed values of $Q_{ads}^{C_3H_8}$ are independent of the stripping procedure there are no diffusion or desorption complications, or the errors therefrom have been satisfactorily eliminated. Another difficulty of the potentiostatic method is that charge from unwanted processes, e.g. H-atom oxidation, can also be included. For example in a potentiostatic step from 0.2 v to 0.9 v, some charge is passed corresponding to this process of H-atom oxidation. During the progress of C_3H_8 adsorption at 0.2 v some of the H-atoms adsorbed at 0.2 v are oxidized and are not, therefore, found subsequently in the stripping procedure. Clearly, the charges found potentiostatically must be corrected for the amount of H on the electrode at the lower potential. This correction may be made with a subsidiary set

of galvanostatic experiments to determine the amount of H on the electrode at the lower potential as a function of time of adsorption.

The simplest way to measure the stripping charge with a potential step is to record the current-time transient and to integrate the area under the curve, say with a planimeter. There are severe disadvantages with this method: - (1) The obtaining of charges is tedious and cannot be done readily during an experiment; this limits rapid feedback from the results into the experiment. (2) The currents to be measured, particularly towards the end of the stripping, are small and require high sensitivity on the cathode-ray oscilloscope with consequent interference from noise. (3) When the potential is stepped, a large (~ 350 ma) capacity current flows. This overdrives the oscilloscope amplifier, particularly if it is set up to read the small currents towards the end of the stripping. We have found that Tektronix oscilloscopes will not tolerate more than 100% of full-scale vertical overdriving. If such overdriving is allowed, the oscilloscope zero changes and it slowly reverts back to its original position. This effect can lead to errors of the order of several hundred percent in the present circumstances but, usually, gives rise to errors of the order of 10%. This effect is not very reproducible since the zero "drift" after overdrive is, itself, not quantitatively very reproducible. To overcome this problem, we are building an active voltage limiter, i.e. a device which, when interposed between the signal and the oscilloscope, will not allow more than a specified voltage (e.g. 100% of full-scale) to be applied to the Y-plates. In the meanwhile, we have adopted an alternative technique which overcomes all the defects of this method. The current is passed through a resistor, as before, inserted in the counter electrode path, and is integrated electronically. The voltage output of the integrator (proportional to charge) is displayed on the oscilloscope and gives an instantaneous charge-time relation with much the same directness as a galvanostatic chronopotentiogram. Ideally, both the current and the charge would be displayed side by side with a dual beam oscilloscope and this we will be able to do with the voltage limiter.

The circuit is shown in Fig. I.6. The potential drop across the sampling resistor R is fed to the input of the first of two Philbrick P25AH differential amplifiers. This amplifier converts the differential signal across the resistor to a single-ended output, which is the more convenient to integrate. Integration is effected with the second amplifier. A closed relay is connected across R and is opened with a trigger pulse from the potential step generator when it is desired to begin the integration. Under favorable circumstances, signals of duration from 10^{-5} sec to several minutes may be integrated, with an accuracy better than that of the oscilloscope.

In Fig. I.7, a comparison is made between the galvanostatic method and the potential step method. These data refer to the adsorption of C_3H_8 at 0.3 v and 130°C. The galvanostatic charge was computed using 1.9 v as the end-point at the anodic end. This potential is within the range found for the end-point we have used previously (as described in Fig. I.5) and was the most appropriate for the given experiment. Our belief is that the most conservative general practice in this system is to use 1.95 v as the end-point if the galvanostatic method is being used alone. The difference between using 1.9 v and 1.95 v is about 2% of $Q_{ads}^{C_3H_8}$ and this is certainly no worse than the repeatability of the measurements between different experiments. The line in the figure is drawn through the origin with a slope of unity. If the two methods do in fact measure the same quantity we expect random scatter about this line. As can be seen, the agreement between potential step and galvanostatic stripping is excellent over a wide range of adsorbate concentration. Values for the potential step procedure are shown with steps to 0.9 and 1.1 v, integrating charge at these potentials for 1 sec and 0.8 sec, respectively. Anodic galvanostatic charging from these potentials (however you determine the anodic end-point) shows that the electrode is completely clean after these times. The excellent agreement between the results for the two potential steps confirms that no non-faradaic desorption of $C_3H_{8_{ads}}$ is occurring and that the charge measured is an accurate estimate of $Q_{ads}^{C_3H_8}$.

CHARGE FOUND IN POTENTIOSTATIC STRIPPING (...) 100 200 300

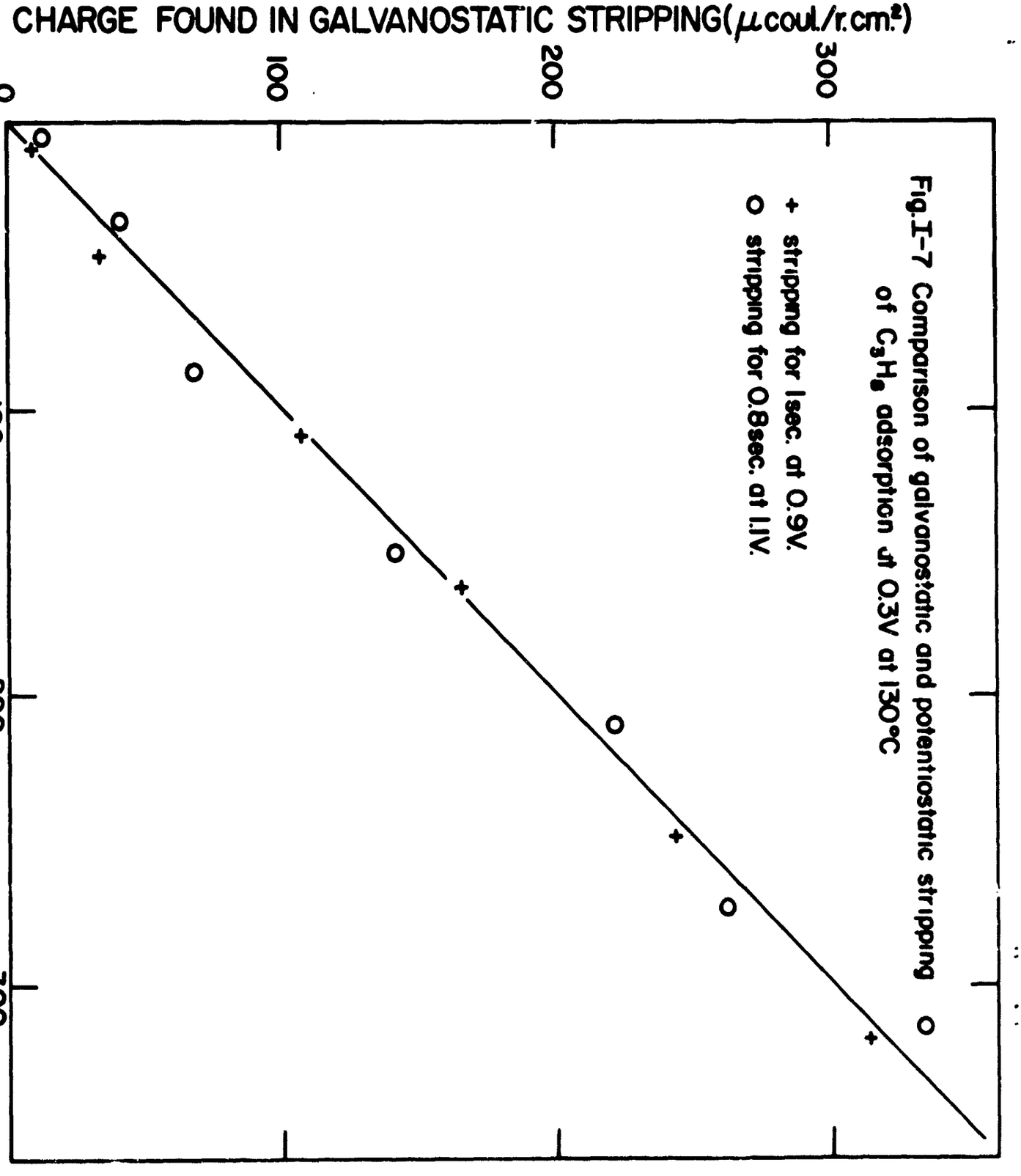

Fig.I-7 Comparison of galvanostatic and potentiostatic stripping of C_3H_8 adsorption at 0.3V at 130°C

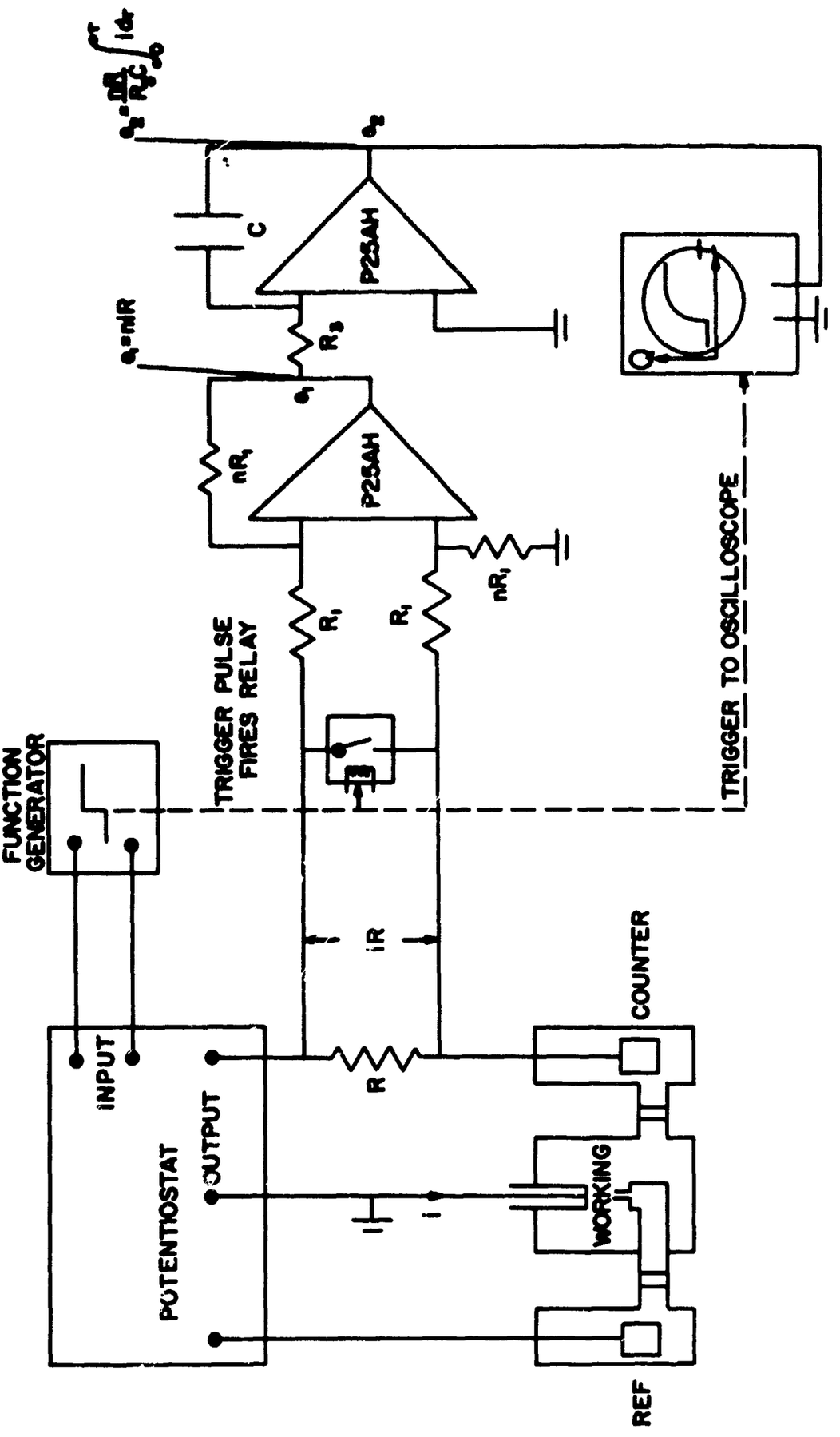

Fig.I-6 Electronic circuit for integration of charge passed after a potentiostatic step pulse

These experiments show conclusively that the procedure we have used previously, which is equivalent to, although not as precise as, choosing 1.95 v as the anodic end-point, gives an accurate estimate of $Q_{ads}^{C_3H_8}$.

5. Adsorption of C_3H_8 as a Function of Temperature and Potential

In Figs. I.8 and I.9, we present our most complete data for the limiting adsorption of C_3H_8 as a function of potential and temperature. The results at the higher temperatures (130° and 140°C) are experimentally indistinguishable from those found at lower temperatures and this is a revision of some of the data presented in our last report where it appeared that adsorption at 130°C is less than at 80° and 110°C. A comparison of the anodic and cathodic data to give [e] the average number of electrons involved in the high potential oxidation of the adsorbate per Pt atom that it covers, is shown in Fig. I.10. Concerning the reproducibility of this data, we may say that with the exception of occasional experiments, where we have found large discrepancies, the limiting $Q_{ads}^{C_3H_8}$ values may be repeated from experiment to experiment to $\pm$ 10% or $\pm$ 20 μcoul/r.cm^2, whichever is the lesser. The θ_H^t values for limiting adsorption (i.e. at "infinite" time) are repeatable to about $\pm$ 15%. Scatter on the [e] values is thus about $\pm$ 25% and we believe that in the region from 0.3 v up, we can quote [e] as 2.5 $\pm$ 0.6 electrons per covered Pt surface site. Any variation in [e] with E in this region is concealed by this scatter.

We may summarize the following conclusions from the steady-state adsorption-potential-temperature relations:

1. To within $\pm$ 10% or $\pm$ 20 μcoul/r.cm^2, whichever is the lesser, the adsorption at a given potential against the reversible hydrogen electrode is independent of temperature.

2. Similarly the number of adsorbed C atoms and their average state of oxidation, are independent of temperature.

3. Adsorption, as measured anodically, is highest at ~ 0.2 v vs. R.H.E., but cathodic measurements show a much broader range of high adsorption, from about 0.2 v to ~ 0.35 v.

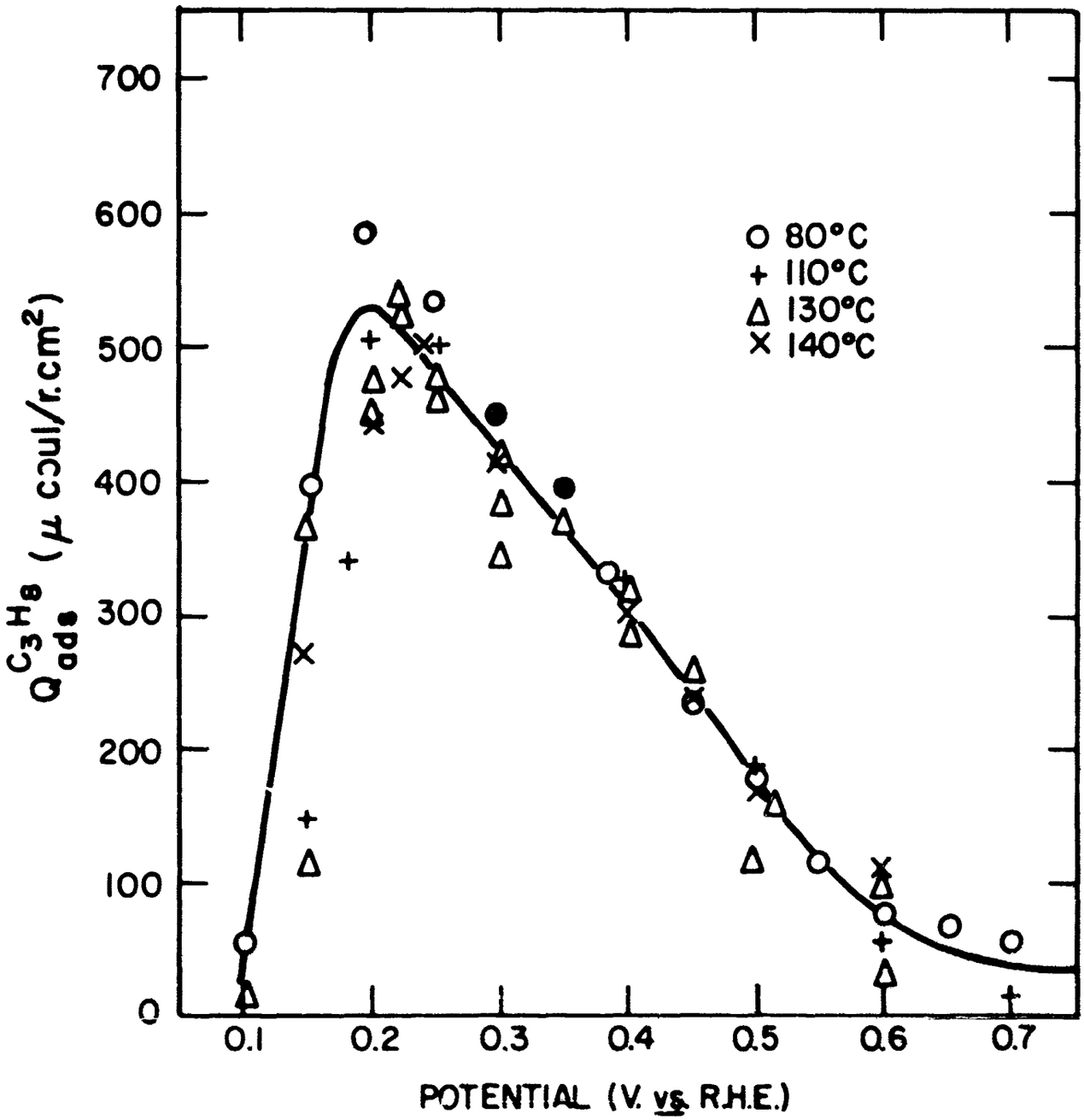

Fig. 1-8, Propane adsorption as a function of potential and temperature

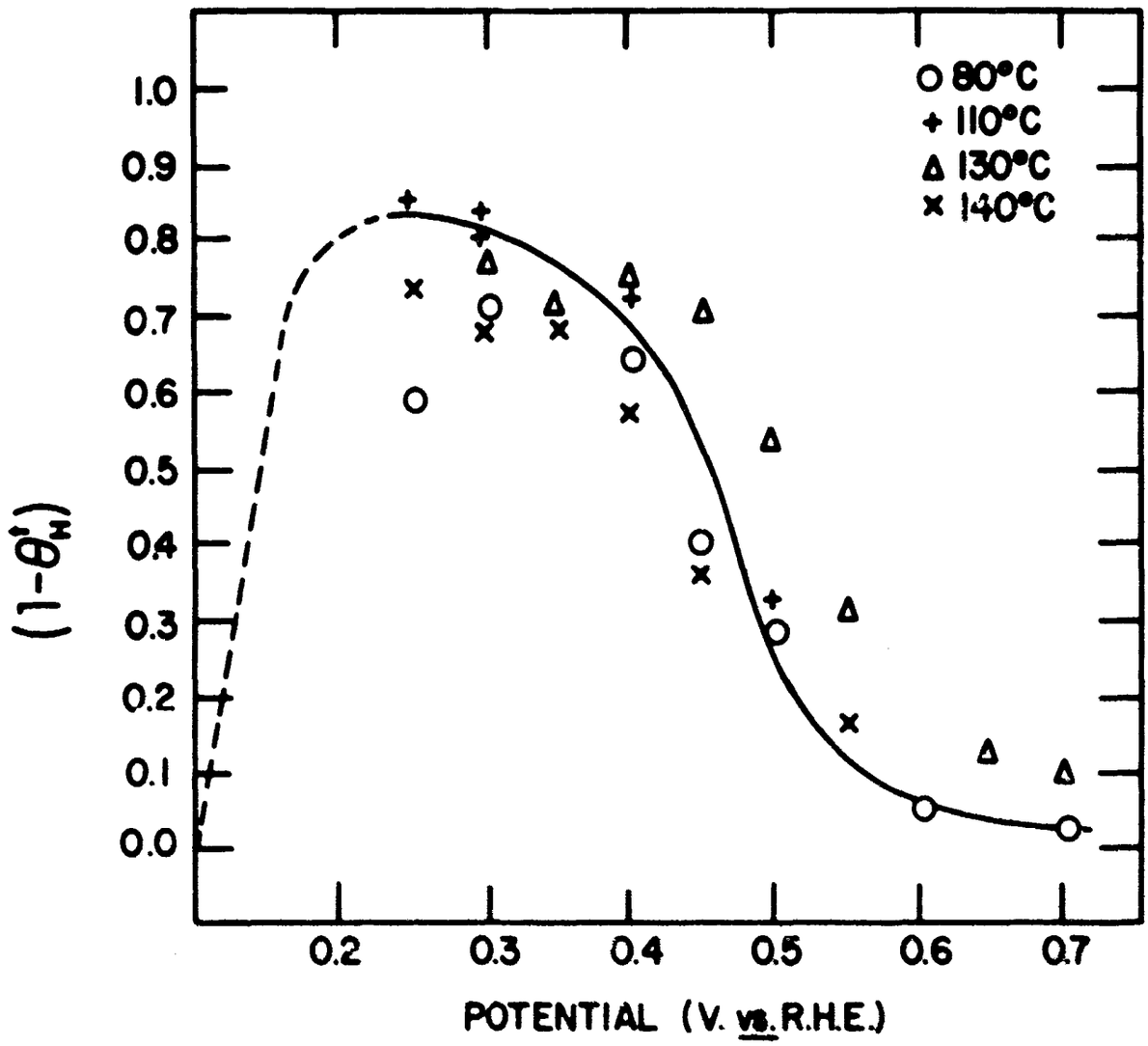

Fig. I-9 Coverage of Pt with irreversibly adsorbed material as a function of potential and temperature.

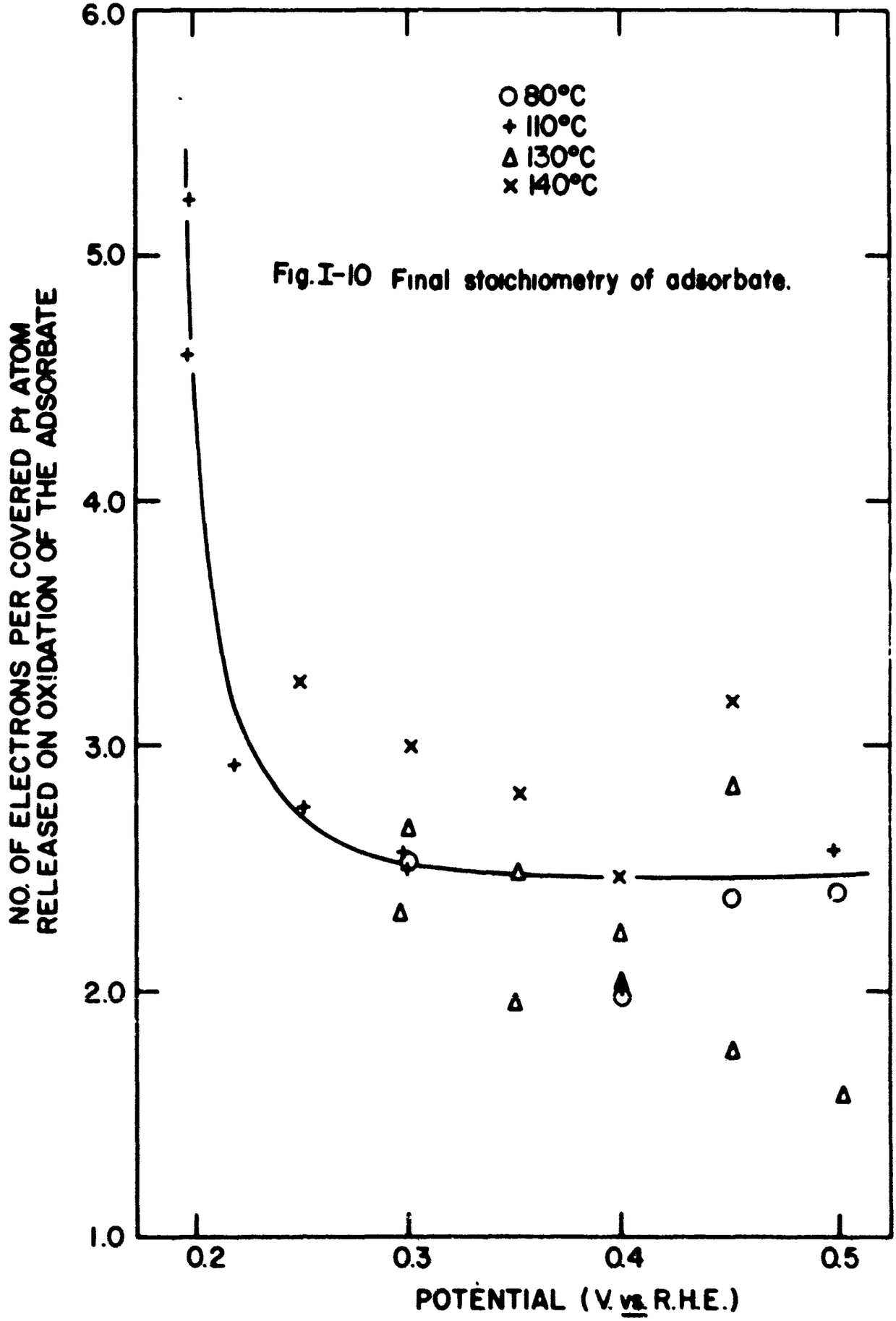

Fig. I-10 Final stoichiometry of adsorbate.

4. The anodic charges indicate that considerably less than a monolayer of C_3H_8 is adsorbed. Cathodic measurements show, rather, that a considerable fraction of a monolayer of organic material is adsorbed whose oxidation state is higher than that of C_3H_8 itself. The description of the properties of this material has been the object of the experiments described in the two sections that follow.

6. Studies of Adsorbed C_3H_8 Residues by Anodic Desorption

In our last report[2], we gave the results of some preliminary experiments designed to examine, with greater sensitivity than is possible with the techniques typified by Fig. I.10, the structure of the finally-adsorbed residues. The preliminary observation, then was that there are qualitative differences in the properties of the adsorbate, depending on the potential at which it is formed. (This discussion refers to the region from 0.3 v up, where Fig. I.10 would suggest that the residue is essentially the same independent of temperature and potential.) These measurements have been extended and confirm the initial finding that there is a qualitative difference in the adsorbate as we change the potential of adsorption. They show, in addition, a small variation of the properties of the adsorbate with temperature. The main effect is that at higher temperatures for a given potential the adsorbate is somewhat more highly oxidized.

The basic notion of the experiment we have used is to adsorb the residue until it is at its steady state surface concentration and then to desorb it. During desorption, we follow changes in the surface concentration of the adsorbate ($1 - \theta_H^r$) and in the charge to oxidize it ($Q_{ads}^{C_3H_8}$) and this procedure, as will be seen, gives very detailed information on the structure of the adsorbate. This experiment is similar in concept to the studies of θ_H^r and $Q_{ads}^{C_3H_8}$ during adsorption, which we have reported[1, 2] and which themselves say a great deal about the disposition on the electrode surface of the adsorbed C atoms. In the desorption experiment we seek to examine the reactivities of these adsorbed C atoms in their final condition. When there are variations in reactivity during

the progress of desorption, we have prima facie evidence for different adsorbed species or at least for different modes of bonding. The desorption potential has been chosen as 0.7 v vs. R.H.E. This is a compromise between the normal absence of adsorbed C_3H_8, on the one hand, and of electrode oxidation on the other[2]. Also, the rate of desorption is convenient at this potential. Most of these experiments have been carried out at 130°C, but some data taken at 110°C are also reported.

Fig. I.11 shows the desorption of material adsorbed at 0.3 v at 130°C. Data for 30 and 100 sec of adsorption seem to be superposable. This would be expected from the observations that after 30 sec at 0.3 v, the anodic charge (Fig. I.16) and the cathodic charge[2, 4] have both become constant, implying steady state for the adsorbate. We find that desorption is virtually complete after about 1 sec at 0.7 v and that the $Q_{ads}^{C_3H_8}$ vs. $(1 - \theta_H^t)$ curve, during desorption, seems to have two linear regions. The slopes of these linear regions correspond to ~ 1.35 electrons and ~ 7 electrons per covered Pt atom for the oxidation (to CO_2) of the adsorbate. Since we believe that each $C_3H_{8_{ads}}$ occupies three surface sites at 0.3 v[1-4], we infer that these [e] values refer directly to adsorbed C atoms. As indicated by the arrow in Fig. I.11, desorption proceeds from the right to the left of the figure. The easiest material to be desorbed, i.e. the first material to be desorbed, is then the material for which [e] is ~ 1.35. The hardest to oxidize to CO_2 is the material for which [e] is ~ 7. In the terminology of ref. (4), these are referred to as residues (B) and (C) respectively - we will use this nomenclature in the present discussion although we specifically reserve judgment at this juncture as to whether (B) and (C) (and later, (A)) are separate adsorbed species as such. We will for simplicity, however, refer to them as species. Then the easiest of the adsorbed residues to oxidize to CO_2 is the one most highly oxidized during adsorption, (B). We have invariably found that this is the case for adsorbed C_3H_8. This means that (C) cannot be an intermediate between C_3H_8 and (B) and that the C_3H_8 to (C) reaction is a parallel path to the C_3H_8 to (B) reaction.

Fig.I-11 Desorption at 0.7V of material adsorbed for various times at 0.3V and 130°C

At 0.32 v (Fig. I.12), the results are rather similar to 0.30 v but at 0.35 v (Fig. I.13) there is a marked change. Some species akin to (C) still manifests at the extreme end of desorption but instead of (B) we find a slope of ~ 1.75 electrons/covered Pt for the more highly oxidized part of the adsorbate. We will call this "species" residue (A). At 0.4 v (Fig. I.14) we only find residue (A) (slope 1.8 electrons/covered Pt atom).

Before we discuss the 130°C data in detail it is interesting to examine data at 110°C (Fig. I.15). Data at 0.3 v are comparable to those at 130°C showing two slopes equivalent to ~ 1.3 and 6 electrons respectively. The only real difference is that at 110°C the more highly reduced species (C) occupies more of the surface. At 0.4 v similar remarks apply; (A) is found but now we detect something akin to (C) also. The effect of raising the temperature is, then, to restrict the appearance of (C), the most reduced form of the adsorbate. In this sense the adsorbate is more highly oxidized at higher temperatures, although the same "species" are present on the electrode.

The first question we must ask about (A), (B), and (C) is whether they are necessarily to be regarded as separate "species" per se. In this connection we will refer to variations in oxidative reactivity of adsorbed C atoms in terms of different "species" although they could arise from different structural groups on a larger adsorbed "molecule". A simple way in which a single adsorbed species could appear, for example, at 0.3 v to be more than one species during its desorption would be if it could undergo more than one oxidative reaction. For example consider the species X originally solely present at 0.3v. It could perhaps undergo the following reactions (written per site):

$$X_{ads} - ne^- \xrightarrow{k_1} Y_{ads}, \text{ rate} = r_1, \tag{I.5}$$

$$Y_{ads} - me^- \xrightarrow{k_2} CO_2, \text{ rate} = r_2. \tag{I.6}$$

Fig.I-13 Desorption at 0.7V of material adsorbed for 60sec. at 0.35V and 130°C

Fig.I-12 Desorption at 0.7V of material adsorbed for 100sec. at 0.32V and 130°C

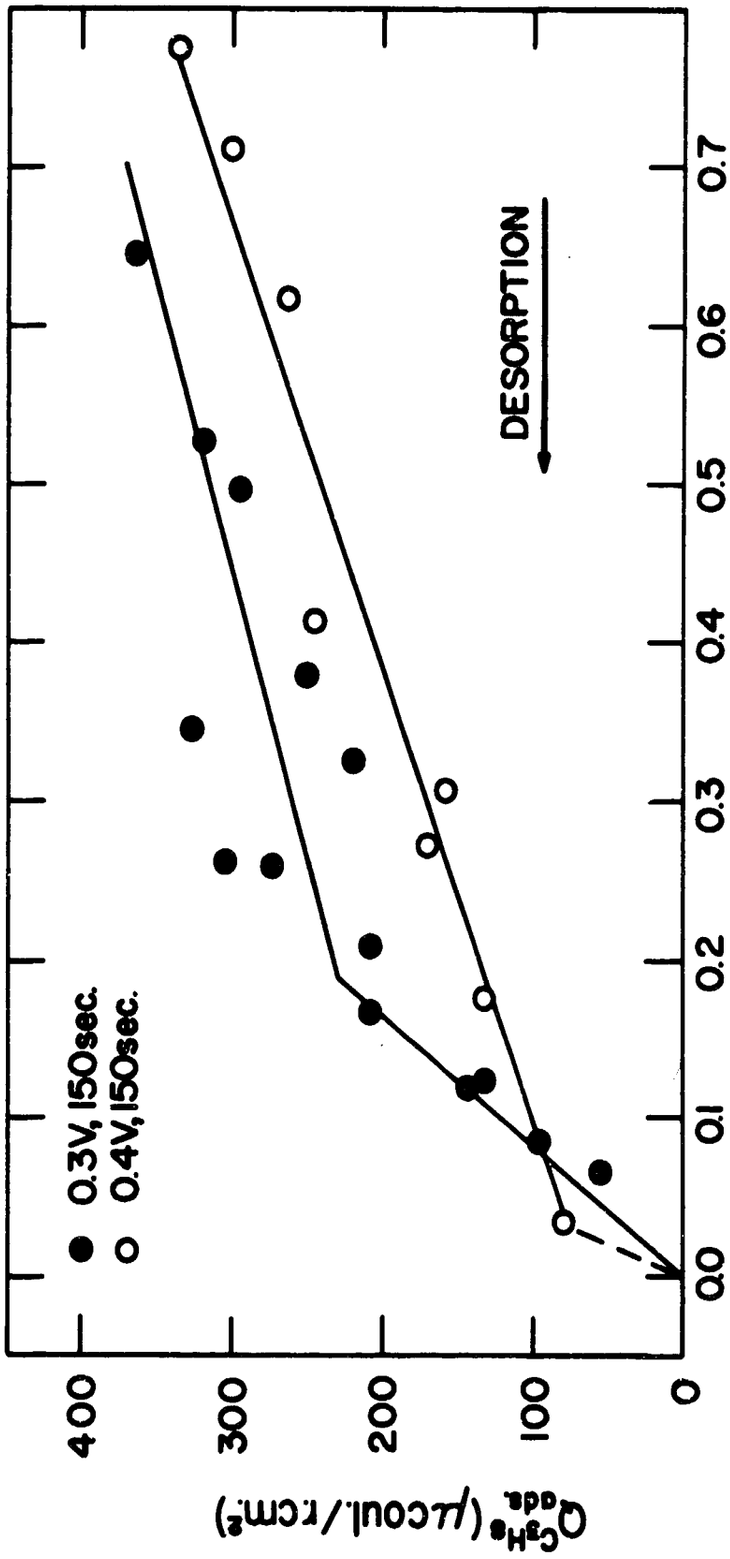

Fig. I-15 Desorption at 0.7V of material adsorbed at 110°C

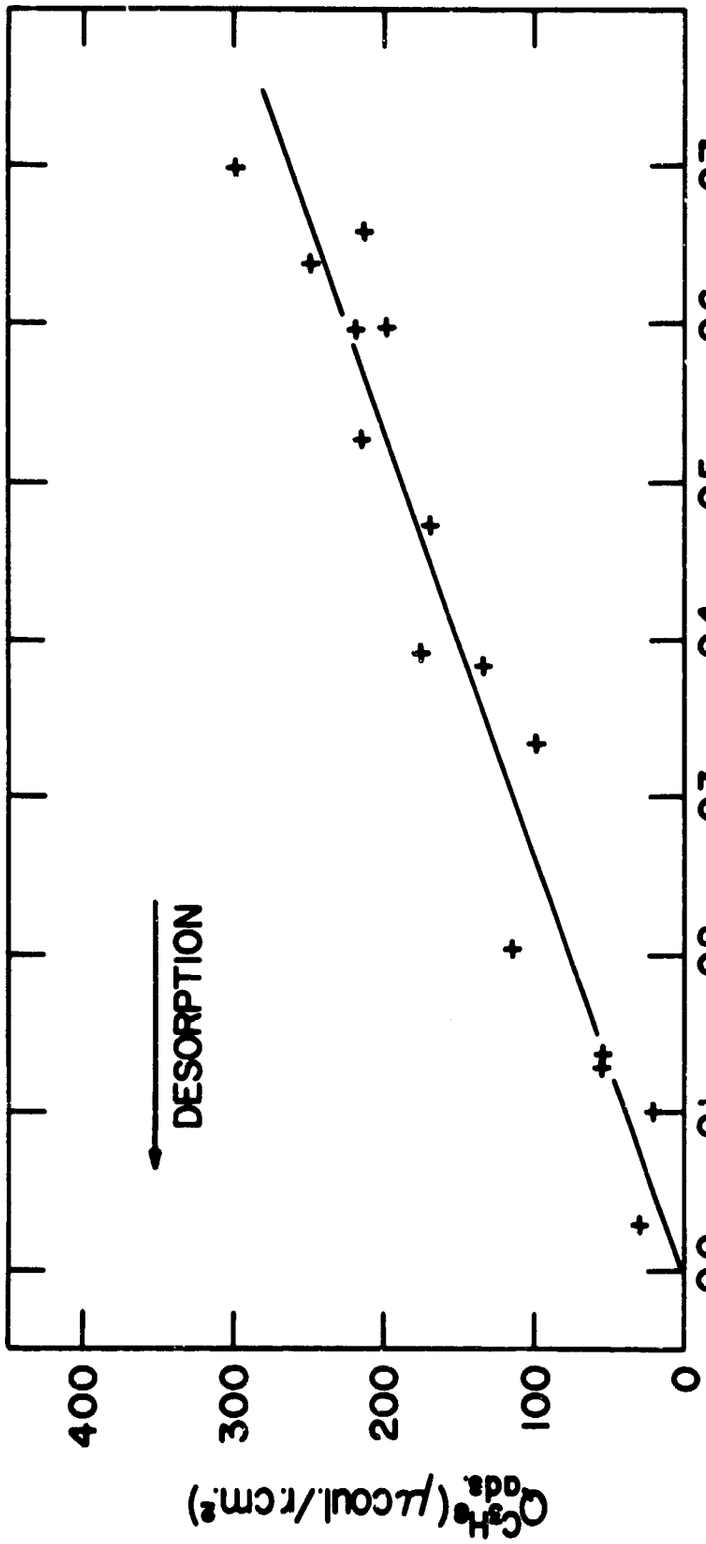

Fig. I-14 Desorption at 0.7V of material adsorbed for 60sec. at 0.4V and 130°C

and

$$X_{ads} - (m+n)\, e^- \xrightarrow{k_3} CO_2, \text{ rate} = r_3 . \qquad (I.7)$$

Then, the observed value of [e] would be given by

$$[e]_{obs} = [e]_X \left(\frac{r_1 + r_3}{r_2 + r_3} \right) + [e]_Y \left(\frac{r_2 - r_1}{r_2 + r_3} \right) . \qquad (I.8)$$

If $r_1 \to 0$ (so that $\theta_Y \to 0$ and, hence, $r_2 \to 0$), $[e]_{obs}$ tends to its correct value of $[e]_X$. Similarly, if $r_1 = r_2$, we find $[e]_X$. If these conditions do not obtain, as in general they would not, $[e]_{obs} \neq [e]_X$. Since reactions (I.5) - (I.7) are potential dependent, we would expect $[e]_{obs}$ to depend on the desorption potential and on the time of desorption. Our tentative conclusion is that there is no such dependence. However, extremely sensitive measurements would be necessary to find this effect if it existed.

A number of powerful inferential arguments can be advanced to suggest that at 0.3 v there must be at least two surface species and that the complication described above is substantially absent. If this were not so, we would have to equate X with (C) (or with something rather similar to (C). The difficulty with such an assumption is that the adsorbate occupies $\sim$ 0.7 of the surface and has an oxidation state such that the average value of [e] for the removal of all of it is $\sim$ 2 (Figs. I.10 and I.11). But (C) is so highly reduced that if it occupied as much as 0.7 of the surface it would raise $Q_{ads}^{C_3H_8}$ to about 5 times the value actually observed. Similarly, (B) could not be X because it just does not have enough electrons per site to give a signal for (C). We cannot on the basis of these arguments exclude the possibility that due to some overlapping of the oxidations of (B) and (C) the values of $[e]_B$ and $[e]_C$ are wrong. Specifically, the true value of $[e]_B$ might be lower than the 1.35 given by Fig. I.11.

Additional arguments which suggest that at 0.3 v we have at least two adsorbed species, substantially without the kind of complication represented by reactions (I.5 - 1.7), may be made from the data for 0.32 v at 130° and 0.30 v at 110°C. Here, differing amounts of (C) are found in the presence of (B) and this supports the notion that there must be two species, since the kinetic relations which would apparently give (B) should vary considerably with θ_C and T.

We now consider whether (B) and (C), together, could react so as to give a false signal for (A) at 0.4 v. Considering adsorbed species (B) and (C) and assuming that they both oxidize to CO_2 at 0.7 v, contemporaneously, as in (I.6) and (I.7), we could write

$$[e]_{obs} = [e]_B \left(\frac{r_2}{r_2 + r_3}\right) + [e]_C \left(\frac{r_3}{r_2 + r_3}\right) \quad . \tag{I.9}$$

Assuming Langmuir adsorption for (B) and (C), we may write

$$r_2 = - \frac{d\,\theta_B}{d\,\tau} = k_2\,\theta_B, \tag{I.10}$$

and

$$r_3 = - \frac{d\,\theta_C}{d\,\tau} = k_3\,\theta_C. \tag{I.11}$$

Then,

$$\theta_B = \theta_B^\circ \exp - k_2\tau,$$

and,

$$\theta_C = \theta_C^\circ \exp - k_3\tau, \tag{I.13}$$

where θ_B° and θ_C° are the initial values of θ_B and θ_C before any desorption occurs. Then, we can transform (I.9):

$$[e]_{obs} = \frac{[e]_B + [e]_C\, f(\tau)}{1 + f(\tau)} \tag{I.14}$$

where

$$f(\tau) = \frac{k_3\,\theta_C^\circ}{k_2\,\theta_B^\circ}\ \exp\ -\ (k_3 - k_2)\,\tau. \qquad \text{(I. 15)}$$

The observed value of [e] would then be a function of τ (time of desorption) unless $k_2 = k_3$. In fact at 0.4 v we observe that [e] is constant right across the $(1 - \theta_H^t)$ axis, which would argue against the possibility of (B) and (C) contriving to give a spurious signal for the species (A). However, we cannot rule out the possibility that a small amount of (C), oxidizing approximately contemporaneously with (B), would lead to the appearance of (A). The arguments against this are: (1) At 0.3 v, (B) and (C) react essentially separately, as discussed above. The relationship required between k_2 and k_3 to give (A) would be dependent only on the desorption potential (0.7 v) and not on the adsorption potential (0.3 v vs. 0.4 v). If (B) and (C) contrived to give (A) from 0.4 v they should also do so at 0.3 v. (2) Different relative concentrations of (B) and (C) do not lead to the appearance of (A) (cf. Figs. I.12 and I.15). (3) Under some conditions we appear to find both (C) and (A) (cf. Figs. I.13 and I.15).

The final conclusion must then be that (A) could not arise as the result of the interaction of the oxidation kinetics of (B) and (C). It is not excluded, however, that a small quantity of some other adsorbed species (especially if it is highly reduced) could alter the observed value of $[e]_A$ (1.8 electrons) or, for that matter, also, the observed values of $[e]_B$ and $[e]_C$. We will present some evidence in the next section that, in fact, this does occur and we will postpone discussion of the possible identity of the various species until then. We will note in passing that the presence of (A), which is more highly reduced, in preference to (B) at the more anodic adsorption potential is anomalous.

7. Studies of Adsorbed-C_3H_8 Residues by Cathodic Desorption

We will now discuss some cathodic desorption experiments which help to resolve some of the questions raised in the last section. The basic notion of the experiment is to adsorb, as usual, at fixed potential and then

to desorb by lowering the potential such that adsorption does not usually occur. From Fig. I. 8, we can see that 0. 1 v and below would be a reasonable potential region to choose for this purpose. To avoid H_2-evolution we have not gone below 0. 03 v and, in fact, most of our experiments were done at 0. 06 v. Some of the adsorbate is removed at the cathodic desorption potential and is not available for subsequent oxidation. We can also study changes in θ_H^t after desorption. In this way, we obtain a different kind of information about the adsorbed residues which, in conjunction with the previous measurements, allows a more complete description of the residues adsorbed on Pt in C_3H_8-saturated solution.

Initial experiments showed that cathodic desorption is complete in less than 1 sec, the actual rate being higher at lower potentials. The extent of desorption was not a sensitive function of the potential of desorption, at least not in the range 0. 03 v to 0. 1 v. Extensive measurements on this point were only possible, when these experiments were performed, for long times of adsorption when a considerable quantity of adsorbate is present. This was because of the rather imprecise technique previously used for determining (Q_{anodic}^{total}) (cf. Fig. I. 5). With the techniques which we have developed recently, (sec. 4) it should be possible to verify this point for short times of adsorption. For this reason we have omitted values of the charge for the residue where the scatter was unsatisfactorily large. The values of $Q_{ads}^{C_3H_8}$, after desorption at 0. 06 v, become constant for $\tau_{0.06} \geq \sim 0.6$ sec (this is known only for long times of adsorption e. g. $\geq$ 10 sec) and do not change up to 100 sec of desorption (the longest time investigated). Thus the adsorbate consists of two parts, one of which is relatively easy to desorb cathodically and one which cannot be desorbed readily. In the adsorption range 0. 2 - 0. 4 v (at 130°C) these two types of adsorbate are always found. In Figs. I. 16 - I. 18 we show the variation of $Q_{ads}^{C_3H_8}$, Q_{res} (the charge to oxidize the nondesorbed residue), Q_{des} ($Q_{ads}^{C_3H_8} - Q_{res}$) and θ'_{res} ($Q_{res}/Q_{ads}^{C_3H_8}$) with $\tau_{ads}^{\frac{1}{2}}$ at 130°C. The general observation is that Q_{res} and θ'_{res} increase with τ_{ads} at each

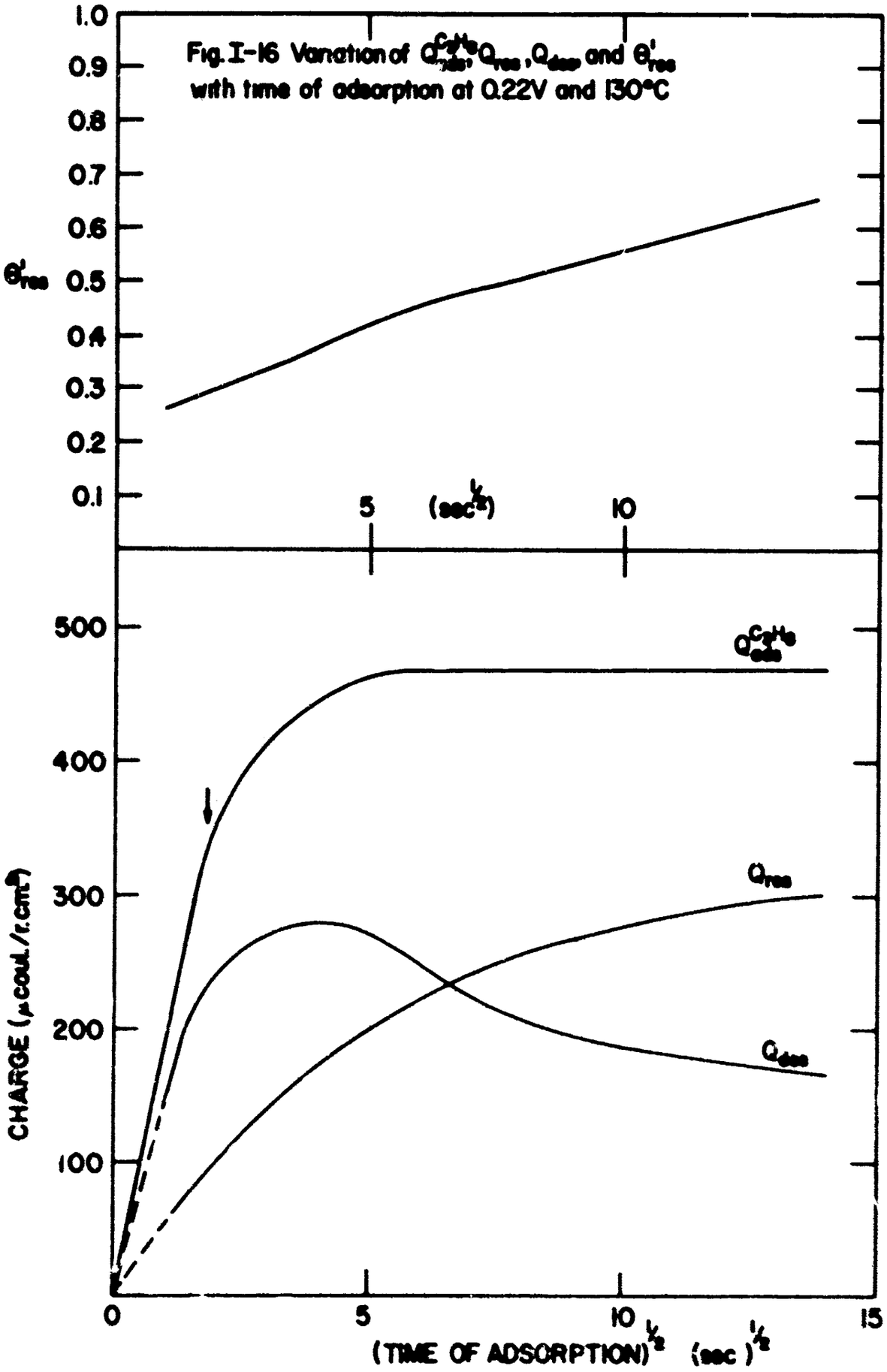
Fig. I-16 Variation of $Q^{C_2H_6}_{ads}$, Q_{rev}, Q_{dep} and θ'_{rev} with time of adsorption at 0.22V and 130°C
θ'_{rev}
1.0
0.9
0.8
0.7
0.6
0.5
0.4
0.3
0.2
0.1
5
$(sec^{1/2})$
10
500
400
300
200
100
CHARGE (μcoul./r.cm^2)
$Q^{C_2H_6}_{ads}$
Q_{rev}
Q_{dep}
0
5
10
15
(TIME OF ADSORPTION)$^{1/2}$ $(sec)^{1/2}$

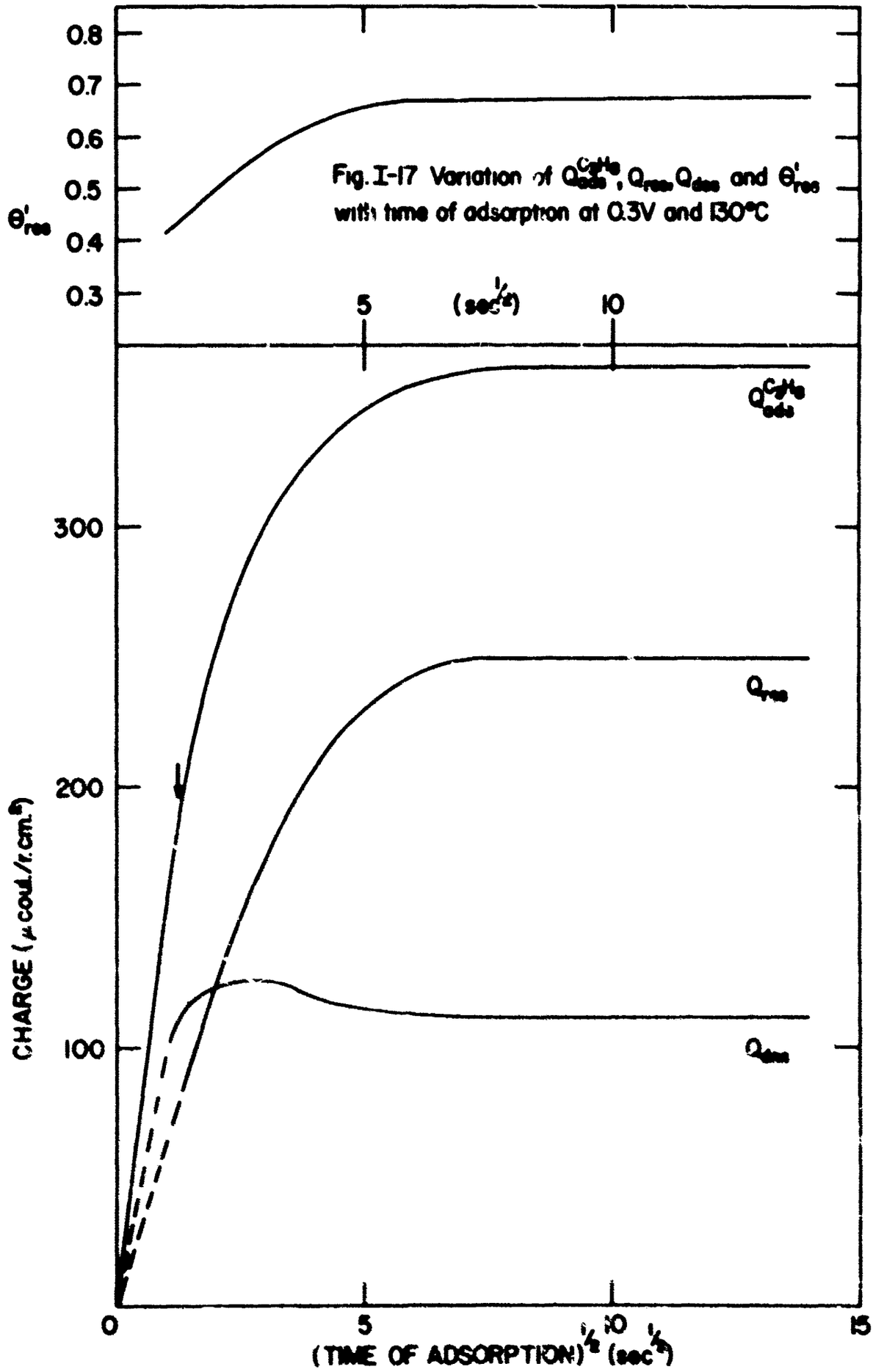

Fig. I-17 Variation of $Q^{C_3H_8}_{ads}$, Q_{rec}, Q_{des} and θ'_{rec} with time of adsorption at 0.3V and 130°C

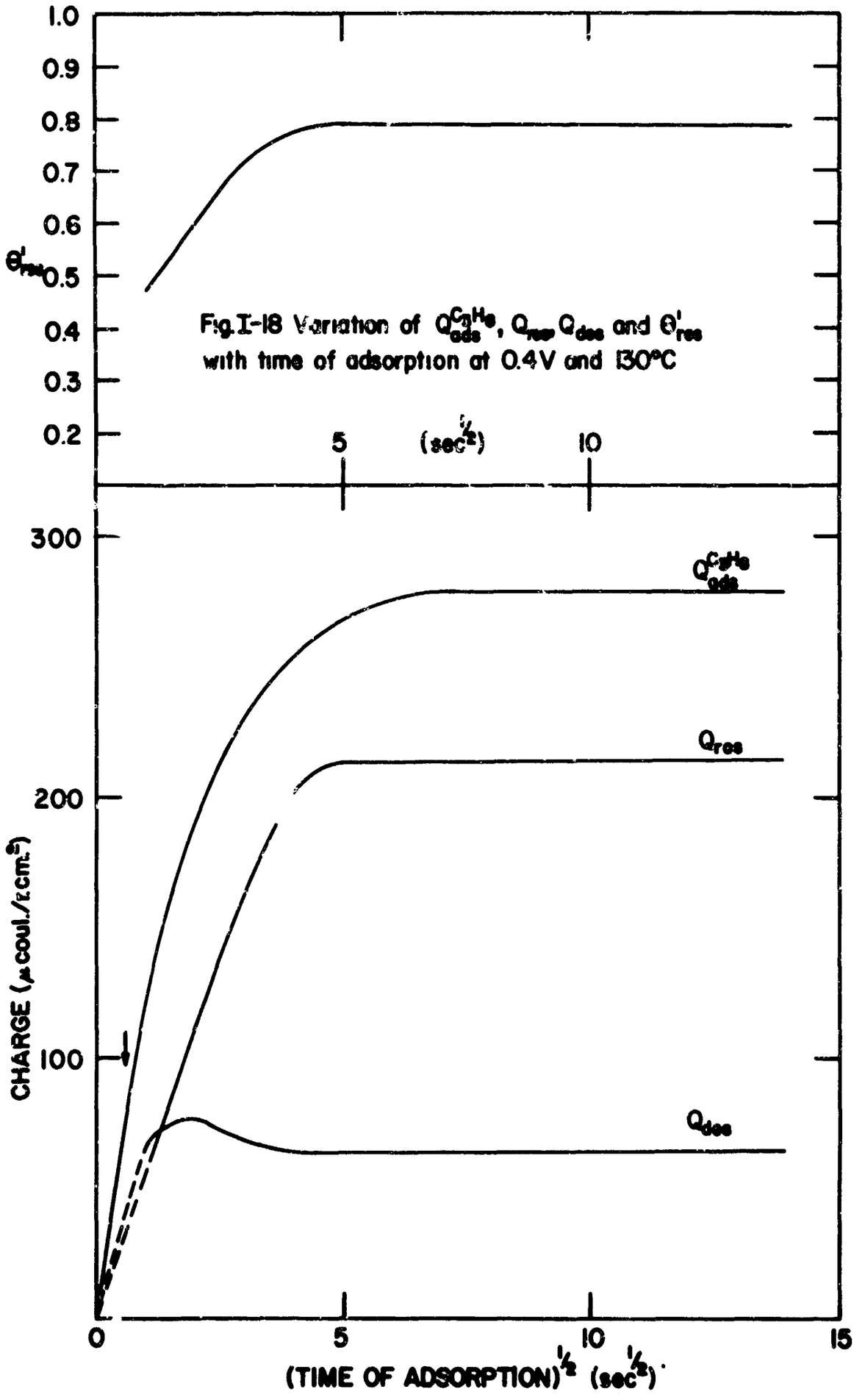

Fig.I-18 Variation of $Q^{C_3H_8}_{ads}$, Q_{res} Q_{des} and θ'_{res} with time of adsorption at 0.4V and 130°C

potential. Eventually at long τ_{ads}, $Q_{ads}^{C_3H_8}$, Q_{res} and θ'_{res} become constant. The observation that θ'_{res} increases with τ_{ads}, and more rapidly at the more anodic potentials, suggests that the non-cathodically desorbable material.

These results raise a difficulty for the initial adsorption region in which it is clear that diffusionally controlled adsorption is occurring. The explicit assumption in our analysis of this region (see section 3 and references (1-4)) is that the material which is adsorbed is not too dissimilar from C_3H_8 itself. This assumption is involved in the value we choose for n in equation (I. 4) and in consideration of the semi-infinite linear diffusion model. The values of $D^{C_3H_8}$ which have been obtained would approximately substantiate the value chosen for n, particularly as n appears in the expressions for $D^{C_3H_8}$ raised to a power greater than one. How then can it be that part of the C_3H_8 is cathodically desorbable while some of it is not desorbable? This implies that there is more than just the single species we have assumed during the initial stages of the adsorption process. It would be required that the two (or more) species suggested by these measurements be both not very dissimilar from C_3H_8 itself and that their proportions are constant, independent of the potential of adsorption. The latter is necessary if we are to see similar $Q_{ads}^{C_3H_8}$ vs. $\tau_{ads}^{\frac{1}{2}}$ line at each potential, for short τ_{ads}, which we do.

It is of interest to examine the extent of this cathodic desorption, as measured by the hydrogen charging method, since we have noted previously that anodic and cathodic charging are not always equivalent. The variation of θ_H^t with time of adsorption at 0.3 v, with and without the cathodic desorption step, is shown in Fig. I. 19. Within the precision of the measurement, θ_H^t is apparently not affected by the interposition of the cathodic desorption step. Other experiments (cf., for example, Fig. I. 21) confirm that $(1-\theta_H^t)$ is, if anything, lowered only slightly by the cathodic desorption step. There is however a remarkable change in shape of the H-charging curve as the result of the cathodic desorption step. This is illustrated in Fig. I. 20. Thus, while θ_H^t is hardly changed when we

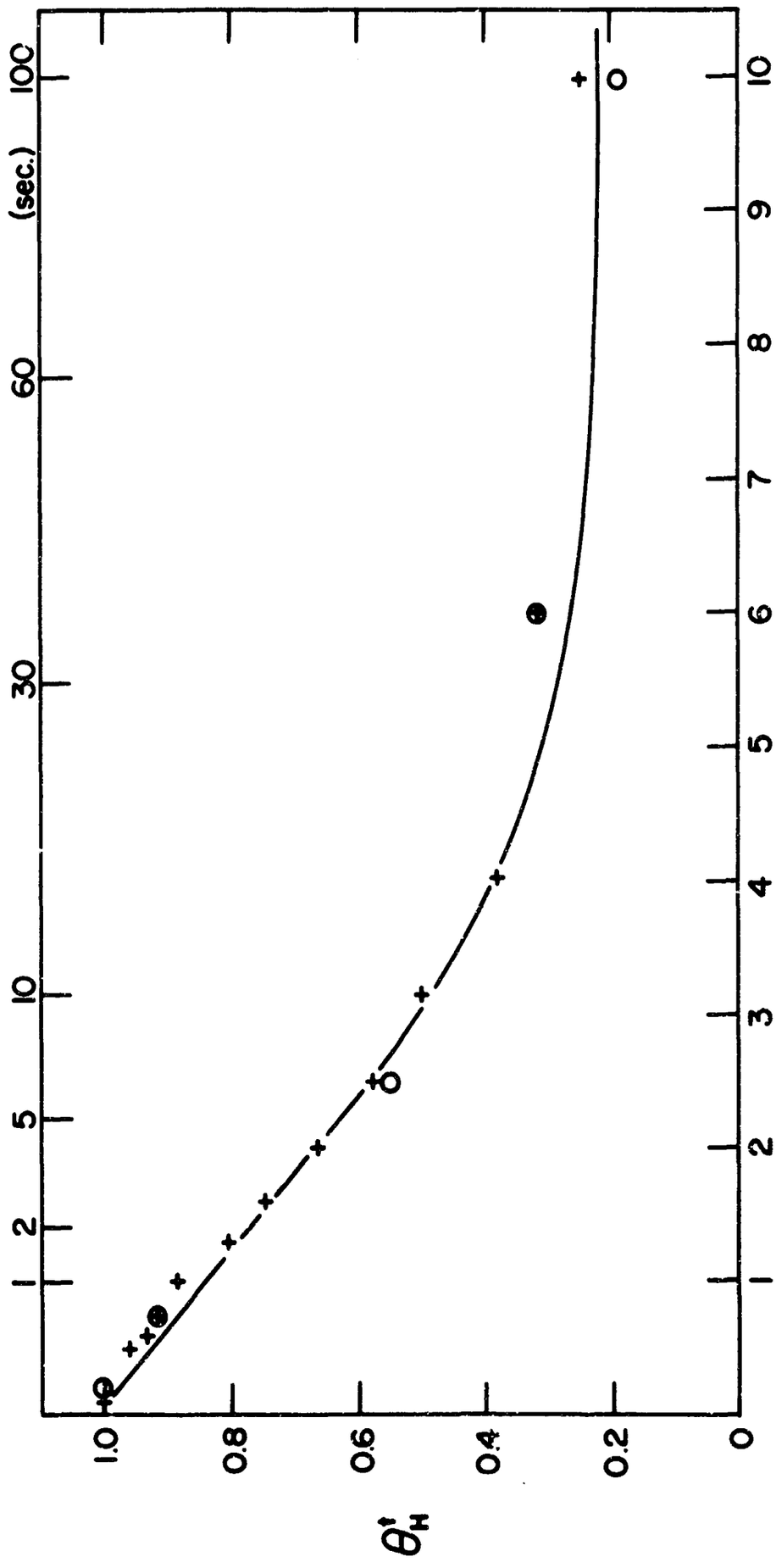

Fig.I-19 Variation of θ'_H with $\tau^{1/2}_{ads.}$ at 0.3V and 130°C with, +, and without, O, cathodic desorption (0.06V for 10sec.)

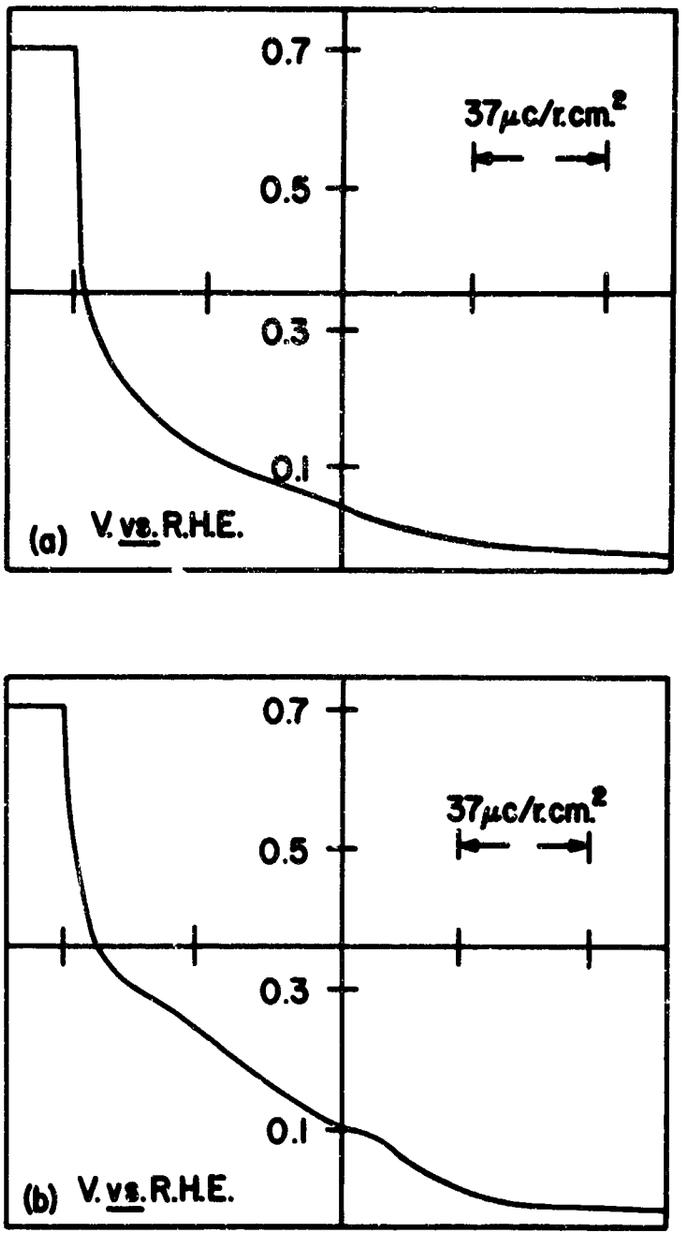

Fig. I-20 Hydrogen charging curves taken at 187mA/r.cm.^{2} after allowing adsorption for 6.3sec. at 0.3V and 130°C. (a) taken directly, (b) taken after cathodic desorption at 0.06V (10sec.). Notice the restoration of the "kinky" character of the H-charging curve in (b).

interpose the step at 0.06 v, this step does have the effect of restoring much of the original "kinky" character of the charging curve. This suggests that there is, in fact, a change in θ_H^t, i.e. surface coverage, during the 0.06 v desorption, but that it is small and consequently easily concealed by the lack of character in the directly taken H-charging curve. These effects might well be caused by the presence of a small amount of relatively weakly adsorbed material which is in a high state of reduction. That it is in a high state of reduction follows from the relatively large contributions it makes to $Q_{ads}^{C_3H_8}$ (cf. Figs. I.16 - I.18). Such a species could, for example, be the physically adsorbed C_3H_8 which was earlier[1, 3] postulated to be present during the initial phases of adsorption. The existence of such a species will also be postulated when we return to the discussion of the possible identities of the partially oxidized adsorbed materials (A), (B), and (C).

The experiments described in the last paragraph indicate either that all the cathodically desorbable material is always completely desorbed during the θ_H^t measurements, irrespective of whether we interpose the 0.06 v desorption step, or that it occupies very little of the surface. Either way, its presence involves a modification in the description of the number of sites occupied by the adsorbed material. The extent of this modification can only be judged when we know how many sites the desorbable material occupies. It is clear that we must expect θ_{res} (≡ true ratio of residue to total) to be much higher than θ'_{res} ($Q_{res}/Q_{ads}^{C_3H_8}$) since the desorbate is almost certainly in a higher state of reduction than the residue. θ_{res} cannot be determined with cathodic hydrogen charging, as indicated, but it should be accessible with anodic hydrogen charging. In this experiment, we adsorb as usual and then follow the cathodic desorption at say 0.06 v, using the anodic hydrogen wave and also measuring Q_{res}. To date, we have had difficulty in making this measurement due to impurities in the solution. Another experiment which helps to elucidate this problem is to study the anodic current during adsorption. Once again, however, we have had difficulties with impurities in the solution. Further purification of

the electrolyte will be necessary before we can carry out these important experiments.

We now consider again the possible identity of the species (A) (B) and (C) in light of the cathodic desorption experiments. The limiting values of Q_{res} and Q_{des} for the adsorbate at 0.3 v are 250 and 110 μcoul/r. cm^2 respectively (Fig. I. 17). Similarly, Q_B and Q_C are 145 and 200 μcoul/r. cm^2 (Fig. I. 11). These values are close enough to lead to the conjecture that Q_{res} and Q_{des} may be alternative expressions of Q_B and Q_C, a highly satisfactory synthesis. Support for this view comes from our previous conclusion that Q_{res} is the most highly oxidized material between Q_{res} and Q_{des} and, also, from the observation that galvanostatic oxidation of the adsorbed material occurs at lower potentials when we have only Q_{res} present. To test this theory, we have adsorbed C_3H_8 at 0.3 v for 100 sec, desorbed Q_{des} at 0.06 v, and then studied the anodic desorption of the remaining Q_{res} at 0.7 v. On the basis of the above theory, we expect to see that part (C) of Fig. I. 11 will be eliminated, leaving part (B); where the line now passes through the $Q_{ads}^{C_3H_8}$ - $(1 - \theta_H^t)$ origin. This is only partly confirmed by experiment (Fig. I. 21). Thus the slope of part (B) is about the same (1.3 against 1.35 electrons) but there is incomplete elimination of part (C). This finding of a similar slope for (B), in the substantial absence of (C), confirms the view expressed in the last section that (B) and (C) are separate species. The value for $[e]_B$, ~ 1.3 electrons per site covered, is thus confirmed.

It might have been expected, from Fig. I.14 where $Q_{ads}^{C_3H_8}$ vs. $(1 - \theta_H^t)$ is a straight line passing through the origin, that there is only one species adsorbed at 0.4 v. The cathodic desorption experiments (Fig. I. 18) show clearly that there must be at least two kinds of material present, one desorbable cathodically and one not desorbable cathodically. The resolution of this difficulty can be made in the following way: If we assume the presence of a small amount of highly reduced material which oxidizes stepwise (eventually to CO_2) with a variety of rate constants, we may still see a linear anodic desorption plot even when two species are adsorbed. It is too early to conjecture the identity of this material - it

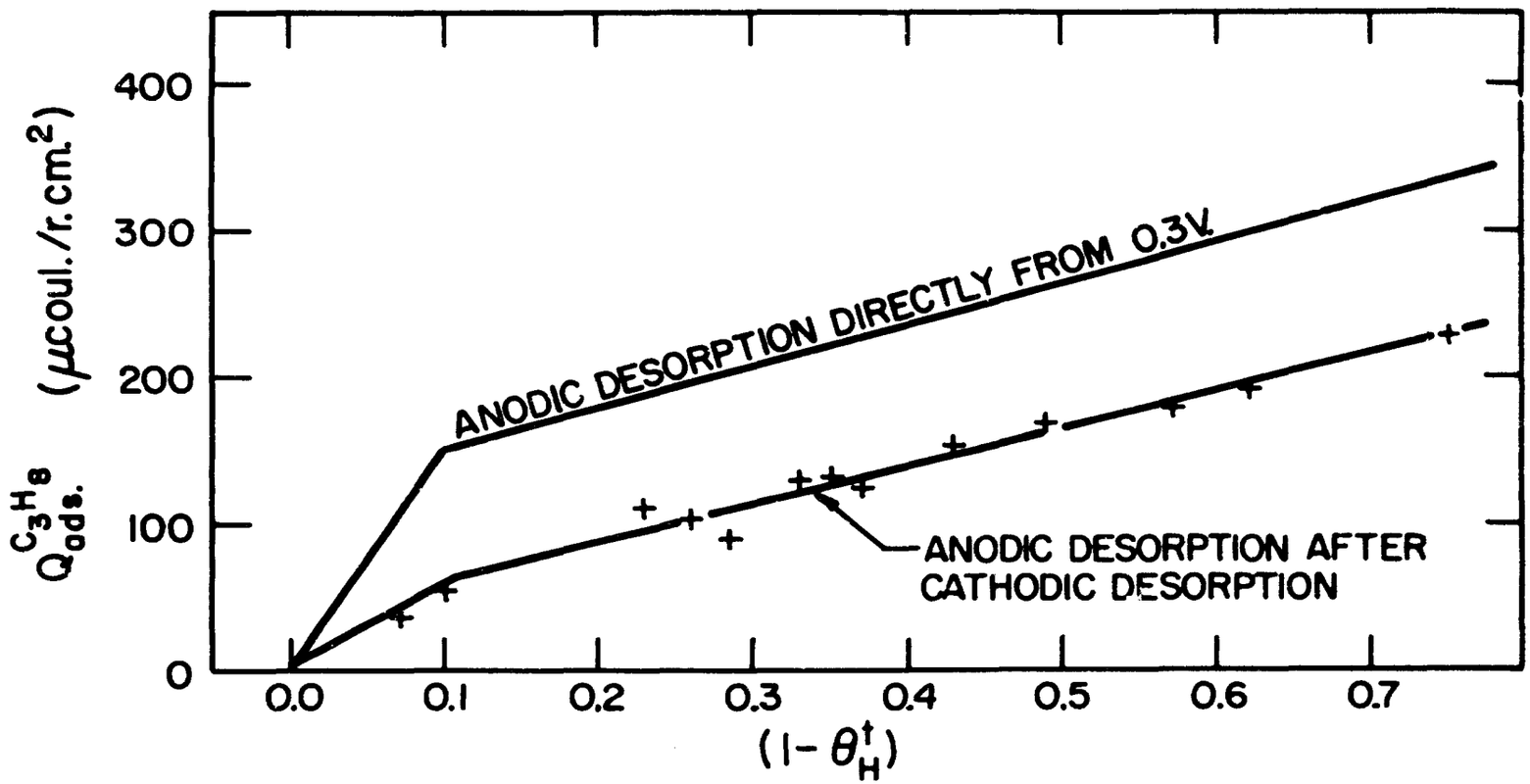

Fig. I-21 Comparison of anodic desorption characteristics (0.7V) of material adsorbed at 0.3V for 100 sec. with and without subsequent cathodic desorption (0.06V, 1 sec.)

could, for example, be the physically adsorbed C_3H_8 postulated earlier[3]. This would mean that $[e]_{obs}$ is higher than the true value of $[e]_A$. To estimate $[e]_A$, we equate Q_{des} ($\sim$ 65 μcoul/cm^2) with the second species and note that this species probably occupies very little of the surface. Then $[e]_A \simeq 1.3$. This value is similar to that of $[e]_B$ and this would suggest that (A) and (B) are actually the same.

If this is so, it removes two substantial difficulties we have mentioned, the disagreement between Figs. I. 14 and I. 18 and the presence of (A), a more highly reduced species, as the finally-adsorbed residue at the more anodic potentials. A definitive test of this thesis will be a comparison of the oxidation kinetics of (A) and (B) under conditions where only they are present on the electrode and where their surface concentrations are the same.

Until the difficulties raised earlier concerning the number of sites occupied by the adsorbed molecules are resolved it is somewhat speculative to consider in detail the identity of the adsorbed species. If (B) does turn out to be the major final residue on the electrode, its actual composition really depends on the number of C atoms on the surface. On the basis of the original 3-site per C_3H_8 molecule adsorption model, the value of $[e]_B$ would correspond to the oxidation state of single C atoms. Then the only possibilities would seem to be an average of various oxidation states, e.g. HCOO (Pt) and CO (pt). If multi-attachment were occurring the C atoms would have to be in a more reduced state. It does seem probable, at this time, that since the maximum charge to oxidize a full monolayer of (B) is between 275 μcoul/r. cm^2 it cannot be CO_{ads} itself[16] not could it be the adsorbed material which poisons HCOOH oxidation[17].

8. Summary of Proposed Mechanism for Oxidative Adsorption of Hydrocarbons

It is clear that more experimental work is required to elucidate the full mechanism of this complex reaction. This will involve detailed studies of both simple and complex hydrocarbons and may also involve studies of simpler materials, e.g. "reduced CO_2"[18]. The rewards of such an endeavor will be to define the chemical paths taken during the passage from

saturated hydrocarbons to CO_2 and to reveal the chemical principles whereby control of the reaction may be attempted. The work carried out in this report period has contributed significantly to the description of the adsorptive oxidation of C_3H_8 on Pt in concentrated H_3PO_4 but, as indicated, a number of fascinating problems are still to be resolved. We would summarize our findings in this period as follows:

1. Studies with the rotating disk electrode and with a foil electrode confirm the previous conclusions made with a wire electrode, that the initial adsorption of C_3H_8 onto a clean electrode is limited by diffusion in the solution.

2. The anodic galvanostatic method, as used previously, gives an accurate quantitative description of the amount of oxidizable adsorbed material.

3. Total C_3H_8 adsorption, at a given potential, whether measured anodically or cathodically, is independent of the temperature in the range 80 - 140°C. Comparison of the limiting values of $Q_{ads}^{C_3H_8}$ and $(1 - \theta_H^t)$ would suggest that the average oxidation state of the adsorbate is independent of the potential ($\geq$ 0.3 v) and of the temperature.

4. Anodic desorption studies show, however, that this is not true and show that the detailed "structure" of the adsorbate is a function of the potential and the temperature. Three distinct adsorbed residues appear to be present, labelled (A), (B), and (C). These appear to release, respectively, 1.8, 1.3 and $\sim$ 6 electrons per covered Pt site when oxidized.

5. Cathodic desorption measurements indicate the presence of another highly reduced adsorbed material. When the presence of this material is allowed for, (A) and (B) appear to be the same and release about 1.3 electrons/site when oxidized. These last measurements throw, however, some doubt on the assignment of the number of sites occupied by each adsorbed molecule.

The following is a summary of a tentative mechanism for the over-all C_3H_8 - CO_2 reaction: -

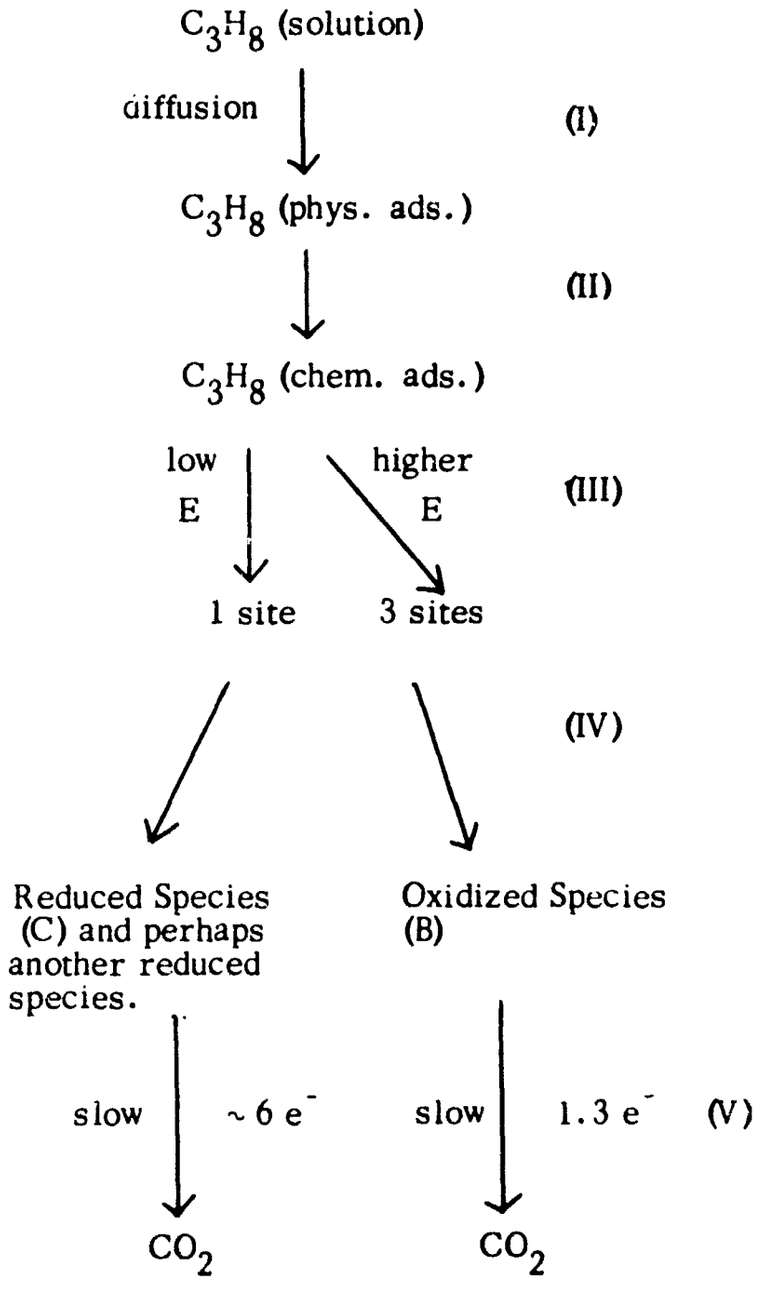

(I) is rate-limiting on a clean electrode. Physically adsorbed C_3H_8 required to account for observation of diffusional control at high coverage.

(III) is subject to review.

(IV) proportions of (B) and (C) vary with E.

(V) are certainly slow steps in the paths of C_3H_8 to CO_2 via (B) and (C). Of these, (B) to CO_2 is faster, at least at 0.7 v. It is not established whether C_3H_8 usually proceeds to CO_2 via these reactions, or in spite of the blockage of the electrode by (C) and (B), i.e. via another mechanism on the remainder of the surface.

9. Glossary of Symbols

$C^{C_3H_8}$	Concentration of C_3H_8 (moles/ml).
$D^{C_3H_8}$	Diffusional coefficient of C_3H_8 (cm^2/sec).
E	Potential (v vs. reversible H^+/H_2 (R.H.E.)).
$[e]_i$	Average number of electrons involved in the complete oxidation to CO_2 of adsorbed species i per surface Pt atom which it covers.
geom. cm^2	Geometric area of the electrode.
i_a	Anodic current density (amp/r.cm^2).
i_c	Cathodic current density (amp/r.cm^2).
n	Number of electrons involved in complete oxidation to CO_2 of adsorbed species (not per site covered).
Q	Charge (μcoulomb/r.cm^2).

Q_{des}	$(Q_{ads}^{C_3H_8} - Q_{res})$.
Q_H or Q_H^t	Cathodic H atom charge at t°C.
$(Q_{anodic}^{total})^i$	Either charge passed during anodic galvanostatic transient in solution saturated with gas i as defined in Fig. I.5 and section I.4, or total charge passed in a suitable potential step as discussed in section I.4.
$Q_{ads}^{C_3H_8}$	Charge to oxidize adsorbed C_3H_8.
Q_{res}	Charge to oxidize cathodically non-desorbable residues.
r . cm^2	Real area (one real cm^2 ≡ 210 μcoul. for Q_H^t on a clean electrode).
t	Temperature (°C).
T	Temperature (°K).
θ_i	Fraction of surface covered by species i.
θ_H or θ_H^t	Ratio of the H-atom charge under a given circumstance to the maximum value at the same temperature.
θ'_{res}	$Q_{res}/Q_{ads}^{C_3H_8}$ (both measured for same τ_{ads}).
τ	Time (sec).
τ_{ads}	Time of adsorption.
τ_E	Time at potential E.

10. References

1. Report by Tyco Laboratories, Inc. on this contract (Nov. 1964).
2. Ibid., (April 1965).
3. S. B. Brummer, J. I. Ford, and M. J. Turner, J. Phys. Chem. 69, 3424 (1965).
4. S. B. Brummer and M. J. Turner, "Hydrocarbon Fuel Cell Technology", The Proceedings of the A.C.S. Fuel Symposium in Atlantic City, N.J., Sept. 1965. To be published by the Academic Press, New York, N.Y.
5. P. V. Popat and A. Kuchar, Interim Report No. 1 on contract DA 44-009-AMC-479T (Apr. 1964).
6. H. A. Laitinen and I. M. Kolthoff, J. Amer. Chem. Soc. 61, 3344 (1939).
7. S. Gilman, Priv. Comm.
8. V. G. Levich, Acta Physichim. U.S.S.R., 17, 257 (1942); Disc. Faraday Soc., 1, 37 (1947).
9. D. Gregory and A. C. Riddiford, J. Chem. Soc., 1956 (3756).
10. "Phosphoric Acid, Its Physical and Chemical Properties", Technical Bulletin No. P-26, Monsanto Chemical Co., St. Louis, Mo.
11. Report by General Electric Company on Contract DA 44-009-AMC-479T (Dec. 1964).
12. D. N. Saraf, P. A. Witherspoon and L. H. Cohen, Science, 142, 955 (1963).
13. S. B. Brummer and G. J. Hills, Trans. Faraday Soc., 57, 1816, 1823 (1961).

14. J. R. Van Wazer, "Phosphorus and Its Compounds", Vol. 1, (Interscience Publisher Inc., New York, N.Y. 1958).

15. V. G. Levich, "Physicochemical Hydrodynamics", (Prentice Hall, Englewood Cliffs, N.J., 1962) p. 358 et seq.

16. S. B. Brummer and J. I. Ford, J. Phys. Chem., 69, 1355 (1965).

17. S. B. Brummer, ibid, 69, 562 (1965).

18. J. Giner, Electrochimica Acta, 8, 857 (1963); 9, 63 (1964).

II. DEVELOPMENT OF PLATINUM BASED ELECTROCATALYSTS FOR HYDROCARBON FUEL CELL ELECTRODES

1. Introduction

A program for the development of improved platinum anodes for direct hydrocarbon fuel cells was initiated during the last year. The approach we have taken is to prepare, characterize, and test platinum-based alloys and compounds and then attempt to relate their catalytic activity to their properties and structure, these last being in turn relatable to the conditions of preparation. A systematic study along these lines will enable us to understand, predict, and control the electrocatalytic activity of platinum-based electrodes and will allow us to prepare fuel cell electrodes of maximum activity and, hopefully, minimum cost.

The main tasks under this program fall into the three operations stated above: prepare, characterize, and test. Our main effort in this first phase of the program was to develop methods of characterization suitable for high surface-area platinum blacks. Up to now catalyst powders have been studied largely by adsorption measurements; consequently, little or no information is available on particle geometry and shape, on surface morphology, on stored energy, and on crystalline imperfections - although all of these quantities affect directly the activity of an electrode prepared from platinum black.

Parallel to the development of characterization methods, we have put together a working hypothesis about the way in which blacks are precipitated. We have attempted to identify the main variables which control nucleation and growth and outline a systematic approach which will allow us to control the preparation, and hence the properties, of platinum black.

Finally, testing of a given platinum black in the form of a practical electrode presents distinct problems associated with the physical structure of the final electrode. The electrode structure determines the transport to and from the active centers on the electrode of all species taking part in the reaction (including electrons) and must be controlled if measurements

of the activity are to be meaningful. We have therefore designed electrodes and techniques for studying them which will permit us to arrive at an unambiguous measure of the activity of the electrode.

2. Preparation of Platinum Blacks

There are two distinct steps during the precipitation of a platinum black: primary nucleation and growth. The primary nucleation is a purely molecular reaction described by classical kinetics, while growth occurs to some extent as an electrochemical process with two electro-reactions occurring simultaneously, and to some extent independently, on the formed nucleus. One reaction is the electrochemical oxidation of the reducing agent and the other is the electrochemical reduction of the Pt salt. Accordingly, the classical theory of a mixed electrode applies (ref. 1) as shown schematically in Fig. II. 1.

The main factor which determines the number, and therefore the size, of precipitated particles is the ratio between the rate of formation of primary nuclei and the growth rate. However, the kinetics of electro-deposition during the growth process (compact deposition or powdery - dendritic deposition) can also be decisive in determining the size of particles. The extreme case of a single primary nucleation center with a dendritic electrogrowth (or electrodeposit of powder) with very fine particles illustrates this point.

In general, the size of particles formed during the second step (electrogrowth) is determined by the ratio between the rate of crystal growth and the rate of formation of secondary nuclei (to some extent also by the intergrowth of crystals).

We consider in the following only the factors which cause dendritic growth (high ratio of nucleation rate to growth rate) during the second step. It is reasonable to expect that the factors which favor the formation of secondary nuclei on existing crystal surfaces also favor the formation of primary nuclei.

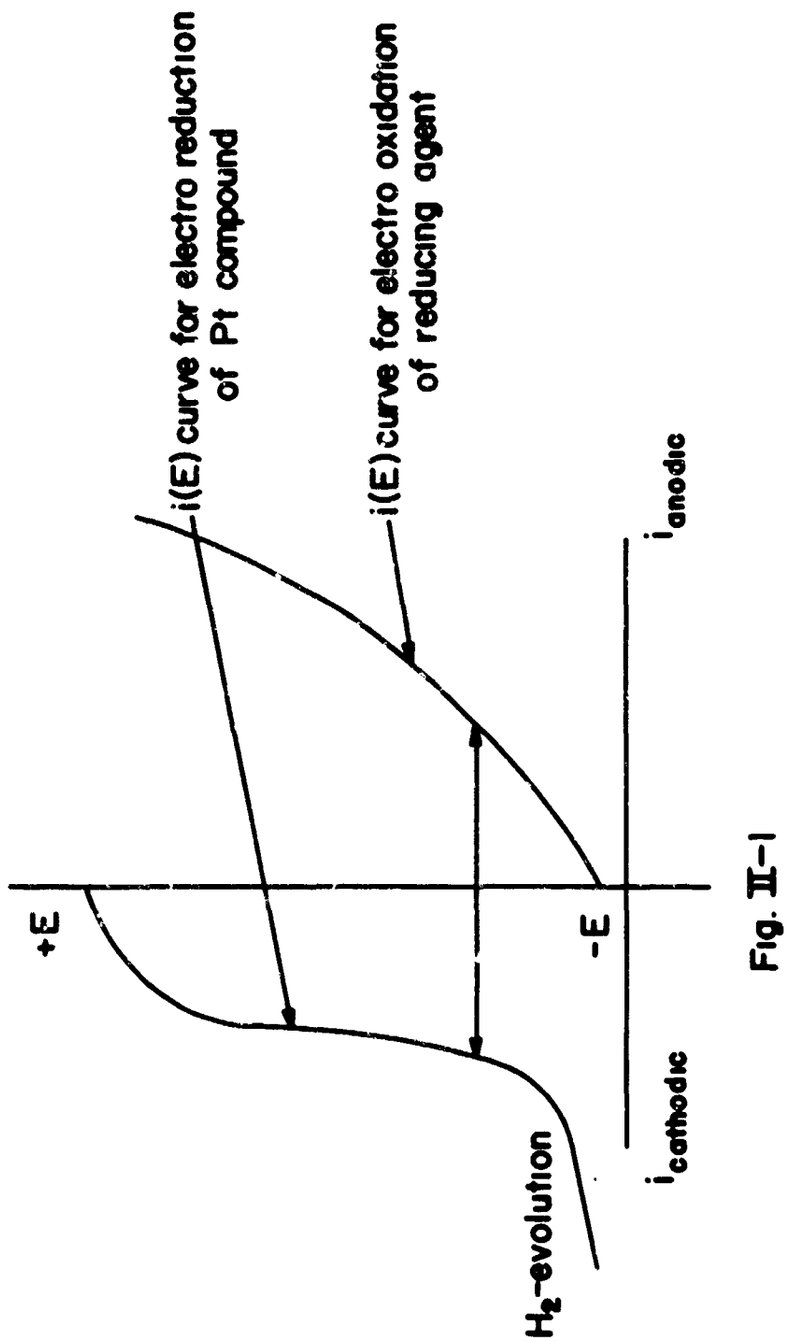

Fig. II-1 Schematic diagram of platinum precipitation according to a mixed electrode mechanism

A. Factors Which Determine the Particle Size of Electrodeposited Powders (and Dendrites) and of Chemically Reduced Blacks

Although the phenomenon of powder deposition (or dendritic growth) is not well understood and conflicting mechanisms have been suggested, it is generally agreed that factors which favor deposition under conditions of diffusion-limited transport favor, at the same time, the formation of powder, i.e. the formation of small crystallites (ref. 2).

Current: In general, the higher the ratio between actual current and diffusion-limited current during conventional powder electrodeposition the smaller the particle size. The current has to be controlled, however, in order to avoid violent hydrogen evolution; it will be shown later that this is not a contradiction.

When the mixed electrode theory for the chemical deposition of blacks is used, the current (local current) is determined by the concentration and reactivity (oxidation rate) of the reducing agent. From this point of view, the higher the concentration and the higher the reactivity of the reducing agent, the smaller the expected particle size of the black.

Concentration of Metal Salt: The lower the concentration of the metal salt being deposited, the lower is the diffusion-limited current and therefore the smaller the expected particle size. This criterion can be translated without much modification from the electrodeposition process to the chemical process. In practice, the effect of concentration of powder electrodeposition is larger than that expected from the change of the diffusion-limited current.

Rate of Stirring: Since stirring increases the diffusion-limited current, it tends to increase the particle size. By extrapolating this to the chemical precipitation, one expects that a decrease in the rate of stirring would lead to the formation of finer particles. This effect may be limited by coagulation which may occur without stirring. Ultrasonic agitation may also be a special case.

H_2-evolution: Since hydrogen evolution during electrodeposition causes very effective stirring, it is expected to increase the particle size. This effect has, in fact, been found in several cases.

When selecting a reducing agent for chemical reduction of black, the possibility that this reducing agent may cause a sufficient negative potential on the Pt nuclei to cause H_2-evolution must be considered.

Viscosity: According to the general transport effect, an increase in viscosity causes a finer particle size.

Temperature: In electrodeposition, the only effects of temperature seem to be an increase in the diffusion rate and a decrease in the activation polarization. Disregarding for the moment the last factor, which is not clear, the statement may be made that an increase in temperature causes a larger particle size by increasing the diffusion-limited current.

In the chemical precipitation of blacks, the effect of temperature is more ambiguous because it acts to increase the transport rate (hence, to increase particle size) but, at the same time, also increases the rate of oxidation of the reducing agent and, if we assume that this increases the local current, this leads to a decrease of particle size.

The relative importance of these opposite effects may be ascertained by estimating their activation energies.

Inhibitors: The effect of poisoning of the electrode surface on the size of electrodeposited powders is not very clear; however, there seems to be some agreement that strong inhibitors promote small grain size by poisoning the rate of metal growth and increasing the rate of nucleation, while weak inhibitors promote large grain size.

When precipitating blacks one should keep in mind that the reactants or their decomposition products may act as inhibitors. In addition, inhibitors used in the electrodeposition of powders will be investigated to see if they act in the same manner during precipitation. Lead acetate will be examined from this point of view.

Concentration of Indifferent Electrolyte: Increasing the concentration of an inert salt leads to a decrease of the particle size. The origin of this effect is not clear.

Other Factors: Several other factors have been shown to have an effect; however, clear interpretations of their effects are lacking.

Activation Polarizations: The role of activation polarization in determining particle size is unclear and contradictory interpretations have been offered in the literature (see, for example, ref. 2, pp. 69-71).

Colloids: Gels seem to favor powders, while sols favor a fine-grained, even deposit (favor intergrowth).

Complexes: It has been claimed that if dissociation of the complex occurs previous to the electrodeposition, the deposit will be compact, while if the complex is discharged directly, the deposit will be powdery.

B. Factors to Study or to Control During Precipitation of Pt Black

In order to study the precipitation of Pt black as a mixed electrode process the following factors will be studied under similar conditions to those maintained during precipitation.

Electro-oxidation of the Reducing Agent: Potentiostatic i(E) curves of the oxidation of the reducing agent will be obtained on bright Pt. The concentration of the redox agent and temperature will be equal to those used during precipitation.

Electrodeposition of the Pt Salt: Similarly, potentiostatic i(E) curves of the electrodeposition of the Pt salt (no reducing agent present) will be obtained.

It has to be kept in mind that transport to a flat electrode is by linear diffusion, while diffusion during precipitation is spherical, at least before very large agglomerates have formed. It may be advisable to work with a very small spherical Pt electrode in order to simulate the conditions of spherical diffusion.

Galvanic Potential During the Electrodeposition: The potential of the Pt particles could also be measured with the help of a Pt micro-electrode. The measurement of this potential and the comparison with that estimated theoretically from the combination of the previous two i(E) curves will tell us how close the working hypothesis is to reality. We can also determine whether deposition of Pt is occurring in the diffusion-limiting range or in the activation polarization range, and if H_2-evolution is possible.

Hydrogen Evolution: By working in a closed system with provision for gas volumetric analysis, the extent of this important parameter can be studied.

To summarize, in order to study the effects of the factors discussed above (metal concentration, local current caused by the reducing agent and its dependence on concentration and reactivity, viscosity, temperature, stirring, etc.) we will determine the two separate i(E) curves for the reducing agent and for Pt-deposition, and we will measure the actual mixed potential and the amount of hydrogen evolved during the precipitation.

The use of this electrochemical theory of growth of blacks does not mean that the molecular theory of crystal growth theory will be neglected. On the contrary, the elucidation of the electrochemical aspects of the process will permit us to apply the usual crystal growth theory with confidence. In addition, other points of view, such as the colloid effect (size and magnitude of charge of the double-layer on the particle during precipitation) may be necessary in order to understand fully the precipitation process.

3. Characterization of Platinum Blacks

A. Statement of Problem

The characterization of the Pt-black must be carried out in such a way that the parameters so described can be related on the one hand to the variables in the precipitation (thus leading to good control of the preparation of blacks), and on the other hand to the catalytic properties of the black.

B. Characterization Parameters

Five parameters were selected in order of increasing sophistication so that step by step they can be related to preparation and catalysis.

i) Average grain size and surface area

ii) Grain size distribution

iii) Grain shape (e.g. needle, platelet, dendrite, etc.), grain morphology (e.g. octahedron, cuboctahedron, etc.), and state of aggregation

iv) Locked-in stress

v) Grain perfection and classification of imperfections

a. Stacking faults and twinning

b. Dislocations

C. Methods

In dealing with powders of grain size of the order of 100 Å it is necessary to use several characterization methods since the assumptions inherent in each one cause different errors. This approach will most likely lead to a realistic specification of the powder.

The number of methods which can effectively be applied to the determination of characteristic parameters decreases as more sophisticated parameters are sought. We will, therefore, discuss the methods available for the determination of the average grain size and then show which of these methods are most useful for the determination of the other required parameters.

Two different samples of platinum black have been used to test the characterization methods, compare the results, and try to estimate possible errors by comparison. One of the blacks is a commercial material, obtained from Engelhard Industries; the other was prepared by reduction of a chloroplatinic acid solution with sodium borohydride. Results have been obtained for the average size by all methods described and for grain size distribution by electron microscope shadowgraphy and selected area electron diffraction.

The following methods have been used to determine the average grain size.

i) Electron microscope shadowgraphy

ii) X-ray line broadening

iii) B. E. T. method

iv) Selected area electron diffraction

a) Electron Microscope Shadowgraphy

This method provides the silhouette outline (shadowgraphy) of the enlarged particles in the electron microscope. An ultrasonically dispersed sample of the black is placed on a copper grid which is covered with a carbon film. The electron beam outlines the particles, since the electrons are generally totally absorbed in the platinum particles. There are always some particles which are partially transparent because of their small size, but in general, only the contours of the particles are visible. Only very rarely is a particle sufficiently transparent to allow deductions as to its internal structure. This differs from the case of the carbon blacks, in which the same method results in clearly visible details of the particle habit.

The areas of well outlined particles are measured using a "Zeiss" particle size analyzer[3, 4, 5, 6]. The average particle diameter, as well as the size distribution, can be computed taking into account the magnification of the electron micrograph. Measurements obtained in this way on the commercially prepared black indicate an average grain size of 108 A; those on the sodium borohydride-reduced material give a diameter of 77 A.

The shape of the particles can also be discerned from the electron microscope shadowgraph. This method appears to be the only one which gives a definite indication of the state of aggregation or, at least the state obtained with the particular dispersion method used. This last statement also reveals a major drawback of the method: the particle size measured is dependent on the dispersion method and the fundamental question arises as to whether even advanced dispersing methods (such as ultrasonic agitation)

provide total dispersion without breakage of particles, particularly if the black consists of needles or dendrites. (For a general discussion of this point see Reference 7).

b) X-ray Line Broadening

It was first observed by Scherrer that if the particle size falls below a certain limit ($\sim 10^{-4}$ cm), the X-ray lines begin to broaden. This phenomenon is due to the limited resolution of a diffraction grating of only a few lines and has been treated mathematically[8]. In a first approximation, the following simple relation holds:

$$\epsilon_{hkl} = \frac{K\lambda}{\beta \cdot \cos\theta}$$

Here, ϵ_{hkl} is the mean apparent crystallite size normal to the reflecting plane, K is the Scherrer constant, taken here as 0.9. β is the pure diffraction broadening and cos θ is the cosine of the Bragg angle of the reflection. This equation gives reasonable values for the crystallite size, if no factors other than the smaliness of the grains contribute to line broadening. Various instrumental factors make if necessary to correct for the fact that the linewidth is finite even if the grain size is on the order of $\sim 10^{-4}$ cm. This is done by subtracting the experimentally obtained width at half-height of a diffraction line of the same powder obtained under optimum size conditions ($\sim 10^{-4}$ cm), from the experimental diffraction broadening.

The average grain diameters obtained in this manner for the commercial black and the sample reduced by borohydride were 110 Å and 71 Å respectively, in good agreement with the values obtained by shadowgraphy.

More precise results, however, can be obtained following methods developed by Jones[9]. Initial values of linewidth are obtained using CuKα radiation, and the correction for splitting due to the Kα_1 - Kα_2 doublet are made for both the specimen and the standard linewidths. The instrumental corrections are then applied to the corrected experimental linewidth, using

a method, also due to Jones, in which the pure diffraction profile, $f(\epsilon_{hkl})$, is assumed to obey the relation

$$f(\epsilon_{hkl}) = \frac{1}{K^2\epsilon^2 + 1} \quad .$$

One sample of the commercially prepared Pt black was analyzed by this technique. The particle sizes in Å of this sample obtained for several hkl reflections were as follows:

G_{111}	G_{200}	G_{220}	G_{311}
165	136	138	130

At present it is not clear why these values are higher than those found by the other methods described in this section. It is possible that the deviation apparent in the (111) peak may be due to a shape factor.

It has been shown, however, that other factors inherent in the material besides small size cause line broadening. This is the case when microstress as well as twinning and stacking faults are present. Fortunately these factors have different influences on the line intensity so they can be mathematically separated by an inconvolution operation using Fourier series.

The Warren-Averbach method entails a complete Fourier analysis of the line shape. It has been shown by Warren[10] that in order to separate the effects on the line broadening of particle size, faulting and microstrains, one must express the diffracted intensity, $p^1(2\theta)$, as a Fourier series, i.e.

$$p^1(2\theta) \alpha \sum_L A_L^{PF} \cdot A_L^{D} \cdot \exp\left[2\pi i L (S - S_o)\right] \qquad (1)$$

where $S = 2 \sin\theta/\lambda$, $S_o = 2 \sin\theta_o/\lambda$, θ_o being the position of the peak maximum; the index L is the distance normal to the reflecting plane (hkl) with an interplanar spacing d; the terms A_L^{PF} and A_L^{D} are the particle size faulting coefficient and the distortion coefficient respectively.

The coefficients obtained from a well annealed powder are used in the Stokes method[19] for the elimination of the instrumental contribution to the peak shape.

The strain coefficients are approximated by the relation

$$A_L^D = \exp\left[- \frac{2\pi^2 L^2 < \Sigma_L^2 >}{d^2} \right] \qquad (2)$$

where $< \Sigma_L^2 >$ is the mean-square strain at a distance L normal to the (hkl) plane of spacing d. Since the distortion coefficients are dependent upon the order of reflection, they can be separated from the particle size faulting coefficients by the relation

$$\ln A_L = \ln A_L^{PF} - 2\pi^2 L^2 < \Sigma_L^2 > \frac{h_o^2}{a^2} \qquad (3)$$

where the A_L are the observed coefficients, corrected for the instrumental broadening, $h_o^2 = (h^2 + k^2 + l^2)$ and a is the lattice parameter. Using equation (3), one obtains A_L^{PF} as a function of L, for each direction in the lattice normal to the reflecting planes.

The intercept value of $\ln A_L$ at $h_o^2 = 0$ gives the particle size faulting coefficient A_L^{PF}, and the slope is proportional to the mean-square strain component $< \Sigma_L^2 >$. When the particle size faulting coefficients obtained from the (hkl) reflections are plotted as a function of L, the intercept on L of the initial slope is termed the effective particle size, D_e(hkl) normal to the (hkl) planes, i.e. in the <hkl> direction for cubic crystals and from the idea of the effective particle sizes, the faulting probabilities can be evaluated.

For the recording of the diffraction spectra a "Norelco" X-ray diffractometer was used, equipped with step scanning gear and a counting-rate computer. The output (time used to achieve a given number of counts) was fed directly into a paper-tape-puncher. The paper tape is converted on an automatic IBM keypunch into punched IBM cards which are subsequently

processed on an IBM computer. The paper punch attachment was not commercially available and has therefore been built in our laboratory. The results obtained by this method await computer evaluation.

c) B.E.T. Area Determinations

This method, which is primarily used to determine the total surface area, can also be employed to calculate the average size if assumptions are made about the shape of the particles. Generally particles are assumed to be spheres as a first approximation. Correlation of the size arrived at here with that found by other methods allows conclusions to be drawn as to the extent of the deviation of the particles from spherical shape even on a submicroscopic scale (roughness factor), or overlapping of surfaces. Conclusions as to the degree of agglomeration of particles and associated pore size can also be derived.

A measurement by B.E.T. on the $NaBH_4$-prepared black resulted in an average diameter of 106 Å. This seems quite high in comparison to diameters obtained by other methods, but the assumption of isolated spherical particles is rather stringent, and it is not unreasonable to assume that some of the area for absorption is blocked by overlap of the particles.

d) Selected Area Electron Diffraction Methods

In an electron microscope with a selected area diffraction attachment, the effective irradiated area of a specimen can be made sufficiently small so that it is possible (even if the grains are in the 100 Å range) to keep the number of single crystallites inside the irradiated area limited; the diffraction rings are then resolved into a series of diffraction spots. Grain size measurements can then be carried out by counting the number of reflection spots present following the methods of Stephen and Barnes[11], or by measuring the spot sizes following the method of Clark and Zimmer[12].

The first method used here differs from that of Stephen and Barnes inasmuch as it is possible with an electron microscope to change the

irradiated area within wide limits, thereby extending their method to the range of much smaller grain sizes than is possible even with a micro-beam X-ray technique. A typical electron diffraction picture obtained of commercial platinum black under these conditions is shown in Fig. II-2.

It is assumed that the electron beam cannot penetrate beyond one particle thickness, and that the area seen by the beam is entirely filled with particles. The first assumption is justified by interpretation of the transparency thickness curve for gold found by Lenz[13] and the second by observation of the sample under the beam. Therefore, the number of spots observed in one diffraction ring is directly proportional to the number of particles filling the area seen by the beam. It can be shown[13] that the average grain size, G, obeys the relation

$$G = \left(\frac{A\,p\cos\theta\,d\theta}{2N}\right)^{\frac{1}{2}}$$

where

A = irradiated area

θ = Bragg angle for the reflection under consideration

p = multiplicity (number of planes with indices {hkl})

N = number of spots counted in the hkl ring

$d\theta$ = beam divergence

Since the divergence of the electron beam is not accurately known, a particle size of 100 Å was obtained for one sample by shadowgraph technique, and a $d\theta$ value was estimated by taking the average over-all hkl rings seen in the diffraction photograph. This value was found to be in agreement with the estimate made by Thomas[14] and has been applied to photographs of other samples to obtain average grain sizes. The results, for various samples of the commercially prepared Pt black, appear in Table II-1.

TABLE II-1

Average Particle Size in Å Obtained by Counting Diffraction Spots

Sample	Irradiated Area, μ^2	G_{111}	G_{200}	G_{220}	G_{311}	Gav. of 111 and 200
1	.1668	96	84	101	112	90
2	.2112	111	101	118	134	107
*3	.1806	101	92	103	108	97
**4a	.3429	99	108	129	153	103
4b	.2065	108	104	112	133	106
4c	.1296	99	100	100	122	100
4d	.3062	115	105	123	147	110
4e	.3085	114	105	121	149	110

* The beam divergence was calculated from this sample

** All data labelled 4 are from photographs of the same sample, with varying areas and beam intensities.

In each case, grain sizes found by counting spots in the first two (111 and 200) reflections are consistent, and smaller than those obtained from the (220) and (311) reflections. This may be due to a shape factor, but the fact that diffraction spots are faint for high hkl (and thus less likely to be counted) indicates that a larger grain size would be found from higher order reflections regardless of whether a shape factor is present or not.

The second method used with these same samples extends the range of spot size measurements to much smaller diameter particles than those investigated by X-ray methods. It is potentially a very powerful method of general applicability for the determination of average grain size as well as of grain size distribution.

The chief assumption inherent in this method is that the spots formed by diffraction of crystallites of diameter smaller than that of the incident beam are linearly proportional to the size of the crystallites. This is borne out by extrapolation from the results obtained by Clark and Zimmer[12] for larger particles, using X-rays.

The spot sizes on a diffraction photograph are measured on a Zeiss particle size analyzer and divided by the magnification of the photograph. Thus the size distribution is obtained, and the mean grain diameter (at least within a factor) is calculated. The results for several samples appear in Table II-2 for mean grain diameters on several hkl rings and their average over all rings.

TABLE II-2

Average Particle Size in Å Obtained by Measurements of Diffraction Spots

Sample	Irradiated Area, μ^2	G_{111}	G_{200}	G_{220}	G_{311}	Gav.
1	.1668	99	93	94	96	95
2	.2112	92	85	82	81	85
3	.1806	81	---	76	80	79
*4a	.3429	103	92	92	95	95
4b	.2065	106	109	112	112	110
4c	.1296	107	101	109	103	105
4d	.3062	100	96	101	96	98
4e	.3085	96	102	106	103	102

* All data labelled 4 are from photographs of the same sample, with varying areas and beam intensities.

We can draw several conclusions from the above results. Since the diameters obtained agree well with those found by other methods, it appears

that the diameters of the diffraction spots do, in reality, represent the diameters of the particles. There is no significant variation of spot size with hkl reflections, indicating that the particles are in fact symmetrical (at least with respect to the reflections observed). Comparison with Table II-1 indicates close agreement with the grain sizes obtained by counting the number of spots on the (111) and (200) rings, and it would seem that the larger values obtained with the (220) and (311) rings are likely due to errors in observation.

4. Discussion

A number of methods have been described which were used to measure grain size, size distribution, shape of grains, state of agglomeration and locked-in stress, stacking faults and twinning. Table II-3 compares grain size values obtained by these methods. It can be seen that the results are indeed reasonably close, particularly since one cannot expect the error in any one method to be less than about + 15%. The good agreement of shadowgraph and B.E.T. methods with the results from the diffraction methods suggests that the greater majority of particles seen in the shadowgraph and deduced from its surface are indeed single crystals. Some future efforts will have to be directed towards better ultrasonic dispersion for electron microscope shadowgraph counts.

TABLE II-3

Average Grain Diameter of Two Platinum Black Specimens

Sample	E. M. Shadowgraph	B.E.T.	X-ray Line Broadening	Elec. Diff. Spot Counting	Elec. Diff. Spot Size
Commercial	108	---	110, 130	96, 104	96, 99
SBHI	[illegible]	106	71	84	--

Grain size distribution in the same powders is presently being determined. Results have been obtained by shadowgraphy from pictures

typical of that shown in Figs. II-2 and II-3. Figures II-5 and II-6 show the distribution curves (cumulative probability vs. the logarithm of size) for commercial material and the sodium borohydride-reduced preparation as determined by shadowgraphy. It can be seen that the borohydride sample follows very well a second order Gaussian distribution, whereas the commercial material deviates quite markedly from such behavior. Figure II-7 shows a similar curve for commercial material, obtained by electron diffraction spot size measurements. In this case there is excellent agreement with a second order Gaussian distribution.

Although shadowgraphy is here considered the most absolute and accurate method of particle size and particle distribution determination, the limited success in dispersion techniques has so far reduced its usefulness. In particular, since the number of the larger particle sizes is depressed because of the tendency of the investigator to avoid counting agglomerates, the average particle size is also depressed. As mentioned before, improvement in the ultrasonic dispersion technique will eliminate this difficulty.

The results obtained by the novel technique of spot size determination on electron diffraction photographs appear to be most convincing. This is somewhat surprising in view of the fact that all spots are round, which implies that they are not projections of the crystallites, and thus may render the approach inapplicable. The fact is, however, that average particle size as well as size distribution match very well with the results obtained by shadowgraphy. The rounding of the spots is probably a diffraction effect which, through averaging, does not affect the reproduction of the particle size but does affect the determination of the particle shape.

It is necessary to relate particle size and particle size distribution to the activity of the material as measured in fuel cell catalytic action. It is, therefore, mandatory to be informed about both the average surface area of the particles of a particular sample (preferably expressed per particle weight or volume), and the spread of the particle sizes (i.e. particle size distribution). This is a necessary requirement for the determination of whether the catalytic fuel cell activity of the (platinum powder) catalyst increases for constant area with decreasing grain size.

Fig. II-2 Electron microscope shadowgraph of commercial platinum black

Fig. II-3 Electron microscope shadowgraph of platinum black prepared by reduction with sodium borohydride

Fig. II-4 Selected area electron diffraction photograph of commercial platinum black. In order of increasing radius the rings represent {111}, {200}, {220}, and {311} reflections

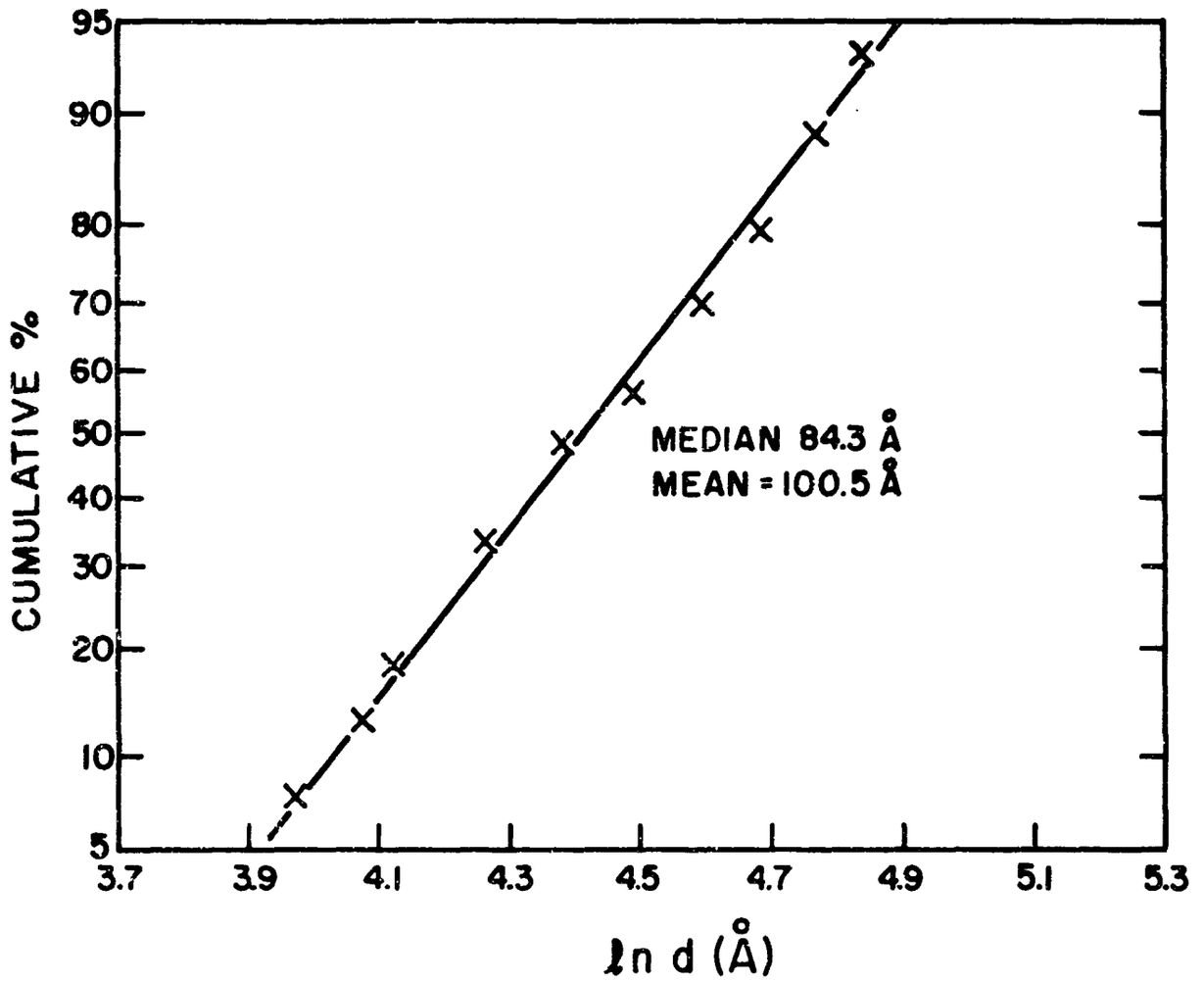

Fig. II-5 Cumulative log-probability distribution of particle size for commercial platinum black (from shadowgraph).

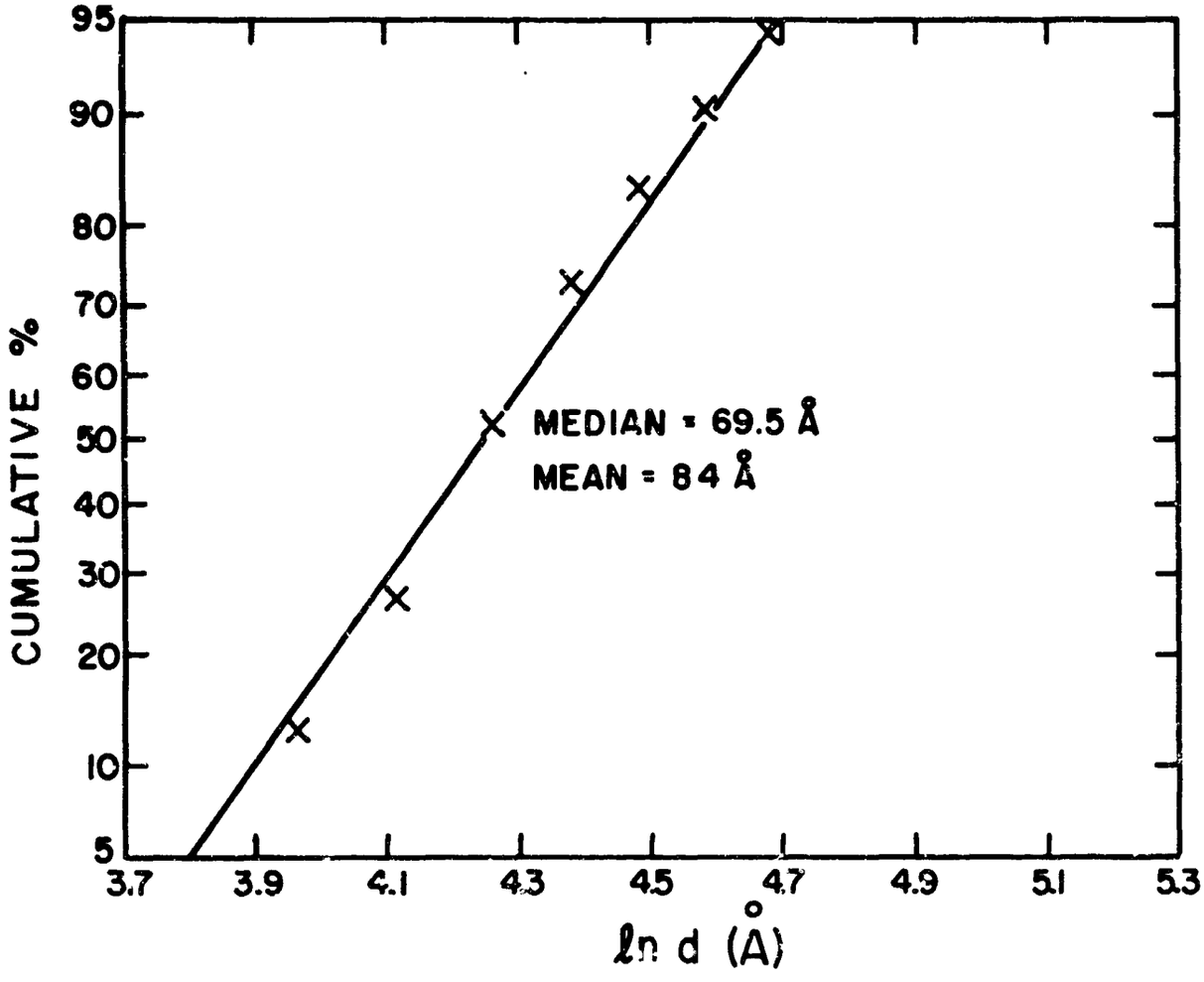

Fig. II-6 Cumulative log-probability distribution of particle size for platinum black prepared by sodium borohydride reduction (from shadowgraph).

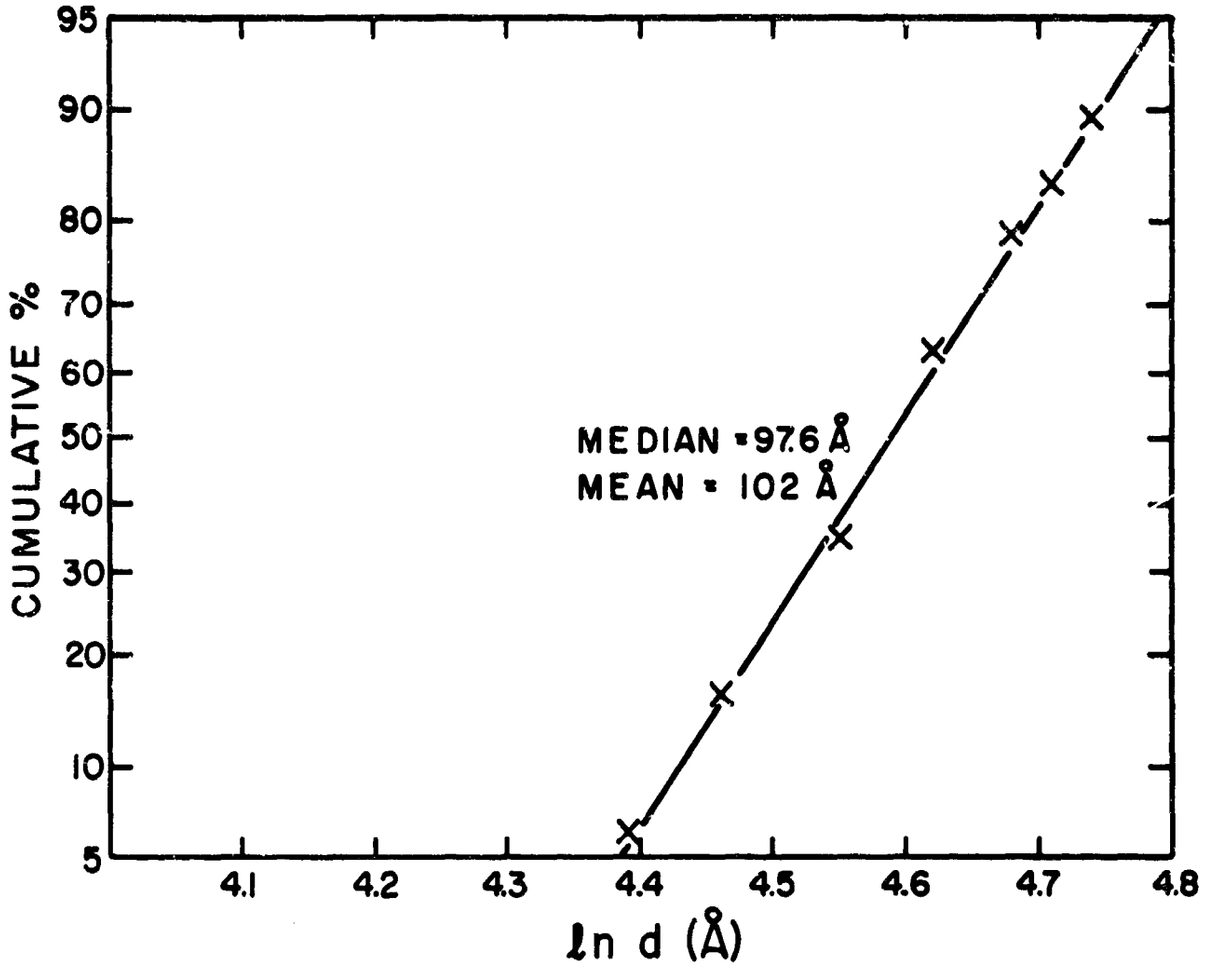

Fig. II-7 Cumulative log-probability distribution of particle size for commercial platinum black (from electron diffraction).

Given a particular particle size distribution (and shape) it is possible to calculate average particle size, surface area, and volume. These values can be derived algebraically from the observed log-normal or second order Gaussian distribution. The existence of this distribution is sufficiently manifested by the linearity of the cumulation distribution plot on the log-arithmic probability charts, as shown in Figs. II-5, II-6, and II-7. The probability function P(x) of the grain size (= x) distribution can be expressed by

$$P(x) = A \exp (- h^2 \ln^2 a x)$$

where A, h and a are constants.

Normalization by setting

$$\int_0^\infty P(x)\, dx = 1$$

yields

$$P(x)\, dx = \frac{a h}{\sqrt{\pi}} \exp (- \frac{1}{4 h^2}) \cdot \exp (- h^2 \ln^2 a x)\, dx$$

The most frequent value of the diameter (mode) is given by

$$x_{mode} = \frac{1}{a} ,$$

(as derived from $dP/dx = 0$), while the median x_{median} follows from $\ln ad = \frac{1}{2h^2}$ yielding $x_{median} = \frac{1}{a} (\frac{1}{2h^2})$.

The average grain size $\bar{x}$ is found by calculating $\int_0^\infty x P dx$, and is

$$\bar{x} = \frac{1}{a} \exp \frac{3}{4 h^2}$$

with the mean deviation

$$\sigma_x = \left(\int_0^\infty (x - \bar{x})^2 P\,dx \right)^{\frac{1}{2}}$$

or

$$\sigma_x = \bar{x} \left[\exp \frac{1}{2h^2} - 1 \right]^{\frac{1}{2}} .$$

The values relating to surface area and volume can be calculated in a similar way. Average surface area per particle is

$$\bar{s} = \frac{\pi \exp (2/h^2)}{a^2}$$

and the average volume, $\bar{v}$, is

$$\bar{v} = \frac{\pi \exp (15/4h^2)}{6\, a^3} ,$$

in both cases assuming a spherical particle shape. The associated mean deviations are

$$\sigma_s = \bar{s} \left[\exp \left(\frac{2}{h^2}\right) - 1 \right]^{\frac{1}{2}}$$

and

$$\sigma_v = \bar{v} \left[\exp \left(\frac{9}{2h^2}\right) - 1 \right]^{\frac{1}{2}}, \text{ respectively.}$$

Graphs of the probability function derived for several samples appear in Fig. II-8 and Fig. II-9. Fig. II-10 shows the grain size surface area, and volume distribution functions derived for one sample of platinum black. Assuming a different particle shape the surface area should generally increase, but not more than by a factor of 2; the average volume would not increase by more than a factor of 2.5.

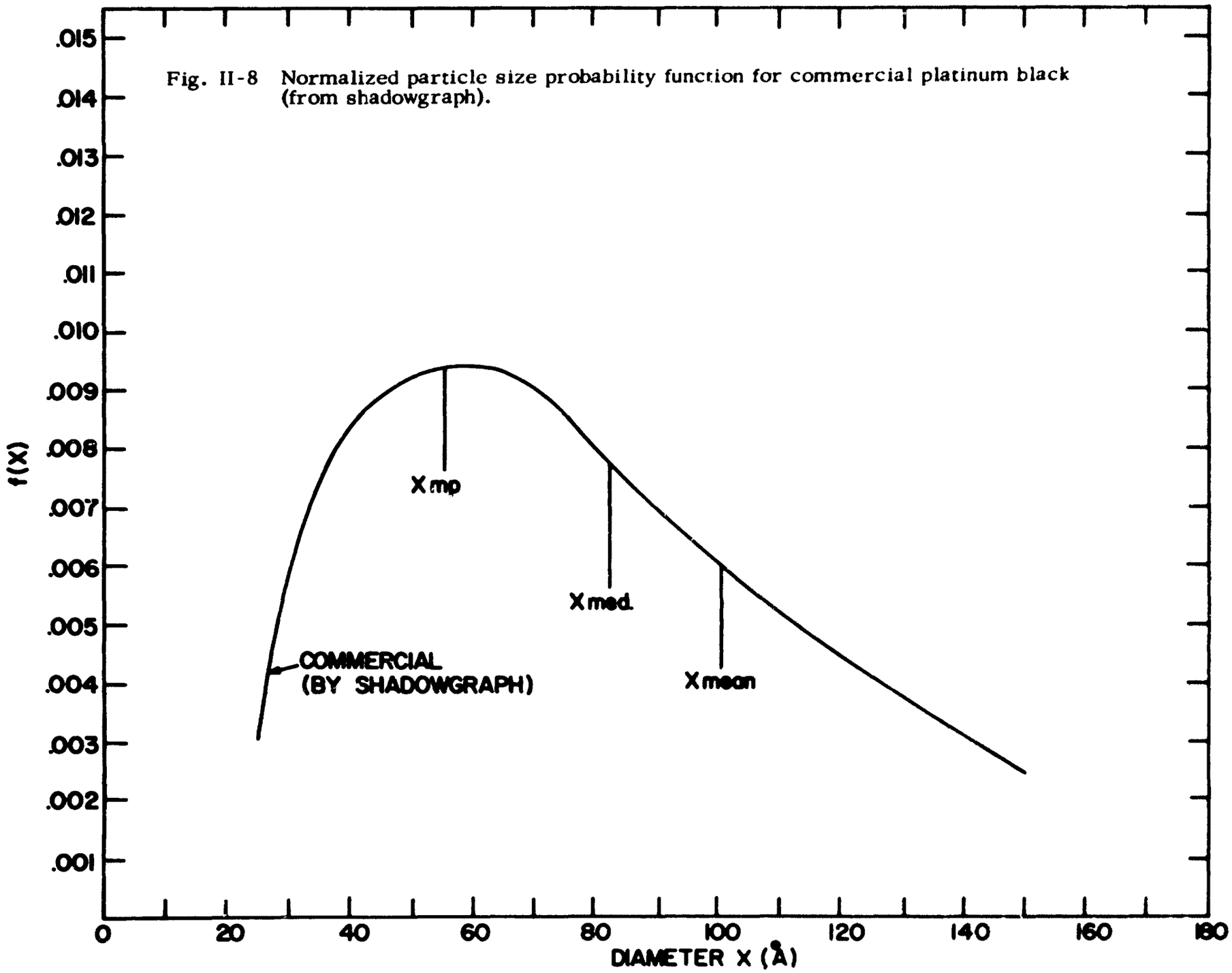

Fig. II-8 Normalized particle size probability function for commercial platinum black (from shadowgraph).

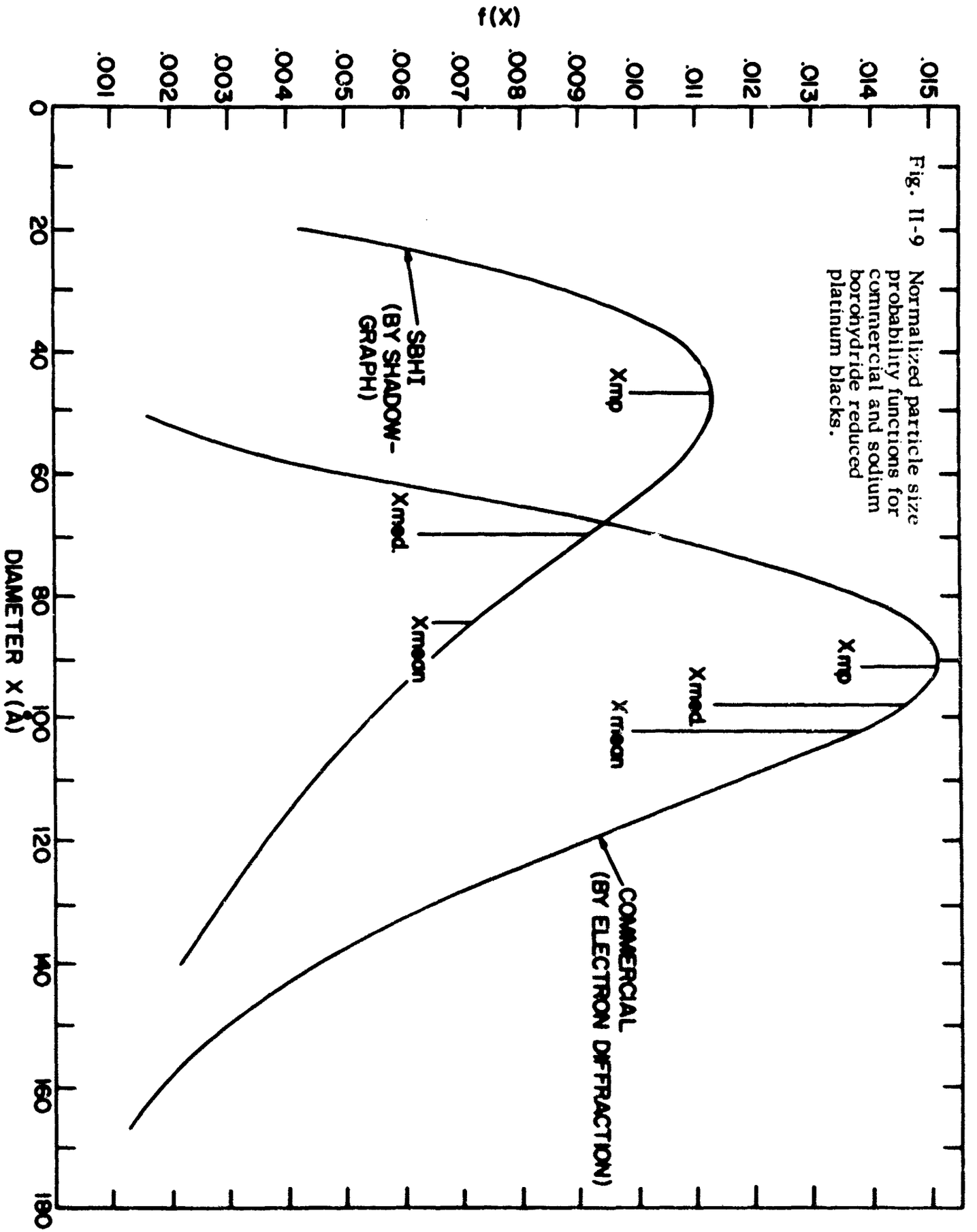

Fig. II-9 Normalized particle size probability functions for commercial and sodium boronhydride reduced platinum blacks.

Fig. II-10 Probability function (a) and distribution function for grain diameter (b), surface area (c), and volume (d), for commercial and sodium borohydride reduced sample. Curve (a) is identical to the curve for commercial platinum black shown in Fig. II-8.

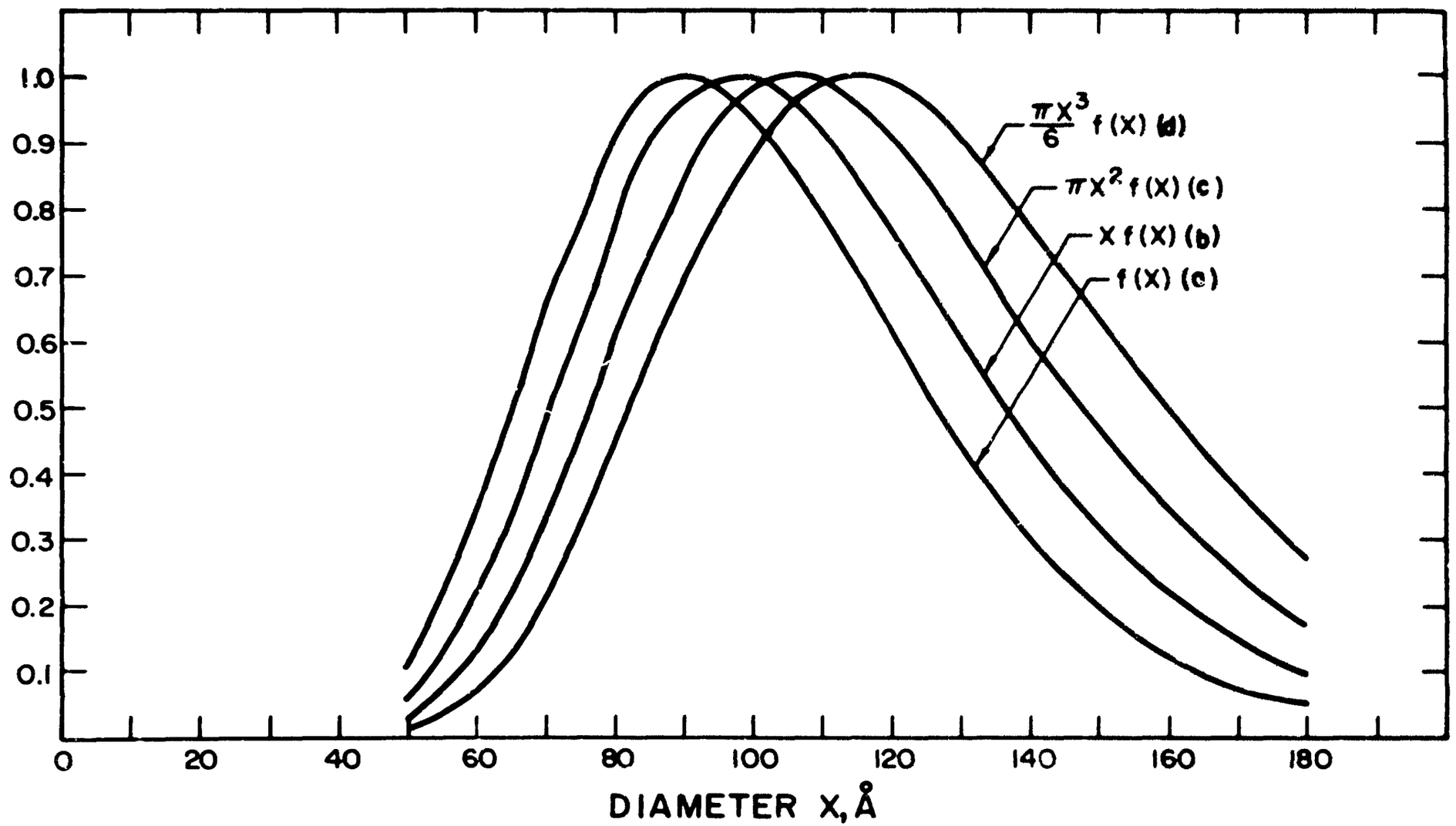

Comparison of these curves with the ones to be obtained by Fourier methods from the broadened X-ray lines will further clarify these results.

5. Remarks on the $NaBH_4$ Reduced Preparation

It has been reported by B. D. Polkovinkov et al[15] that the reduction of $H_2[PtCl_6]$ with $NaBH_4$ leads to the formation of Pt_2B rather than Pt. No cognizance of these reports seems to have been taken by workers in this country. A number of them have reduced chloroplatinic acid with sodium borohydride without reporting the formation of platinum borides. In our preparation, analysis of the diffraction spectrum indicated the presence of Pt_2B as well as Pt[16]. In addition, the diffraction peaks of platinum itself have been shifted, implying a solid solubility of B in Pt. Chemical analysis is being used to determine the amount of Pt_2B present. A study is underway to find the reason for its appearance in such small quantities, and to elucidate the absence of Pt_3B, a compound intermediate in boron content between Pt and Pt_2B. Since Pt_2B is formed it seems necessary to separate this problem from the investigation of pure Pt black, particularly since Polkovnikov et al[15] detected activities for the borides noticeably different from that of Pt.

6. Activity Tests

A. Model of Hydrophobic Porous Electrode

The more obvious procedure of testing a Pt-based catalyst is to produce a practical electrode by mixing the catalyst with Teflon powder, sintering the mixture on a conductive, inert screen, and testing the resulting electrode as a hydrocarbon anode. This method has the advantage of giving the ultimate answer about the performance of a practical electrode, but it is of limited value for studying the intrinsic activity of a given catalyst black. In order to understand the limitations of the method and the meaning of the results, the following working hypothesis, which seems to be confirmed by electron micrographs, has been suggested.

According to this picture, the Pt black is present in agglomerates (see Fig. II.11) with a size of about 10 μ. These agglomerates, with relatively high internal porosity, are formed by a network of interlocked Pt particles of 50 - 100 Å in diameter. The agglomerates are in electrical contact among themselves and with the conductive screen. Particles of Teflon (C) of about 0.1 μ in diameter fill some of the space between the Pt agglomerates and bind them together.

When the electrode is brought in contact with electrolyte at one of its external surfaces and with a reactant gas at the other surface, electrolyte fills the hydrophilic Pt agglomerates all through the electrode by capillarity, while gas fills the gaps between the Pt agglomerates since these are made hydrophobic by the Teflon particles. Thus, both electrolyte and gas penetrate all through the electrode. It should be noticed here that the main function of Teflon is to hydrophobize the electrode, the binding function being only secondary. In the particular case of an electrode in contact with acid and fed by ethane, the following reaction occurs under anodic current flow:

$$C_2H_6 + 4\,H_2O \rightarrow 2\,CO_2 + 14\,H^+ + 14\,e^- .$$

The electrons will flow between particles, agglomerates, and screen wires (electronic transport (a) of Fig. II-11); the created H^+ ions or the neutralizing anions will flow transversally to the electrode, through the electrolyte-flooded, porous Pt agglomerates (electrolyte transport (b)); the ethane gas and the water vapor will flow transversally to the electrode through the Teflon wetproof channels (gas transport (c)), while the CO_2 will diffuse in the opposite direction. The reaction will happen first on the particles located in the interface formed by electrolyte-flooded channels and gas channels and to some extent in the interior of the agglomerates; in order for the reaction to occur the gas has to dissolve to some extent in the electrolyte and diffuse into the interior of the particles (diffusive transport (d)).

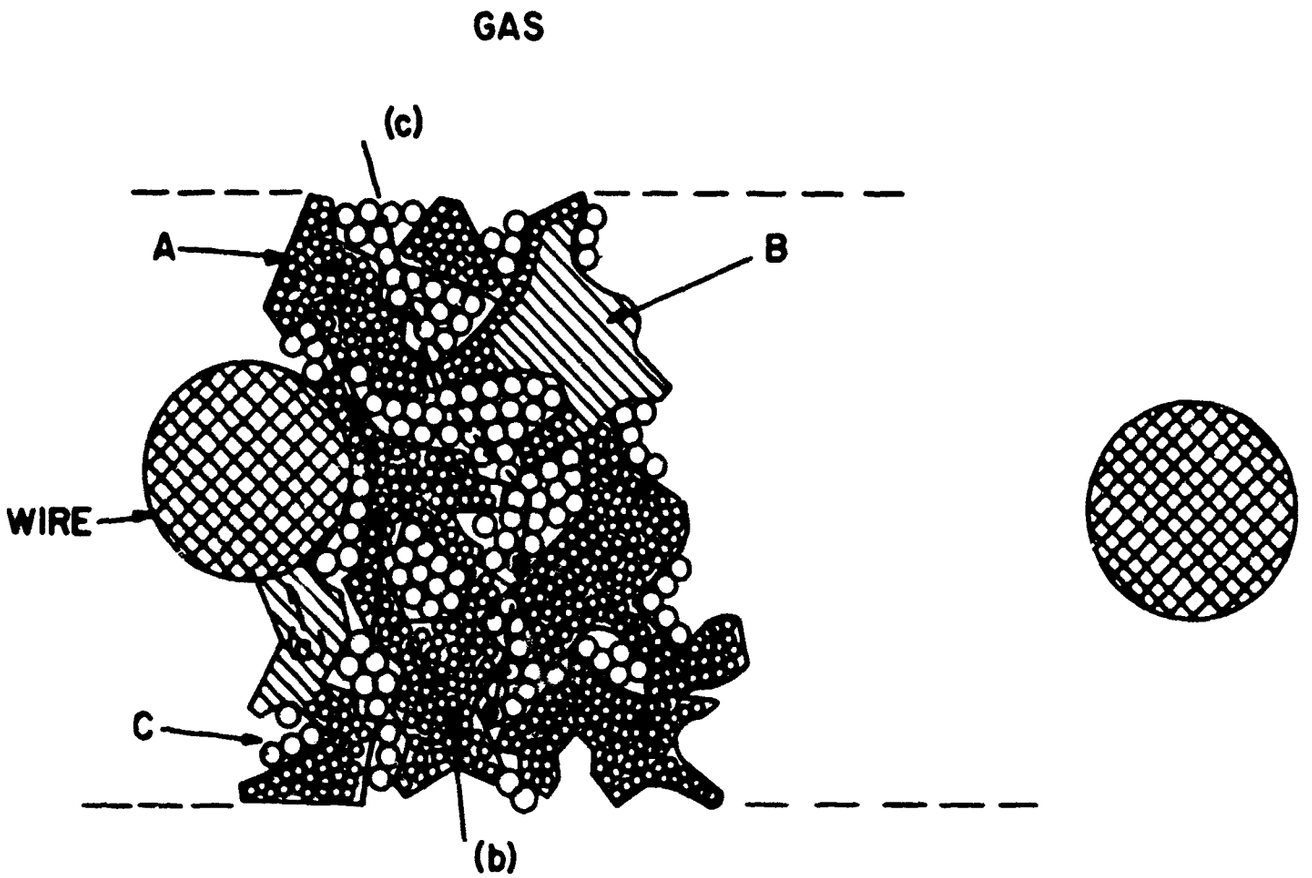

Fig. II-11

Schematic representation of a hydrophobic, porous electrode made of Teflon-bonded platinum black.

The result is that the electrolyte is a compound of three interlocked networks for gas, electrolytic, and electronic transport, respectively, with an additional local diffusive transport of dissolved reactant which helps to utilize the internal surface of the Pt agglomerates. The optimization of such structure calls for a compromise, since the requirements for improving the efficiency of any of the three channels will, to some extent, damage the other ones. For instance, increasing the Teflon/Pt ratio will cause a more hydrophobic electrode and better gas transport (and to some extent better diffusive transport), but will increase at the same time the chance of encapsulating Pt agglomerates in Teflon and hence it will decrease the efficiency of the electronic and electrolytic transport.

Another factor of interest is the size of the Pt agglomerates. With low gas solubility, as is the case with ethane in 85% H_2PO_4 at 150°C, it is possible that under staeady state condition only a thin peripheral part of the Pt agglomerate is used for the oxidation of the hydrocarbon, while the inside is depleted of hydrocarbon and therefore useless. One way to make more rational use of the Pt available is to decrease the agglomerate size. The effect of decreasing the size of the Pt agglomerates can be more easily predicted if the following assumptions are made:

a) The size of the Teflon particle is of no influence on the structure. This will be the case as long as the decrease of agglomerate size does not make the agglomerate size comparable to the size of the Teflon particle.

b) Both microporosity (i.e. porosity inside the agglomerates) and macroporosity (porosity between agglomerates) are independent of the agglomerate size.

c) The tortuosity factor is independent of size.

d) The presence of contacts between agglomerates is independent of size (i.e. electronic conductivity at those points is not interrupted with decreasing size).

If these conditions hold, a decrease of particle size will cause no change on the electronic and electrolytic resistance since these factors are only a function of the porosity and of the tortuosity factor. By reducing the size of the agglomerates and pores in scale, porosity and tortuosity factors remain constant. Also the gas transport, which will be determined by molecular gas diffusion, will be independent of pore size (the gas permeability is pore size dependent, but will not play any role here).

The only effect of reduction of the agglomerate size will then be an increase in the agglomerate surface (inversely proportionate to the radius), i.e. of the surface limiting the gas and electrolyte filled pores, increasing the diffusive transport, and at the same time decreasing the depth through which the dissolved hydrocarbon has to diffuse in order to utilize all the internal surface of the agglomerates (i.e. of the crystallites in the center of the agglomerate). The net result will be an increase of current if diffusion of dissolved hydrocarbon is a rate-determining process.

In general, the preceding assumptions will not hold absolutely and therefore the effects of changes of the agglomerate size are somewhat difficult to predict.

Homogenity of the agglomerate and Teflon dispersion is essential. If the mixture is not homogeneous, aggregation of Pt agglomerates will lead to macroflooding. This will be also the case if too small amounts of Teflon are used. Conversely, Pt agglomerates can be encapsulated in large amounts of Teflon.

It is apparent from the above that besides the catalytic factors that we are looking for, there are also structural factors (some of them inherent to the specific Pt-black) which may be overriding for a gas diffusion electrode in the steady state. In order to test catalytic factors in such types of electrode structure, we are forced to investigate also the structural factors inherent to the black, such as agglomerate size, shape of the agglomerate, internal porosity, internal pore size distribution, macroporosity of Pt-black, besides the structural factors inherent to the electrode (Teflon/Pt ratio, homogenity, etc.).

In the following, the several testing methods which are being developed, and their advantages and limitations, are described.

B. "Steady State" Test

In order to obtain the "steady state" (i(E) curve the electrode will be tested in a "floating electrode"[17] which has been already assembled and is operable. This cell consists of an electrode (~ 1 cm^2 area) placed on the surface of the electrolyte over which reactant gas is passed. This simulates the operation of a half cell without the complications of construction and operation of a complete fuel cell.

The body of the cell is a 500 ml reaction kettle. The cover supports the working electrode, reference electrode, and gas inlet. The gas exits from the cell through the threads in the level adjust screw. The reference electrode and the working electrode holder are made in one piece wo that the capillary tip is always at the same distance from the electrode. With this arrangement the resistance included in the electrode potential measurement is a constant for a given electrolyte and need be measured only once for a series of determinations. This is a distinct advantage, since it is very difficult to have a constant or zero iR drop, if the distance is adjusted with each electrode.

The electrode holder is fitted into the center tube with a screw device which permits a fine control on the level of the electrode with respect to the electrolyte and permits the electrode to be accurately placed in the solution. Using this device it was found that raising or lowering the electrode by 3 mm from a position level with the electrolyte surface made less than 2% change in the current (when used as H_2-electrode); thus, the elevation of the electrode with respect to the solution is not critical.

The i(E) curve will be taken as follows: After anodic pretreatment at 1300 mv the i(E) curve will be taken every 50 mv, starting from E = 150 mv by reading the current after 5 min at constant polarization, or by direct recording with X-Y recorder and slow voltage scan (10 mv/min).

In addition, the current at a given voltage (for instance E = 400 mv) will be recorded for periods of approximately one hour.

The drawbacks of this method for determining the activity of a given catalyst have been discussed above. One of the main problems is, of course, the presence of diffusion polarization. This factor can be eliminated if the following non-steady state test is used with the same electrode structure.

C. Oxidation of Chemisorbed Intermediates

The most important limiting factor during the hydrocarbon oxidation is the formation of intermediate species which are more difficult to oxidize than the pure hydrocarbon and therefore poison the electrode[18]. The activity of the electrode for oxidation of these species is an indication of its over-all catalytic activity.

In order to study the oxidation of the intermediate, the floating electrode will be kept at constant potential (250 - 350 mv) for a given time (recording the current decay during this time). Afterward, the hydrocarbon is replaced by N_2 and a "fast" voltage sweep ($\sim$ 400 mv/min) or galvanostatic pulse will be applied, in order to oxidize the chemisorbed product. This process will be repeated with increasing times at E = 250 - 300 mv, until the charge of the peak (i.e. the amount of chemisorbed species) is constant. The possibility that the nature of the chemisorbed species may change with time, without change of the amount, has to be kept in mind.

While the two first stages, i.e. current decay, and time necessary to reach saturation, will be in part diffusion controlled, the final stage is independent of diffusion. The only factors which will still obscure the determination of the intrinsic catalytic activity will be the degree of electrical contact between particles (or percentage of Pt-agglomerates electrically isolated) and, to some extent, macroflooding. Both effect can be studied by measuring the real surface by charging curves or double layer capacity methods and comparing with B. E. T.

The influence of degree of flooding and degree of electrical contact on the measurement can also be eliminated by studying the oxidation of a hydrocarbon having a high solubility.

7. Methanol Oxidation

The oxidation of methanol has the following advantages:

a) Methanol is highly soluble and reactive even at 25°C.

b) Some limitations of the CH_3OH oxidation (intermediate formation) are common to the oxidation of saturated hydrocarbons.

c) Because of the high solubility of the reactant the electrode can be flooded. Also, since the only Teflon function now is to act as a mechanical bond, its quantity can be reduced greatly. This will insure a minimum of electrically isolated particles.

Summarizing the contribution of diffusion polarization, degree of macroflooding, and imperfect electrical contact, all important factors with gaseous hydrocarbon electrodes, will be insignificant in methanol oxidation. However, if by using this test method a more active Pt-catalyst is found, this catalyst can then be used in a structure favorable for oxidation of saturated hydrocarbons.

8. References

1 C. Wagner and W. Traud, Z. Elektrochem. 44, 391 (1938); G. E. Kimball, J. Chem. Physics 8, 199 (1940).

2 N. Ibl in "Advances in Electrochemistry and Electrochemical Engineering", Vol. 2, edited by C. W. Tobias, John Wiley & Sons, New York, 1962.

3 F. Endner and H. Gebauer, Optik 13, 97-101 (1956).

4 I. Karpenko, R. W. Dye, W. H. Engel, Tappi 45, #1, 65-69 (1962).

5 See for example, Ceramic Age, September 1962.

6 D. W. Montgomery, Rubber Age, September 1962

7 H. F. Fischmeister, H. E. Exner, G. Lindelof, Proceedings of the International Conference on Powder Metallurgy, New York 1965, Paper #5B .

8 H. P. Klug and L. E. Alexander, X-ray Diffraction Procedures, John Wiley & Sons, New York, London 1962, pp. 491-494.

9 F. W. Jones, see: Taylor, X-ray Metallography, John Wiley & Sons, New York, 1961, pp. 687-696.

10 B. E. Warren, Progr. Metal Phys. 8, 147 (1959).

11 R. A. Stephen and R. T. Barnes, see: Taylor, X-ray Metallography, John Wiley & Sons, New York, 1961, pp. 667-671.

12 Clark and Zimmer, see: Taylor, X-ray Metallography, John Wiley & Sons, New York, 1961, pp. 665-667.

13 F. Lenz, see: G. Thomas, Transmission Electron Microscopy of Metals, John Wiley & Sons, New York, 1962, pp. 9-10.

14 G. Thomas, Transmission Electron Microscopy of Metals, John Wiley & Sons, New York, London, 1962, pp. 37-38.

15 B. D. Polkovnikov, A.A. Baladin and A. M. Taber, Dokl. Akad. Nauk. SSSR, 145, 809-11 (1962).

16 F. Wald and A. J. Rosenberg, Trans. A.I.M.E., 233, 796-799 (1965).

17 J. Giner and S. Smith, to be published.

18 J. Giner, 15th CITCE Meeting (London) 1964, Summary 3.17 (to appear in Electrochimica Acta);

18a S. B. Brummer, J. I. Ford and M. J. Turner, J. Phys. Chem. 69, 3424 (1965).

19 A. R. Stokes, Proc. Phys. Soc. (London) 61, 382 (1948).

III. CORROSION IN H_3PO_4 SOLUTIONS

1. General

The successful practical development of the direct oxidation hydrocarbon fuel cell depends largely on improving its performance through understanding its functioning, as outlined in the previous sections. In addition, it is critical to reduce the capital cost of the fuel cell components. Ideally, one would hope to move away from high-cost, low-availability noble metal catalysts towards cheaper, more widely accessible materials. A significant additional cost factor in the present hydrocarbon fuel cell is presented by the structural materials, e.g. electrode supports, the current collectors, the cell walls, and so on. Normally, these materials would not constitute a sizeable fraction of the cost of the cell, particularly as there are no unusual strength requirements. The problem is that the concentrated H_3PO_4 electrolyte presently used is highly corrosive. To date the cheapest conducting structural material which can be employed is tantalum and it is so expensive that, in practice, its total cost is about the same as that of the Pt catalyst. (The Ta is, of course, used in much larger quantities.) Thus, a program of research of corrosion in concentrated H_3PO_4 has been initated with the aim of finding cheaper substitues for Ta.

An extensive literature survey showed that no non-noble metal other than Ta is sufficiently corrosion resistant to the concentrated acid (see also Popat and Kuchar[1]). This corrosion problem is aggravated under the conditions of high anodic potential required at the electrodes of the fuel cell. In the absence of any positive information of alternatives to Ta, the initial approach has been to work from Ta, which is highly corrosion resistant to the acid, and to attempt to alloy the Ta with cheaper metals. In this way, it might be hoped to reduce the Ta content and the cost, but to retain the high corrosion resistance of Ta itself.

It is worth considering, at this juncture, what one might hope to achieve in this way. Ta is not intrinsically very expensive, particularly if one does not mind minor contamination with Nb. The difficulty is that

in order that the Ta be sufficiently ductile, it must be vacuum-melted to remove dissolved interstitials (O_2, N_2). Since the melting point is 2996°C[2], this involves specialized and expensive equipment, the capital cost of which is an important factor contributing to the high cost of the Ta. Thus, an important consideration is that when Ta is alloyed, the melting point should be depressed and also that the need for vacuum melting should be eliminated. Because of this, no high Ta alloy can possibly be much cheaper than Ta itself. (In fact, even those alloys available in quantity, e.g. Ta - 10% W, are as yet more expensive than Ta itself.) However, we have examined some high Ta-containing alloys, as reported below, in order to investigate the general corrosion behavior of the alloy systems because we believe that only a systematic program will allow the development of an alloy with the optimum electrochemical and mechanical properties.

Consider for the moment single phase, binary alloys with less than 50 at. % Ta: the following elements are not suitable for alloying with Ta:[3]
Al, B, Be, C, Co, Cr, Cu, Te, Ga, Ge, Ni, Os, Ru, Si, U.
The metals listed below are possible[3]:

Metal:	Ir	Mo	Nb	Re	Rh	Ti	V	W
M.P. 50% alloy (°C):	(--)	2750	2700	(--)	(--)	(2400°)	(2300°)	(~3000°)
Density, alloying element ($g.ml^{-1}$):	(22.5)	(10.2)	(8.4)	(21.0)	(12.4)	(4.5)	(6.1)	(19.3)

In these cases, the approximate melting points of the 50% alloys are given in the table, as are the densities of the alloying elements. In the present context, lighter alloying elements such as Ti or V would be distinctly favored. This is not a long list, particularly if we exclude, as we must, the noble metals on the grounds of cost. However, it provides a basis from which we can investigate corrosion-resistance in hot concentrated H_3PO_4 of Ta-based systems.

2. Experimental

The basic approach is to survey a system rapidly and, where promising, to investigate it more thoroughly. Since the performance at potentials anodic to H^+/H_2 is important, we have adopted, initially, the current-potential (i - E) curve as a screening technique, with the intention of doing weight loss measurements for promising materials. The i-e curve is obtained potentiostatically, using a conventional three-compartment cell, the electrolyte being saturated with pre-purified N_2. As before, the electrolyte is purified by recrystallization followed by reflux with H_2O_2. Current readings were taken after 2 minutes or 5 minutes, as indicated, during an ascending potential regime starting at the rest potential. Then, once O_2-evolution was reached, readings were taken while decreasing the potential. Electrodes were polished mechanically and then cleaned in chromic acid and/or in a suitable etchant-acid, as indicated. Measurements were taken in 85% or 91.6% (the hemi-hydrate) H_3PO_4, at temperatures up to 150°C.

3. Results

a) Tantalum: For comparison purposes, studies were made of the corrosion of Ta. The Ta was mechanically polished and was cleaned with 5:2:2 (vol:vol:vol) of H_2SO_4, HNO_3, and HF. Before use it was washed in boiling, triply-distilled water. Figure III. 1 shows the i-E curves for Ta in H_3PO_4 at 150°C. For reference, we may note that 0. 1 mm/ yr, which we take to be an acceptable corrosion rate for a structural material, corresponds to about 160 $\mu a/cm^2$ for Ta. Ta is evidently much better than this, even under the most stringent conditions required. It should be emphasized that even the low corrosion rates shown in Fig. III. 1, and also subsequently, are higher than those which would be found in practice, since the data were taken after 2 minutes at each potential (or 5 minutes as indicated) and the current was still falling slowly when the measurement was made. The measurements shown were taken on the ascending potential cycle and the currents during the descending cycle were in all cases considerably

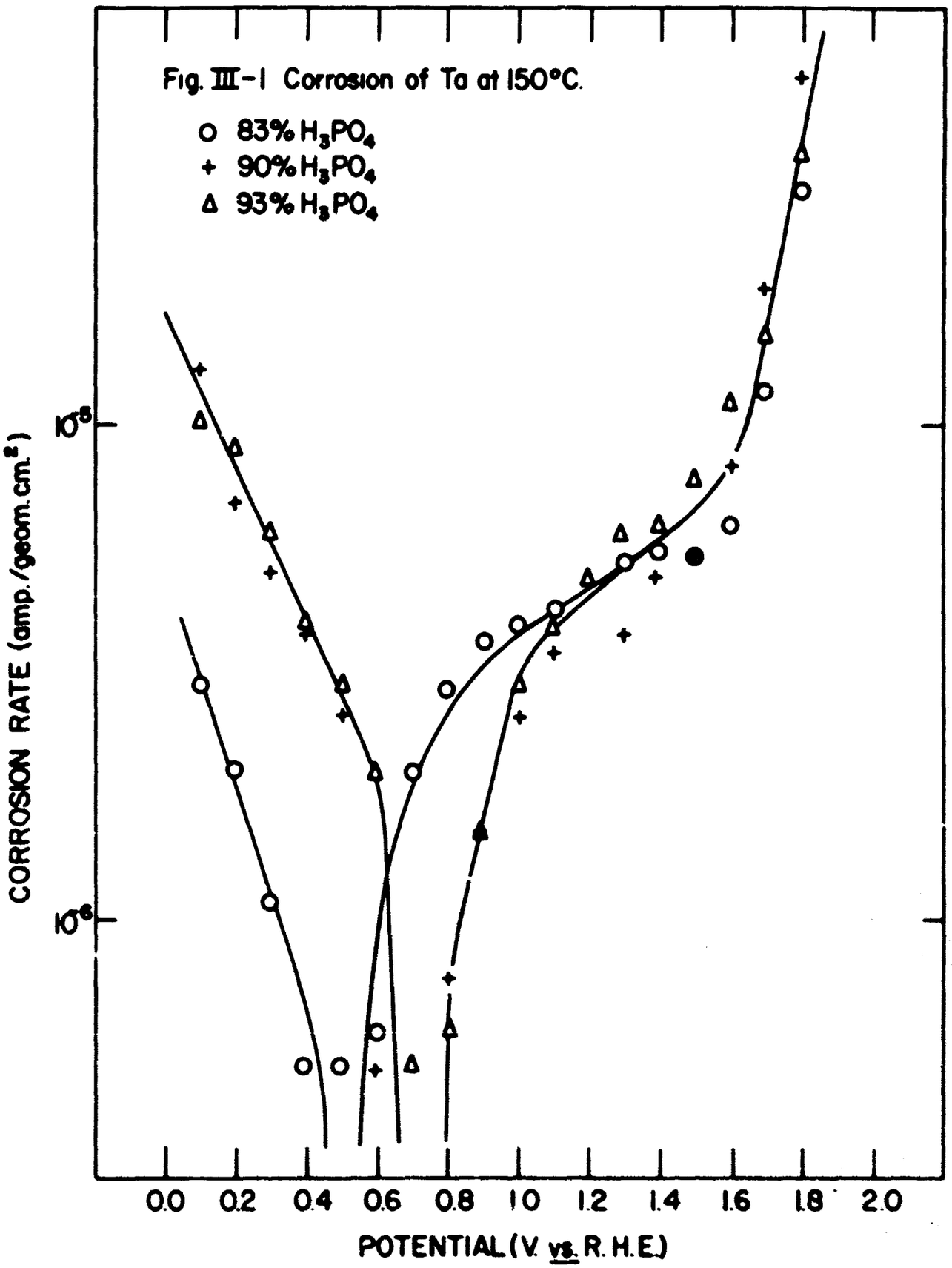
Fig. III-1 Corrosion of Ta at 150°C.
○ 83% H_3PO_4
+ 90% H_3PO_4
△ 93% H_3PO_4
CORROSION RATE (amp./geom.cm.²)
10^{-5}
10^{-6}
0.0
0.2
0.4
0.6
0.8
1.0
1.2
1.4
1.6
1.8
2.0
POTENTIAL (V. vs. R.H.E.)

lower. We do not find any significant effect of H_3PO_4 concentration and we may note that the repeatability of the measurements from sample to sample is about a factor of two.

No Ta alloy has yet been found which has a corrosion resistance superior to Ta itself.

In a recent publication[4], it has been reported that argon-arc melted Ta, which is usually brittle due to inclusions of impurities, may be made ductile by alloying with a small amount of Ni. The Ni evidently acts as a scavenger for the non-metals which would make the Ta brittle. We have made an alloy with 0.33 wt % Ni (alloy compositions are given in atomic % unless otherwise noted) and also, with 1.2% Gd, which is also reported to render the Ta ductile. Both alloys, and also an alloy containing both Ni and Gd, resisted corrosion in H_3PO_4 almost as well as Ta, e.g. their corrosion rate at 1.0 v vs. R.H.E. were about 10 $\mu a/cm^2$. Our samples of these alloys were ductile enough to be rolled, and this method may well be a way to provide cheap Ta which is sufficiently pure for the purposes of fuel cel construction, since it avoids the expensive vacuum melting.

b) Niobium: Nb is much more plentiful than Ta[5] and is potentially much cheaper. Unfortunately, we have found that its corrosion rate is much higher than that of Ta. Thus, for example, at 150°C in 91% H_3PO_4, it corrodes at almost 1 ma/cm^2 at 1 v vs. R.H.E.

c) Alloys with Mo and W: Alloys of Ta and Nb with W and Mo are commercially available due to usage as high temperature corrosion-resistant materials. Ta - 10% W showed excellent corrosion resistance, comparable to Ta, but is quite brittle. Further additions of W seem likely to lead to a brittle alloy. In addition, the melting points are very high in this system. Similar remarks apply to Ta-Mo. Nb-W and Nb-Mo corroded too fast to be useful. Because of these deficiencies, alloying with Mo and W is not presently being considered.

d) Alloys with Ti: Ta-Ti alloys show corrosion resistance towards concentrated acids according to a report by Stern and Bishop[6], although H_3PO_4 is not specifically mentioned. Titanium is potentially a useful alloying element since it is relatively inexpensive and light. It can also be alloyed with Ta up to ~ 60% without introducing a second phase. We have found that alloys up to 60% Ti (argon-arc melted) are reasonably ductile although harder than Ta itself. Their corrosion resistance (so far measured to 120°C) appears to be fairly good, despite the fact that Ti itself dissolves rapidly under these conditions (~ 1 ma/cm^2 at 1 v). Results are shown in Fig. III. 2. At this time, we regard this alloy system as one of the more promising systems in which to attempt ternary additions to improve the corrosion resistance and it is being investigated further.

e) Intermetallic Compounds: Investigating a report[7] that Hastalloy C shows good corrosion resistance to H_3PO_4, we have come across an intermetallic compound of Ta and Ni which has good corrosion resistance and which may be the fore-runner of a whole class of relatively cheap, corrosion-resistant intermetallic compounds. This also suggests the first possibility of even looking for a non-noble-metal catalyst. We found that the Ni-Mo alloy itself corrodes badly at anodic potentials. An alloy of Hastalloy C with 15% Ta also corroded at a high rate but upon metallographic examination it was found that one of the two phases present appeared to be unattacked. This phase was analyzed as $TaNi_3$ (by electron probe microanalysis) and subsequent tests with samples of this compound prepared directly (M.P. 1545°C) have shown that it has good corrosion resistance (Fig. III. 3). This is remarkable for a compound that contains so little Ta, since the corrosion resistance is presumably basically conferred by a film of Ta_2O_5. This contention is being tested by electron diffraction and will help to establish a picture of the corrosion-resistance, or otherwise, of Ta-containing materials. We are also preparing a number of other Ta-containing intermetallic compounds to investigate their general corrosion characteristics.

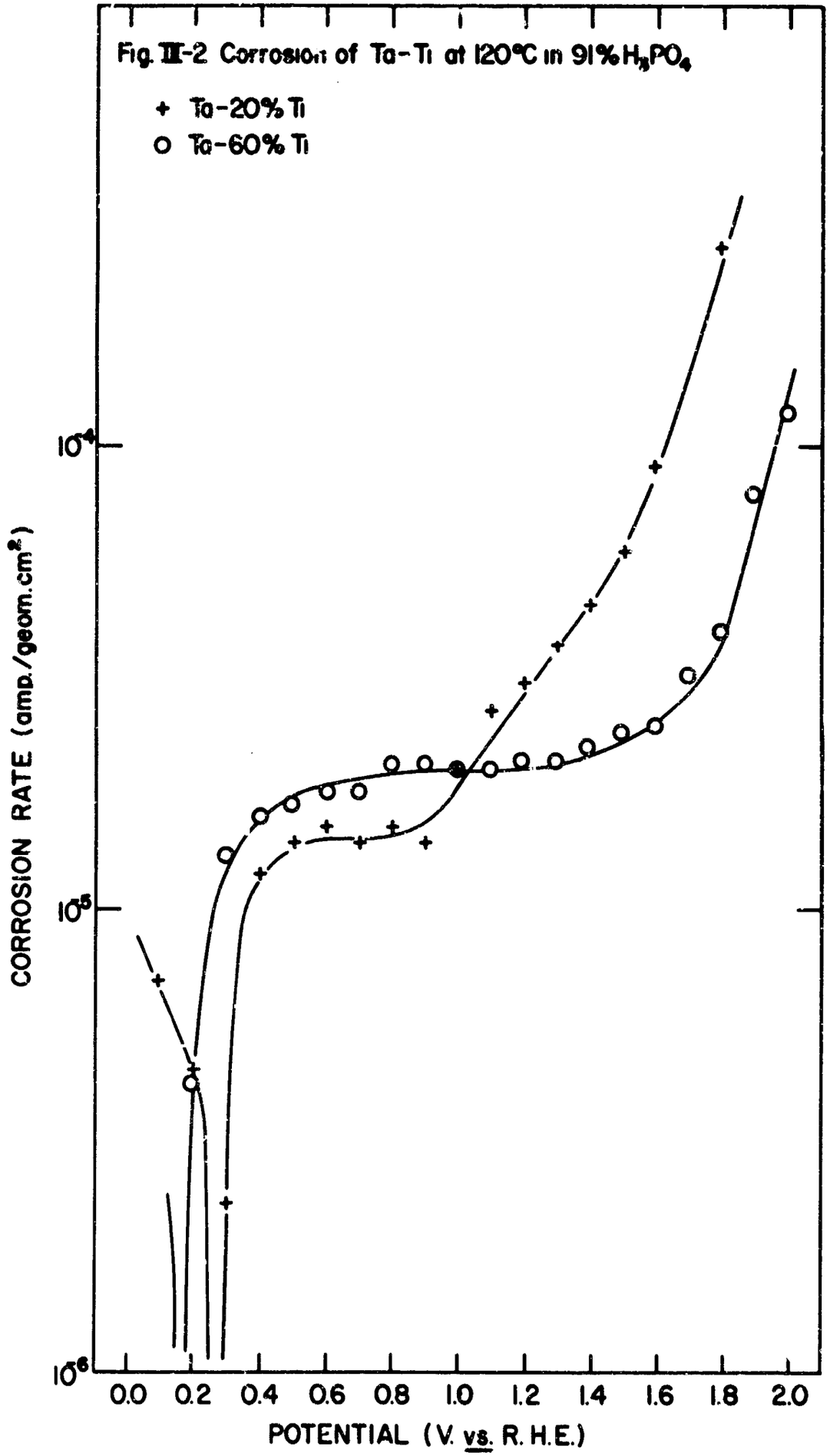
Fig. III-2 Corrosion of Ta-Ti at 120°C in 91% H_3PO_4
+ Ta-20% Ti
O Ta-60% Ti
CORROSION RATE (amp./geom.cm²)
10^{-4}
10^{-5}
10^{-6}
0.0 0.2 0.4 0.6 0.8 1.0 1.2 1.4 1.6 1.8 2.0
POTENTIAL (V. vs. R.H.E.)

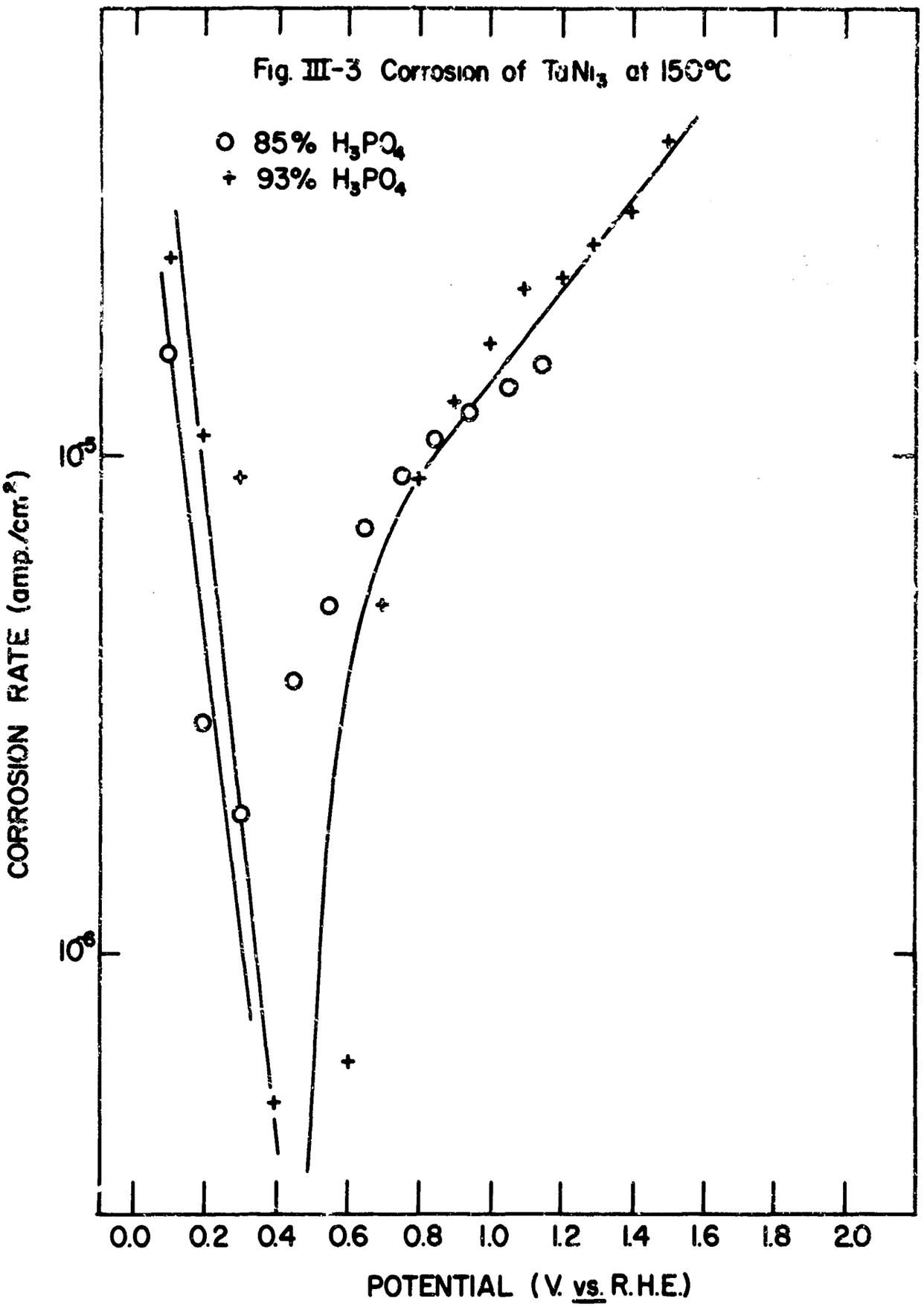
Fig. III-3 Corrosion of $TaNi_3$ at 150°C
○ 85% H_3PO_4
+ 93% H_3PO_4
CORROSION RATE (amp./cm.²)
10^{-5}
10^{-6}
0.0
0.2
0.4
0.6
0.8
1.0
1.2
1.4
1.6
1.8
2.0
POTENTIAL (V. vs. R.H.E.)

4. Future Work

The immediate aim is to investigate the Ta-Ti system more fully and to attempt ternary alloying to improve its corrosion resistance and its ductility. In addition, a number of Ta intermetallic compounds is being prepared and these are being selected on the basis of expected ductility.

5. References

1. P. V. Popat and A. Kuchar, Interim Report No. 10 on contract DA 44-009-ENG-4909 (Dec. 1963); Interim report No. 1 on contract DA 44-009-AMC-479(T) (Apr. 1964).
2. D. R. Stull and G. C. Sinke, "Thermodynamic Properties of the Elements," American Chemical Society, Washington, D.C. 1956.
3. W. F. Sheely in "Columbium and Tantalum" (Ed. Frank T. Sisco and Edward Epremian), John Wiley, New York, N.Y., 1963, p. 444 et seq.
4. E. Raub and E. Roeschl, Z. F. Metallkunde 56, 339 (1965).
5. cf. Ref. (3) p vii.
6. cf. Ref (3), M. Stern and C. R. Bishop, p. 304 et seq.
7. J. Buenger, Werkstoffe und. Korrosion, 6, 369 (1955).